Interaction et diffusion hydrodynamiques dans une suspension de vésicules et globules rouges

Aparna Srivastav

UNIVERSITÉ DE GRENOBLE

THÈSE

Pour obtenir le grade de

DOCTEUR DE L'UNIVERSITÉ DE GRENOBLE

Spécialité : **Physique pour les sciences du vivant**

Arrêté ministérial : 7 août 2006

Présentée par

Aparna Srivastav

Thèse dirigée par **Chaouqi Misbah**
et codirigée par **Thomas Podgorski**

préparée au sein **du Laboratoire Interdisciplinaire de Physique**
et de **l'Ecole Doctorale de Physique**

Interaction et diffusion hydrodynamiques dans une suspension de vésicules et globules rouges

Thèse soutenue publiquement le **(26 Janvier, 2012)**,
devant le jury composé de :

Mme. Miglena Angelova
Laboratoire MSC, Rapporteur
M. Marc Léonetti
IRPHE , Rapporteur
M. François Caton
Laboratoire de rhéologie, Examinateur
M. Bernard Zappoli
CNES, Examinateur
M. Chaouqi Misbah
LIPhy, Directeur de thèse
M. Thomas Podgorski
LIPhy, Co-Directeur de thèse

Hydrodynamic interactions and diffusion in vesicle and red blood cell suspensions

Aparna Srivastav

Ph.D thesis

Grenoble, January 26^{th} 2012

Ph.D thesis supervised by Chaouqi Misbah, Thomas Podgorski
Prepared at Laboratoire interdisciplinaire de Physique
Université Joseph Fourier CNRS/CNES
Grenoble, France

Acknowledgement

The present thesis has been prepared with the help and support of many people, whom I would like to thank with my humble acknowledgement.

First and foremost, I want to express my sincere gratitude to Dr. Gwennou Coupier for his guidance, encouragement, patience, enthusiasm and great technical support from the initial to the final level which enabled me to develop an understanding of the subject. He was always accessible and willing to help his students with their research.

I wish to express my warm and sincere thanks to my co-supervisor Dr. Thomas Podgorski, for enlightening and guiding me with his knowledge. His help and his advices were very fruitful for shaping up my research and thesis. The way they train student is excellent, I will always been indebted for this. I was delighted to interact with my supervisor Prof. Chaouqi Misbah for his detailed review, constructive criticism and excellent advices during the preparation of this thesis.

I have been lucky to have an opportunity to work with Prof. Victoria Vitkova to study rheological property of blood. She has taught me, both consciously and unconsciously, how good experimental physics is done. The joy and enthusiasm she has for her research was contagious and motivated me especially during tough times in the Ph.D. pursuit. I am also thankful for the excellent example she has provided as a successful scientist woman and professor. Thanks to Xavier who recently joined the group in a post-doc position for his support in completing the last set of experiments of my thesis.

In my daily work I have been blessed with a friendly and cheerful group of fellow lab mates, Valentina, Edith, Darja, Michael, Giovanni, Kalpana and Levan for all the emotional support, friendship, entertainment, and caring they provided and for their help they gave me to surmount the difficult times. In particular, Vincent helped me get on the road to LaTeX and provided support to solve problems I had as a beginner in LaTeX practice for writing the thesis. Outside of the lab, plenty of people kept me sane and happy in Grenoble. Among many others, I thank Bernard and Dr. Subodh for their insightful suggestions to look at the problem from different angle and happily overcome it. Their unconditional help and encouragement throughout the thesis were appreciable.

For this dissertation I would like to thank my reading committee members Prof. Miglena Anguelova and Dr. Marc Leonetti for gracefully accepting to be my reporter and contributing to improve my work with their time, interest, and helpful comments. I

gratefully acknowledge the French government and my funding sources, the CNRS/CNES that made my Ph.D. work possible. Lastly, I would like to thank my family for all their love and encouragement.

My elder brothers and younger sister were particularly supportive. The love and firm confidence my parents have for me added enormous energy to work cheerfully. Most important, I express my heartily gratitude to my defunct father who had supported my decision for coming so far from home to prepare a Ph.D. work, I dedicate this thesis to him, he has always been my most enthusiast support. Finally, I would like to thank all the people who contributed to the success of this thesis, and express my apology to those I could not mention personally.

Contents

Chapter 1

Introduction

Blood is a complex fluid whose features lead to unique behavior in flow. The objective of this thesis is to contribute to the understanding of fundamental aspects of blood flow by focusing on particular aspects of red blood cells motion. The model system is briefly introduced. Contributions in understanding fundamental of physics impaired with organisation of the work are detailed.

1.1 Some generic features of blood flow in the microcirculation

Blood is a non-homogeneous dense suspension of red blood cells, leucocytes and platelets (which account for less than 1% of total volume fraction). These cells perform many important biological functions with the help of a transport medium, plasma. In early studies on blood flow, Poiseuille [1] already noticed that in flow these cells are inhomogeneously distributed throughout the cross section of vessels. This non-uniform distribution of red blood cells is influenced by many factors such as hydrodynamic interactions with the vessel walls and interactions between red blood cells. Blood also exhibits Non-Newtonian rheology (shear-thinning) due to the elasticity of cells and their interactions. This complex and Non-Newtonian behaviour of blood has been a fascinating subject that has attracted the attention of many scientists, including biologists, physicists or mathematicians for several decades.

A homogeneous Newtonian fluid is characterized by a constant viscosity, which is an intrinsic material property of the fluid, independent of the conditions or geometry of the flow. Blood is not a homogeneous fluid, it is a suspension. As noticed by Poiseuille, the apparent viscosity of blood depends

on the confinement of the flow in tubes, in particular there is a decrease of the apparent viscosity as the vessel's diameter decreases, with a minimum for capillaries with diameters close to the size of red blood cells. This measure is related to the observation of a cell free layer near channel walls. In other words, in narrow capillaries, red blood cells tend to move close to the center of the vessel, leaving plasma near the wall. This thixotropic effect of blood is known as the Fåhraeus-Lindqvist effect [2].

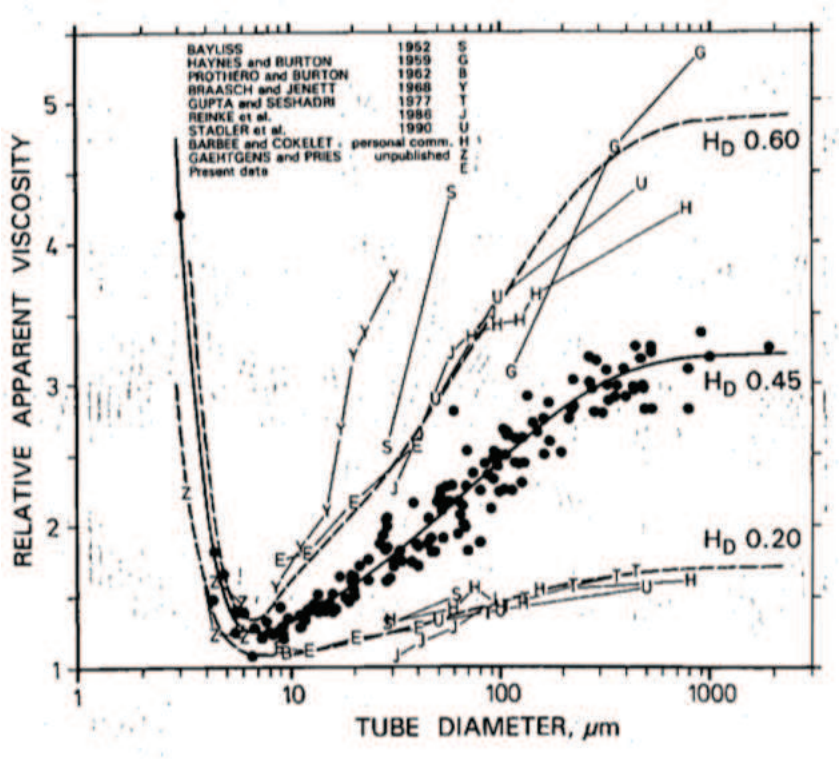

Figure 1.1: Change in apparent viscosity of blood with the change in capillary diameter [2]

Another remarkable feature of blood microcirculation is apparent when measuring the local hematocrit in a complex microvascular network [3]. While the average hematocrit in vessels that are large compared to the size of red blood cells ($> 100\mu$m) is uniform and equal to about 45-50 %, there are large heterogeneities in the smallest capillaries, with unequal distributions of blood cells and plasma at each bifurcation in the network. The general feature is that at bifurcating junctions red blood cells tend to be more concentrated into the higher flow rate daughter vessel [4].

The complexity of this microvascular flow is the consequence of many coupled phenomena which are involved at different levels of microcircula-

1.1. SOME GENERIC FEATURES OF BLOOD FLOW IN THE MICROCIRCULATION

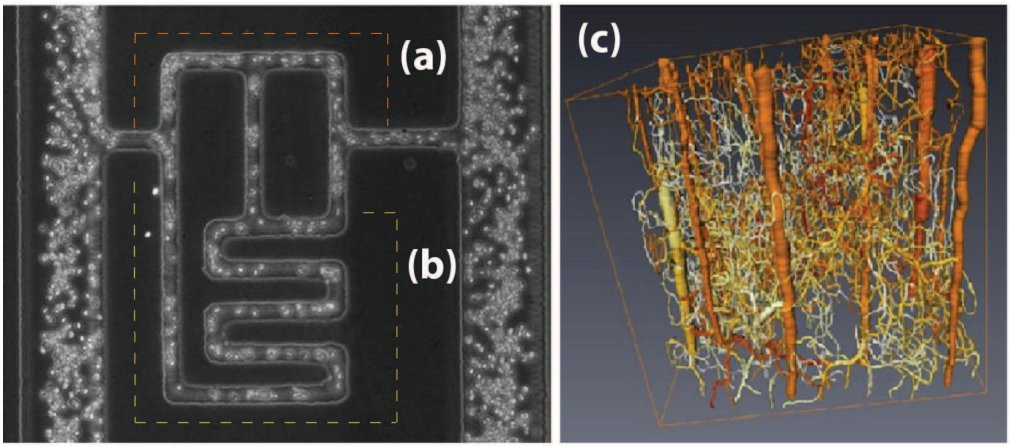

Figure 1.2: Model of microcirculation (a) Flow of blood cells in a model microfluidic network: high concentration of red blood cells (b) lower concentration of red blood cells (c) modelized blood flow in a network of capillaries where structure was measured by tomography from a mouse brain sample (size of network 1mm). Colors shows concentration of red blood cells such as darker colors shows higher concentration whereas lighter colors shows less concentration of red blood cells [3]

tion: (i) blood viscosity depends on hematocrit and capillary diameter, (ii) the distribution of flow rates in the different branches of a network depends on the resistance of each branch, which itself is a function of the local viscosity, (iii) the distribution of blood cells at a bifurcation is a function of the ratio of flow rates in the daughter branches and the spatial distribution of cells in the mother branch, (iv) this spatial distribution is a consequence of the dynamics of individual red blood cells and their interactions.

Based on these considerations, one can therefore easily conclude that a detailed and quantitative study of these various phenomena is a prerequisite to a better understanding of complex features of blood flow that are still a challenge today. In addition to the healthy blood flow, many complications due to pathologies that modify the mechanical properties and hydrodynamic behaviour of blood cells are a stimulation for research at the frontier between medical and physical sciences, to try to establish quantitative relations between the properties of cells and their behaviour in complex flows.

A prominent example, which is being studied in our institute, thanks to a CNES support, is the problem of endothelial dysfunction. Indeed, blood vessels are covered with a monolayer of endothelial cells (endothelium) protected by a brush of biopolymers (glycocalyx). Alteration of shear flow (reduction

of shear stress, as happens in microgravity), as well as flow recirculation (occurring at blood vessel bifurcations), are both known to be favorable terrain for endothelial dysfunction. As a consequence of flow alteration a cascade of events takes place, including platelet activation, lipid (LDL=low density lipoproteins and glycoproteins) deposition on vessel walls, mechanotransduction (such as gene activation, etc...), all have potential impact on cardiovascular diseases.

1.2 The dynamics of blood cells

At a scale smaller than the global blood flow, individual red blood cells exhibit a very rich and unique behaviour due to peculiar membrane properties. Rich scenarios in shape transitions and dynamics in different types of simple flows have been observed, which confer to blood amazing and nontrivial flow properties at larger scales. Under inflammatory and oxidative stress states (mainly cardiovascular) red blood cells aggregability, rigidity and adherence are enhanced, resulting in flow hindrance. Under shear flow it exhibits peculiar dynamics like tank-treading motion consisting in a stationary shape while the membrane undergoes a rotational motion [5, 6], or tumbling and swinging motions ([7, 8]). This rich picture already has an impact on blood rheology: the apparent viscosity of a blood cell suspension shows a macroscopic signature of the microscopic dynamic regime ([9]).

In small capillaries whose diameter is of the same order of magnitude as blood cells, they can exhibit a variety of shapes (axisymmetric parachute shapes or asymmetric slipper-like shapes) [10] [11]. These details naturally have an impact on energy dissipation due to viscous friction and therefore on blood rheology in confined channels, as well as on the ability of red blood cells to interact hydrodynamically with walls or between them to form aggregates.

Indeed, at very low shear rate, RBCs tend to aggregate due to depletion forces promoted by plasma proteins and form structures called rouleaux. These structures are responsible for the shear-thinning behaviour observed at low shear rates [12], [13].

1.3 Objectives and contribution of the present work

The main objective of this thesis is to focus on a few aspects of the behaviour of red blood cells in flow at the microscopic level and relate this dynamics to

properties at a meso and macroscopic level such as the structure of suspensions and their rheology.

In order to study the fundamental phenomena of individual and collective dynamics of red blood cells, we have used, besides real red blood cells, a simplified model of cell: the phospholipid vesicle. Vesicles are closed lipid membranes, encapsulating an internal fluid and are usually suspended in another external aqueous solution. They are similar to red blood cell which are envelopes containing a viscous fluid (haemoglobin solution) dispersed in another fluid (plasma). The membrane of vesicles possesses mechanical properties which are related to those of red blood cells. They are easy to produce with sizes close to the size of red blood cells, are easy to handle and do not need special physiological conditions unlike red blood cells. It allows the experimentalist to play with physical parameters such as viscosity contrast (difference in internal and external viscosity), deflation of the shape. In the present study we explored the situations described below with the help of microfluidic devices reproducing flow conditions similar to micro-vessels in some respect.

1.3.1 Dynamics of deflated vesicles

The dynamics of individual vesicles has been studied experimentally, theoretically and numerically by several authors, for quasi-spherical vesicles or vesicle with moderated deflation. From former works four kinds of dynamical regimes have been found: tank-treading, tumbling, vacillating breathing and kayaking. In the absence of a reliable experimental method for producing stable significantly deflated vesicles, no systematic dynamical study has been reported about vesicles with shapes similar to red blood cells.

We initiated an experimental study on the dynamics of deflation vesicles. The motivation is that former studies revealed that the regime of tumbling of vesicles can only exist in the presence of a viscosity difference between the internal and external fluids. The first results of our study reveal a tumbling-like motion in absence of viscosity contrast. This could shed light on the dynamics of deflated red blood cells and suggest that the shape itself is sufficient to produce such a motion.

1.3.2 Hydrodynamic interaction between two vesicles

The interaction between two objects in suspension in a fluid has been studied since 1970's for drops, bubbles, rigid particles and elastic capsules. They showed trajectory displacements and effective repulsion between objects during the collision or interaction in shear flow, which lead to shear induced diffusion at the scale of the suspension. To understand quantitatively these

phenomena in blood and their consequences on the structure of blood cell suspensions, we performed an experimental study on the interaction between two vesicles of identical size. This study on interactions leads to results in qualitative agreement with the former studies on other systems and provides a way to derive macroscopic diffusion coefficients from microscopic considerations. It should prove to be helpful for a better understanding of the structure of blood and vesicle suspensions in channel flow where shear induced diffusion is balanced by other effets.

1.3.3 Shear induced diffusion of red blood cells in Poiseuille flow

During the circulation of blood in the micro-vascular network, the suspension viscosity depends on the distribution of cells in the cross section of the channels. As a complementary approach to the computation of shear induced diffusion coefficients from the analysis of pair-interactions in suspensions, it is also important to find simple ways to measure the effect of this diffusion in more complex and more concentrated situations. We investigated the diffusion in a focused jet of a red blood cell suspension in a channel from which the coefficient of shear induced diffusion is estimated, this diffusion being a non-linear phenomena where the diffusivity is a function of the local concentration and shear rate.

1.3.4 A separation technique for size-sorting of vesicles

Many studies on vesicles have been performed with polydisperse samples. In specific situations, including some of those we have studied, concentrated samples of monodisperse vesicles are a requisite: for instance diffusion or hydrodynamic interactions in pairs of vesicles.

By following an established principle of pinched-flow fractionation, we have developped and optimized a sorting device dedicated to the sorting of vesicle by size and provide a characterization of its performance. Such a device could also be useful in rheological studies of concentrated suspension of monodisperse vesicle which could be compared to the rheology of real blood to have a better idea of the quantitative effects of the cytoskeleton on rheology.

1.4 Organisation of the manuscript

The core of this manuscript is divided into five distinct chapters, as follows:

1.4. ORGANISATION OF THE MANUSCRIPT

- Chapter 3 is dedicated to an introduction on the structural and mechanical properties of vesicles and red blood cell and physics of the system under study. We present briefly the general materials and methods used during our experiments. The technics of microscopy, the use of high speed cameras and experimental set-up are introduced. The different fabrication steps of the microfluidic systems we used are detailed.

- Chapter 4 presents our experimental methodology for producing vesicles. Since, from electroformation we get polydisperse sample of vesicles, a device dedicated to sort the vesicles according to their size has been developed. Finally, the characteristics and performance of the sorting device are described in details.

- In Chapter 5 we propose a detailed but non-exhaustive presentation of the state of the art concerning the behaviour of vesicles and red blood cells (in a dilute suspension) in response to external flow field through various theoretical and experimental work. In the second section of this chapter, we present the experimental method chosen to produce deflated vesicles. Finally the first observations of the dynamical behaviour of deflated vesicle is discussed.

- In Chapter 6, the phenomenon of hydrodynamic interaction between two vesicles in shear flow is described. To produce interactions between two vesicles in convenient conditions, an interaction device has been created to establish a confined flow with a focused vesicle suspension. The geometry of the device is explained. Results on the interaction between vesicles of an isolated pair are presented and discussed in comparison with theoretical results. A derivation of the shear induced diffusion coefficient from these results is proposed.

- In Chapter 7 we focus on the determination of the diffusion coefficient of Red Blood Cells in Poiseuille flow and on the properties of this non-linear diffusion phenomenon. Experimental results as well as a theoretical study are presented.

Chapter 2

Introduction (français)

Le sang est un fluide complexe dont les propriétés entraînent des comportements uniques en écoulement. L'objectif de cette thèse est de contribuer à la compréhension d'aspects fondamentaux des écoulement sanguins en se concentrant sur certains aspects de la dynamique de globules rouges. Un système modèle est présenté. Les contributions à la compréhension fondamentale des phénomènes physiques mis en jeu ainsi que l'organisation de ce travail sont le préesentés ci-dessous.

2.1 Quelques généralités sur les écoulements sanguins dans la microcirculation

Le sang est uns suspension dense non-homogène de globules rouges, leucocytes et plaquettes (qui représentent moins de 1% de la fraction volumique totale). Ces cellules remplissent d'importantes fonctions biologiques avec l'aide d'un milieu porteur, le plasma. Dans ses études pionnières sur l'écoulement du sang, Poiseuille [1] avait déjà remarqué qu'en écoulement ces cellules sont distribuées de façon inhomogène dans la section des vaisseaux. Cette distribution non-uniforme des globules rouges est influencée par de nombreux facteurs tels que les interactions hydrodynamiques avec les parois des vaisseuax et les interactions entres globules rouges. Le sang a aussi une rhéologie non newtonienne (rhéofluidifiante) due à l'élasticité des cellules et leurs interactions. Ce comportement complexe et non newtonien du sang est un sujet fascinant qui a attiré l'attention de nombreux chercheurs, biologistes, physiciens ou mathematiciens, depuis des décennies.

Un fluide newtonien homogène est caractérisé par une viscosité constante, propriété matérielle intrinsèque du fluide, indépendante des conditions et de

la géométrie de l'écoulement. Le sang n'est pas un fluide homogène, c'est une suspension. Comme noté par Poiseuille, la viscosité du sang dépend du confinement lors de l'écoulement dans des tubes, et en particulier on observe une diminution de la viscosité apparente quand le diamètre du vaisseau diminue, avec un minimum de viscosité pour un diamètre proche de la taille des globules rouges. Cette mesure est reliée à l'observation d'une couche de fluide dépourvue de cellules près des parois vasculaires. Autrement dit, dans les capillaires fins, les cellules ont tendance à se déplacer vers le centre du vaisseau, laissant une couche de plasma pur près des parois. Cet effet thixotrope du sang est connu sous le nom d'effet Fåhraeus-Lindqvist [2].

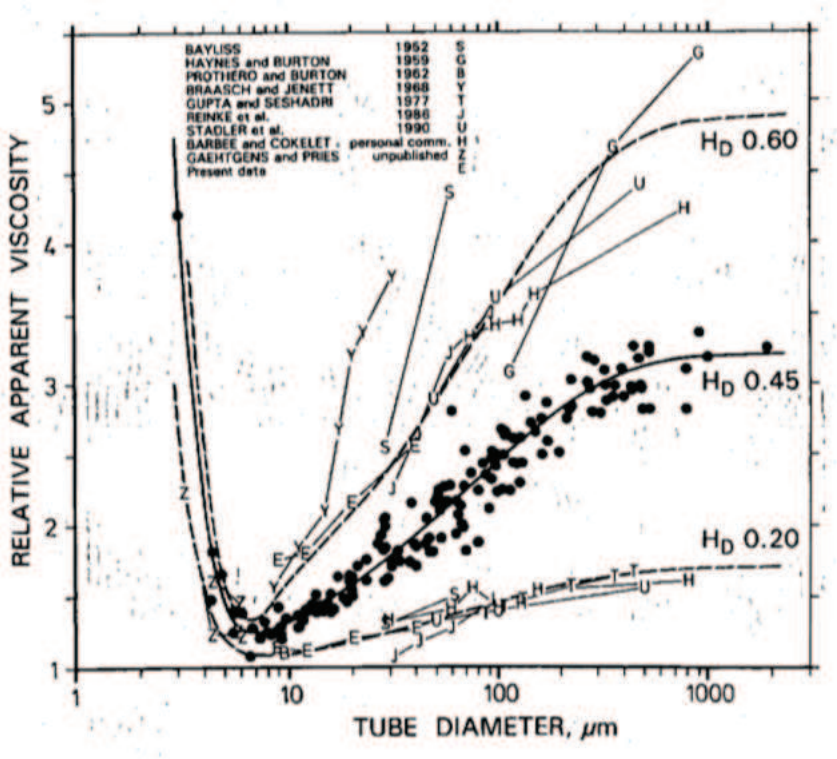

Figure 2.1: Variation de la viscosité apparente en fonction du diamètre du capillaire [2]

Une autre propriété remarquable de la microcirculation du sang apparaît quand on mesure l'hématocrite local dans un réseau microvasculaire [3]. Alors que l'hématocrite apparent dans les vaisseaux larges devant la taille des globules rouges (> 100 μm) est uniforme et égal à environ 45-50 %, il existe de grandes hétérogénéités dans les capillaires les plus fins, avec des distributions inégales du sang et du plasma à chaque bifurcation du réseau. La caractéristique générale est qu'aux bifurcations, les globules rouges tendent

à êter plus concentrés dans la branche fille de plus haut débit [4].

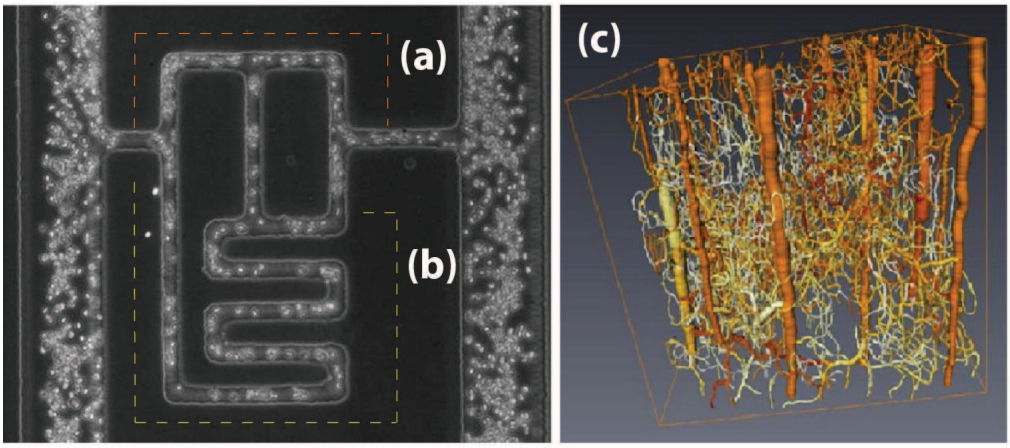

Figure 2.2: Globules rouges dans un réseau capillaire microfluidique modèle (a) Grande concentration de globules (b) concentration plus faible de globules rouges (c) Ecoulement sanguin dans un réseau capillaire (structure mesurée par tomographie) calculé par un modèle simplifié. Les couleurs montrent la concentration locale des globules rouges : les couleurs foncées correspondent à une concentration plus élevée des globules rouges alors que les couleurs plus claires montrent les concentrations plus faibles que la moyenne [3]

La complexité de ce réseau microvasculaire est la conséquence de nombreux phénomènes couplés mis en jeu à différents niveaux de la microcirculation : (i) la viscosité du sang dépend de l'hématocrite et du diamètre du capillaire, (ii) la distribution des débits dans les différentes branches d'un réseau dépend de la résistance de chaque branche, qui elle-même est une fonction de la viscosité locale, (iii) la distribution des globules rouges à une bifurcation est fonction du rapport des débits dans les branches filles et de la distribution spatiale des cellules dans la branche mère, (iv) cette distribution spatiale est une conséquence de la dynamique individuelle des globules rouges et de leurs interactions.

A partir de ces considérations, on peut donc aisément conclure qu'une étude détaillée et quantitative de ces différents phénomènes est un pré-requis à une meilleure compréhension des propriétés complexes d'écoulement sanguins qui reste un défi aujourd'hui. Au-delà des écoulements de sang sain, de nombreuses complications dues à des pathologies qui modifient les propriétés mécaniques et le comportement hydrodynamique des cellules sanguines sont une stimulation à la recherche à la frontière entre les sciences médicales et physiques pour tenter d'établir des relations quantitatives entre les propriétés

des cellules et leur comportement dans des écoulements complexes.

Un exemple saillant, étudié dans notre laboratoire grâce au support du CNES, est le problème de la dysfonction endothéliale. En effet, les vaisseaux sanguins sont recouverts d'une monocouche de cellules endotheliales (endothelium) protégée par une brosse de biopolymères (glycocalyx). Les modifications de l'écoulement (réduction des contraintes de cisaillement qui se produit notamment en microgravité), de même que les écoulements de recirculation (qui se produisent aux bifurcations entre vaisseaux sanguins), sont connus pour être un terrain favorable à la dysfonction endothéliale. En conséquence de la modification de l'écoulement, une cascade d'évènements se met en place, comprenant l'activation des plaquettes, le dépôt de lipides sur les parois vasculaires (LDL = faible densite lipoproteins et glycoprotéines), la mécanotransduction (activation de gènes etc...), ayant tous un impact potentiel sur les maladies cardiovasculaires.

2.2 La dynamique des cellules sanguines

A une échelle plus petite que l'écoulement sanguin global, les globules rouges individuels montrent une richesse de comportements uniques liés à leurs propriétés membranaires particulières. De riches scénarios de transitions de forme et de dynamique dans différents types d'écoulements simples ont été observés, qui confèrent au sang des propriétés d'écoulement étonnantes et non-triviales à plus grande échelle. En présence d'états inflammatoires et oxydatifes (principalement cardiovasculaires), l'aggrégabilité des globules rouge, leur rigidité et leur adhérence sont augmentées, ce qui représente un frein à l'écoulement. En écoulement de cisaillement, ils présentent des mouvements particuliers, comme le mouvement de chenille de char (*tank-treading*) consistant en une forme stationnaire accompagnée d'un mouvement de rotation de la membrane [5, 6], ou les mouvements de bascule (*tumbling*) et de balancier (*swinging*) [7, 8]. Ce schéma riche a déjà un impact sur la rhéologie du sang : la viscosité effective d'une suspension de globules rouges présente une signature macroscopique du comportement microscopique dynamique([9].

Dans les petits capillaires dont le diamètre est du même ordre de grandeur que celui des cellules sanguines, celles-ci peuvent présenter une variété de formes (formes de parachute axisymétriques ou formes asymétriques de pantoufles) [10, 11]. Ces détails ont naturellement un impact sur la dissipation d'énergie liée à la friction visqueuse et donc sur la rhéologie du sang en situation confinée, de même que sur la capacité des globules rouges à interagir hydrodynamiquement avec les parois ou entre eux pour former des aggrégats.

En effet, à très petit taux de cisaillement, les globules rouges tendent à s'aggréger à cause de forces de déplétion favorisées par les proteines du plasma et forment des structures appelées rouleaux. Ces structures sont responsables du comportement rhéo-fluidifiant observé à petit taux de cisaillement [12, 13].

2.3 Objectifs et contribution de ce travail

Le principal objectif de cette thèse est de focaliser sur quelques aspects du comportement de globules rouges en écoulement à l'échelle microscopique et de relier cette dynamique aux propriétés aux échelles méso et macroscopiques telles que la structure de suspensions et leur rhéologie.

Afin d'étudier les phénomènes fondamentaux de dynamique individuelle et collective de globules rouges, nous avons utilisé, en plus de globules rouges réels, un modèle simplifié de cellule: la vésicule de phospholipides. Les vésicules sont des membranes lipidique fermées, encapsulant un fluid le interne et généralement en suspension dans une autre solution externe, de manière analogue aux globules rouges qui sont des enveloppes contenant un fluide visqueux (solution d'hémoglobine) dispersées dans un autre fluide (le plasma). La membrane des vésicules possède des propriétés mécaniques voisines de celles des globules rouges. Elles sont faciles à produire, avec des tailles voisines de celle des globules rouges, sont faciles à manipuler et ne nécessitent pas de conditions physiologiques spéciales contrairement aux globules rouges. Elles permettent à l'expérimentateur de jouer avec des paramètres physiques tels que le contraste de viscosité (différence entre les viscosités interne et externe), le dégonflement de la forme. Dans l'étude présente, nous avons exporé des situations décrites ci-dessous avec l'aide de dispositifs microfluidiques reproduisant des conditions d'écoulement similaires aux micro-capillaires par certains aspects.

2.3.1 Dynamique de vésicules dégonflées

La dynamique de vésicules individuelles a été étudiée expérimentallement par plusieurs auteurs, théoriquement et numériquement, pour des vésicules quasi-sphériques ou modérément dégonflées. Dans ces travaux précédents, quatre types de régime dynamique ont été identifiés: *tank-treading, tumbling, vacillating breathing et kayaking.* En l'absence de méthode fiable pour produire des vésicules stables significativement dégonflées, aucune étude n'a été rapportée sur des vésicules avec des formes similaires aux globules rouges.

Nous avons débuté une étude expérimentale sur la dynamique de vésicules dégonflées. La motivation est que les études précédents ont révélé que le régime de *tumbling* des vésicules ne peut exister qu'en présence d'une différence de viscosité entre les fluides interne et externe. Les premiers résultats de notre étude révèlent un mouvement de type tumbling en absence de contraste de viscosité. Ceci pourrait éclairer d'un jour nouveau la dynamique de globules rouges dégonflés et suggérer que la forme en elle-même est suffisante pour produire un tel mouvement.

2.3.2 Interaction hydrodynamique entre deux vésicules

L'interaction entre deux objets en suspension dans un fluide a été étudiées depuis les années 1970 pour des gouttes, bulles, particules rigides et capsules élastiques. Elles ont montré des déplacements de trajectoires et une répulsion effective entre les objets pendant les collisions ou interactions en écoulement de cisaillement, ce qui conduit à une diffusion induite par cisaillement à l'échelle de la suspension. Pour comprendre quantitativement ces phénomènes dans le sang et leurs conséquences sur la structure de suspensions de globules rouges, nous avons réalisé une étude expériementale de l'interaction entre deux vésicules de taille identique. Cette étude sur les interactions conduit à des résultats en accord qualitatif avec les études précédentes sur d'autres systèmes et fournit un moyend de dériver des coefficients de diffusion macroscopiques à partir de considérations microscopiques. Ceci devrait se montrer utile pour une meilleure compréhension de la structure du sang et de suspensions de vésicules en écoulement en canal où la diffusion induite par cisaillement est en compétition avec d'autres effets.

2.3.3 Diffusion induite par cisaillement de globules rouges en écoulement de Poiseuille

Pendant la circulation du sang dans le réseau microvasculaire, la viscosité de la suspension dépend de la distribution des cellules dans la section des canaux. Dans une approche complémentaire au calcul de coefficients de diffusion induite par cisaillement à partir de l'analyse d'interactions de paires en suspension, il est aussi important de trouver des moyens simples de mesurer les effets de cette diffusion dans des situations plus complexes et plus concentrées. Nous avons étudié la diffusion dans un jet de suspension de globules rouges dans un canal, à partir de quoi le coefficient de diffusion est estimé, cette diffusion étant un phénomène non-linéaire où la diffusivité est fonction de la concentration locale et du taux de cisaillement.

2.3.4 Une technique de séparation pour le tri en taille de vésicules

De nombreuses études sur les vésicules ont été réalisées avec des échantillons polydisperses. Dans des situations spécifiques, y compris certaines de celles que nous avons étudiées, des échantillons concentrés de vésicules monodisperses sont nécessaires: par exemple pour la diffusion ou les interactions de paires de vésicules.

En suivant un principe bien établi de *pinched-flow fractionation*, nous avons développé et optimisé un dispositif de tri dédié au tri de vésicules en taille et présentons une caractérisation de ses performances. Un tel dispositif peut aussi être utile dans des études de rhéologie de suspensions concentrées de vésicules monodisperses qui pourraient être comparées à la rhéologie de cellules sanguines réelles pour avoir une meilleure idée d'effets quantitatifs du cytosquelette sur la rhéologie.

2.4 Organisation du manuscrit

Le coeur de ce manuscrit est divisé en cinq chapitres distincts, de la façon suivante:

- le chapitre 3 est dédié à une introduction sur les propriétés structurelles et mécaniques des vésicules et globules rouges, et à la physique du système étudié. Nous présentons brièvement les méthodes et matériaux utilisés dans nos expériences. Les techniques de microscopie, l'utilisation de caméras rapides et les dispositifs expérimentaux sont introduits. Les différentes étapes de fabrication de dispositifs microfluidiques sont détaillés.

- le chapitre 4 présente notre méthodologie expérimentale pour produire des vésicules. Comme par électroformation on obtient des échantillons polydisperses de vésicules, un dispositif dédié au tri de vésicules en fonction de leur taille a été développé. Finalement, les performances et caractéristiques du dispositif de tri sont décrites en détail.

- dans le chapitre 5, nous proposons une étude détaillée, mais non exhaustive de l'état de l'art concernant le comportement de vésicules et globules rouges (en suspension diluée) en réponse à un écoulement externe à travers différentes études théoriques et expérimentales. Dans la deuxième section de ce chapitre, nous présentons la méthode expérimentale choisie pour produire des vésicules dégonflées. Finalement, les premières observations de la dynamique de vésicules dégonflées sont discutées.

- dans le chapitre 6, le phénomène d'interaction hydrodynamique entre deux vésicules en écoulement de cisaillement est décrit. Pour produire des interactions entre vésicules dans des conditions convenables, un dispositif d'interaction a été conçu pour réaliser un écoulement confiné d'une suspension de vésicules. La géométrie du dispositif est expliquée. Les résultats sur l'interaction entre vésicules d'une paire isolée sont présentés et discutés en comparaison avec les résultats théoriques. Une dérivation d'un coefficient de diffusion induite par cisaillement à partir de ces premiers résultats est proposée.

- dans le chapitre 7, nous nous focalisons sur la détermination du coefficient de diffusion pour des globules rouges en écoulement de Poiseuille et sur les propriétés de ce phénomène de diffusion non-linéaire. Des résultats expérimentaux ainsi qu'une étude théorique sont présentés.

Chapter 3

Vesicles & Red Blood Cells

Ce chapitre introduit les propriétés structurelles et mécaniques de vésicules et globules rouges. Une brève explication des quelques paramètres physiques responsables de la dynamique de vésicules est présentée. Finalement les méthodes expérimentales sont décrites.

This chapter introduces the structural and mechanical properties of vesicles and red blood cells. A brief explanation of few physical parameters responsible for dynamics of vesicles is presented. Finally, an overview of our experimental approach is described.

3.1 Vesicles

A vesicle is a closed lipid membrane encapsulating an internal fluid and suspended in an external aqueous environment. Its size varies from a few nanometers to hundreds of micrometers in diameter. The cell membrane is selectively permeable to ions and organic molecules. Due to this property it controls the movement of substances in and out of cell. Vesicle exhibits major physical and mechanical properties similar to most biological cells. They are easy to produce and their properties such as size, structure and capability to influence internal and external fluid component can be controlled, hence they can be use to mimic certain aspects of biomembranes. Therefore it is essential to know how their membrane structure plays an important role in understanding many physical phenomena like deformation and their dynamics.

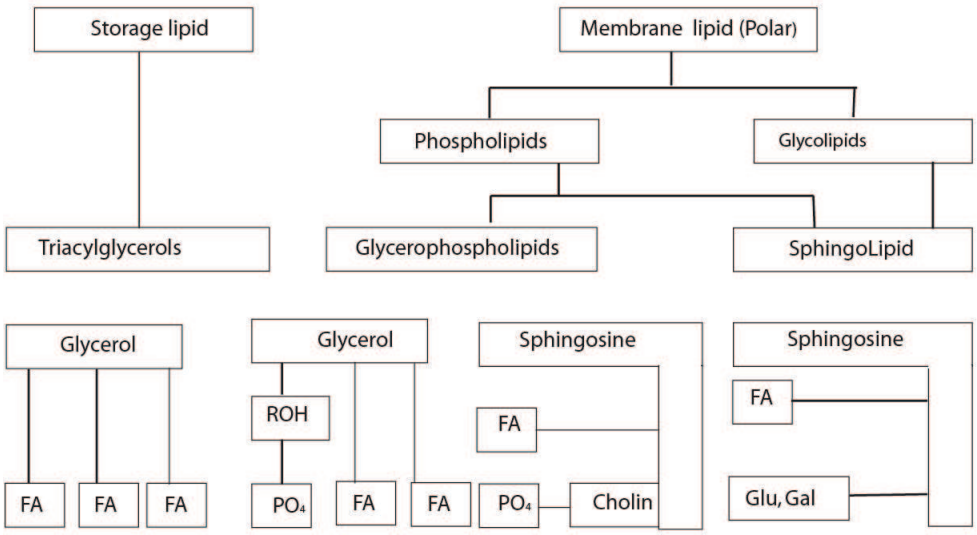

Figure 3.1: Classification of lipid as a basic structural and functional unit of cellular system [14]

3.1.1 Structure of membrane

Lipid : The basic component of biomembrane is a class of molecules called lipid. Lipids are basic building blocks of the membrane of biological cells. There are various types of lipids exist in nature. They can be classified in two categories according to their biological function [14] as represented in fig. 3.1.

(a). Storage lipids: They are non-polar and play functional roles in cells such as energy storage, for example triglycerides, sterols and cholesterols.

(b). Membrane (structural) lipids: They are a major constituent of most

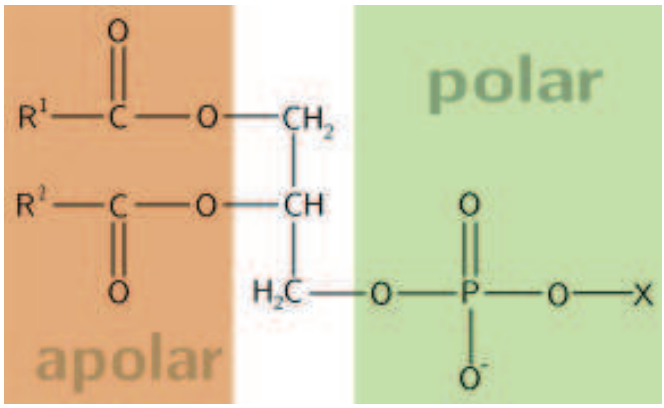

Figure 3.2: A schematic chemical structure of amphiphilic molecule

biological membranes and are polar (phospholipids and glycolipids).

Nature uses a few classes out of an enormous variety of possible lipids for building animal cell membranes. Among these membrane lipids, phospholipids are the ones which ubiquitously exist in all cell membranes. All phospholipids are polar molecules, possess some common structural characteristics which give them an amphiphilic property. The structure of amphiphilic molecules consists in two parts shown in fig. 3.2.

Hydrophilic region : This region of the molecule is polar (favours solubility with aqueous medium). Phosphate head groups are either neutral or negatively charged and may contain other polar groups. In fig 3.2 the backbone is derived from glucose. Its third carbon hydroxyl esterifies (which is represented by 'X'in fig. 3.2) with a phosphate group. Phosphates 'X' head group further esterifies with other groups to produce different phosphate polar heads. Examples of these are mentioned below.

1) Phosphatidylcholine (PC) (X = Choline)

2) Phosphatidylethanolamine (PE) (X = Ethanolamine)

3) Phosphatidylinositol (PI) (X = Inositol)

4) Phosphatidylserine (PS) (X = Serine)

5) Phosphatidylglycerol (PG) (X = Glycerol)

Similarly, another type of membrane lipid which has spingosine-backbone and its Phosphate's 'X' group gives sphingomyelines (SPHM), Cerebrosides and Glycolipids.

Hydrophobic region : This region of the molecule is non-polar hence repels water or any aqueous solution. Hydrophobic tails usually consist of two long fatty acid hydrocarbon chains (R^1 and R^2 as shown fig. 3.2. These fatty acid chain lengths depend on the number of carbon atoms (varying between 16 and 24) and the number of double bonds (ranging from 1 to 6). These two fatty acid chains can have a different length in the same molecule. These chains are either *saturated fatty* acid chain or *unsaturated fatty* chain or both.

Saturated fatty acids have a saturated hydrocarbon chain i.e. no double bond or Kink exists in them. Therefore they are solid at room temperature with higher melting point for e.g. Lauroyl (C 12 :0), Myristoyl (C 14 :0),

Palmitoyl (C 16 :0), Stearoyl (C 18 : 0) and Arachidoyl (C 20 :0).

Unsaturated fatty acids have cis or trans double bond which disrupts intermolecular packing and therefore have a lower melting point (melting point decreases when the number of unsaturated hydrocarbons or double bond increases) for e.g. Palmitoleoyl (C 16 :1) and Oleoyl (C 18 :1). In addition, chain lengths and their unsaturation have an impact on membrane deformation

DOPC (1,2,dioleolyl-sn-glycero-3-phospho choline) is commonly used in experimental studies of vesicle dynamics. Its chemical structure is shown in fig. 3.3. It has a backbone of glycerol and two fatty acid chains a saturated fatty acid chain and an unsaturated fatty acid chain with one double bond.

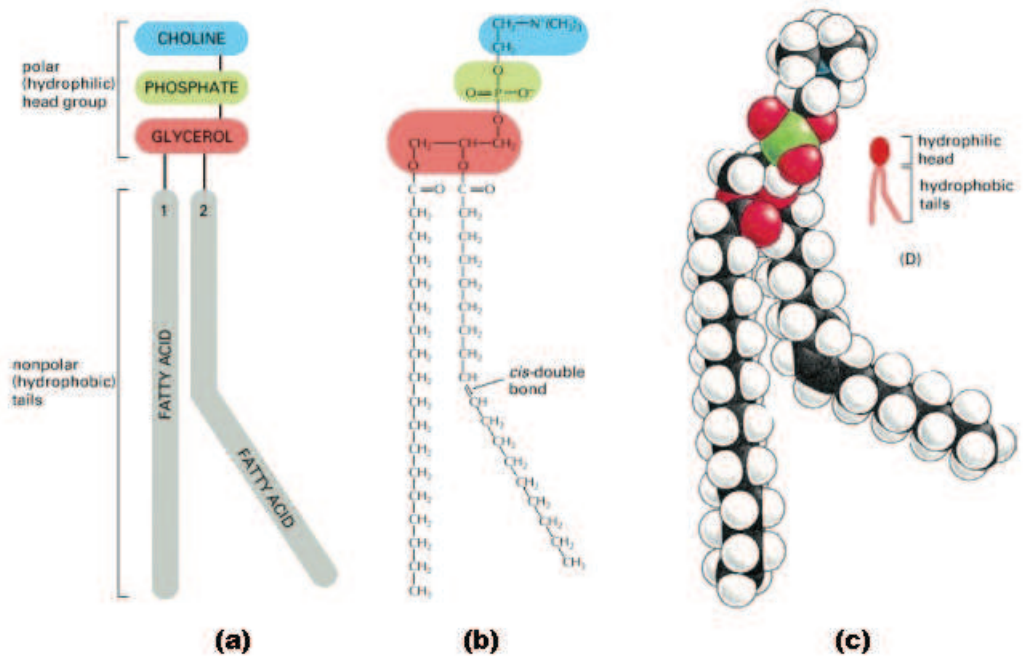

Figure 3.3: Structure of a Phosphatidylcholine, represented (a) schematically; (b) as a chemical formula; (c) as a space-filling model

When these amphiphilic molecules are dispersed in water or other aqueous environment, polar heads face water whereas hydrophobic non-polar tails repelled by water and are forced to aggregate spontaneously. This spontaneous aggregation of hydrophobic tails forms a variety of structures depending on specific properties of the phospholipids. Major varieties of cell membranes have a bilayer structure in nature. Lipid bilayer occurs when hydrophobic

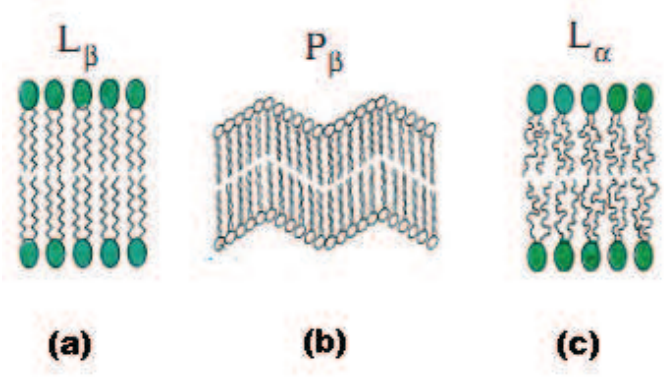

Figure 3.4: (a) Crystalline Phase; (b) Ripple Phase; (c) Liquid-phase

tails line up against one another or in other words two mono-molecular layers are held together by weak non-covalent forces due to the hydrophobic effect. This creates a membrane with hydrophilic heads on both sides facing water. This type of membrane is partially permeable, capable of deformation, and has fluid properties, in which phospholipids molecules are able to move laterally above the gelling temperature of the lipid.

However the structural organization of the lipid bilayer can vary in different liquid or solid phases under the influence of temperature. At low temperature the lipids, which are highly packed in the layers, tend to assemble in a liquid crystal type of conformation which is also called as solid or frozen phase [15]. They have an orientational order fixed by the temperature hence their acyl chains are formed according to surface topology and denoted by L_β or L'_β.

By increasing the temperature, we can evolve from a phase L'_β where the lipids are inclined compared to the bilayer plane to a rippled phase P'_β as shown in fig. 3.4. P'_β phase is commonly observed in lipid molecules having two saturated identical chains, lipid bilayer is then said to be in gel-phase [24]. If the temperature increases above the critical temperature Tc, we can even go from the so-called gel state of the membrane to a phase L_α where the lipids are in a fluid state, all these phases are shown in fig. 3.4. The transition from one phase to another was shown experimentally by Evans and Needham [16] with a micro-pipette aspiration technique, presented in fig. 3.5.

This study reveals, if the system is under stress when going through the transition, that surface area tends to decrease even more dramatically while

the lipids end-up in the P'_β phase. Saturated chains of Phosphatidylcholine exhibit L_β, P'_β and L_α phases. It can be observed from fig. 3.5, that in case of, Dimyristoylphosphatidyl choline (DMPC) is at L'_β solid at equilibrium below $10 - 13°$C, a P'_β solid between $13 - 24°$C and a L_α, liquid surface above 24°C [17][18].

Lipid bilayer structures can be found in most of animal cells in combination with Cholesterols and proteins. Under controlled conditions, some amphiphilic materials are able to produce a type of bilayer structure that enclose a volume of aqueous fluid within a closed shell (see fig. 3.6) with a size similar to animal cells to mimic the mechanical features of natural cells like red blood cells (red blood cells). The resulting bilayers are known as lipid vesicles.

Typical size of the vesicle ranges from the order of 100 nm to the order of 100 μm. Fig. 3.6(b) shows a phase-contrast micrograph of a vesicle.

3.1.2 Mechanical properties of the membrane

When the lipid membrane is subjected to external force, it can be deformed in three independent modes [1] as shown in fig. 3.7. One mode of deformation is *extension* or *compression* (that is by changing its thickness). The second mode is *shear*. The third mode is *bending* by compressing the *innerleaflet* and by extending the *outerleaflet*.

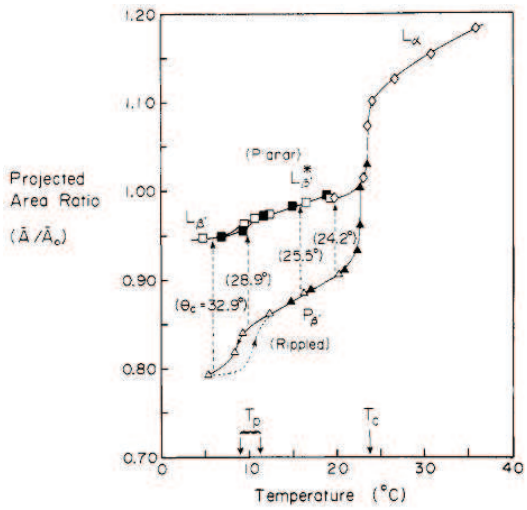

Figure 3.5: Change in Phase of DMPC lipid bilayer with the ratio of temperature and project area

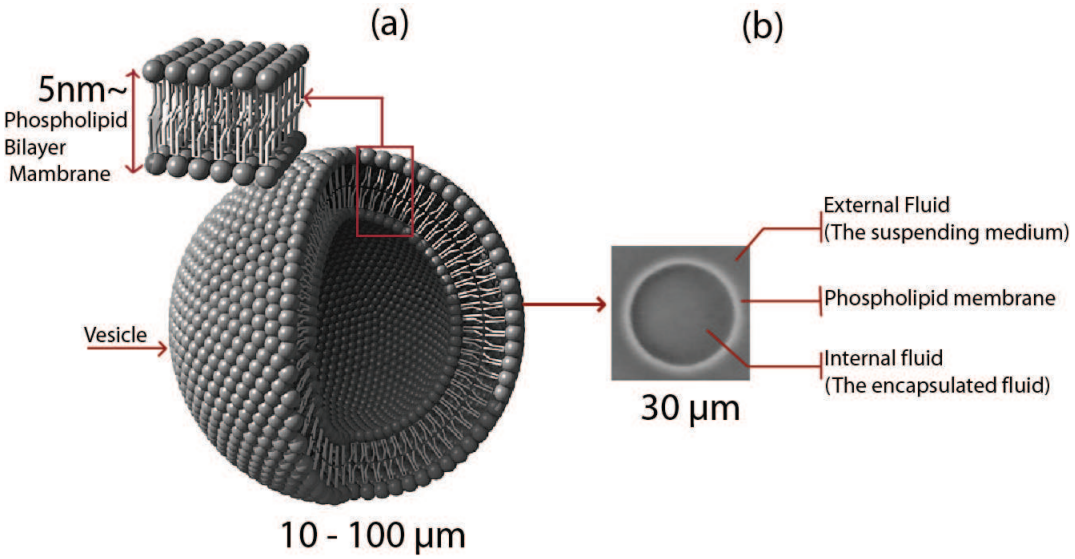

Figure 3.6: (a) Sketch of the arrangement of lipid molecules in a vesicle (b) Phase-contrast image of a vesicle

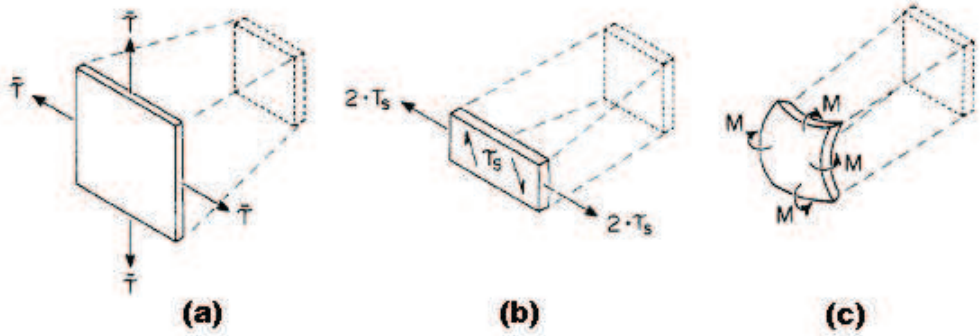

Figure 3.7: Representation of three independent mode of membrane deformation: (a)Extension-compression, (b)Pure shear, (c)Bending

Extension-Compression (*Stretching*)

Extension-compression is the deformation, in which the area per lipid molecule changes. The intermolecular distance between two monolayer in lipid bilayer is about 1nm. The interaction between innerleaflet and outerleaflet molecules is weak. In addition the solubility of phospholipids in water is very low (critical micelle concentration approx $10^{10} mole$) therefore

to balance this energy there can not be any exchange between the bilayer and the external environment. In other words the extension or stretching is a measure of the energy necessary to change a unit area of the membrane and maintain the cohesion between the lipids of the membrane [19]. The extension/compression energy $E_{extension}$ is given by,

$$E_{extension} = \frac{1}{2}\chi\left(\frac{\Delta A}{A_0}\right) \tag{3.1}$$

Where χ is the extensional modulus, A and A_0 being the area before and after deformation ($\Delta A = A - A_0$). A typical value for χ, the stretching modulus, is in the range $100 - 300$ mJ/m^2. Several experimental as well as theoretical evaluation of this energy are presented in table 3.1.

$Phospholipid$	$\chi(10^{-4}mN/m)$	$temp(^\circ C)$
$DAPC$	135 ± 20	18
$DGPG$	160 ± 7	23
$DMPC$	145 ± 10	29
$SOPC$	190 ± 10	18
$SOPC : CHOL$	640 ± 32	15

Table 3.1: Extension modulii of different lipids under temperature [20]

Bending modulus

This deformation represents the curvature elasticity of a membrane. Consider a lipid bilayer deformed according the two principle curvature C_1 and C_2 at constant area, the bending energy per unit area $E_{bending}$ can be written as.

$$E_{bending} = \frac{1}{2}\kappa_c(C_1 + C_2 - C_0) + \frac{1}{2}\kappa_G(C_1C_2) \tag{3.2}$$

where

C_0=Spontaneous curvature of the membrane.

C_1 and C_2=Principle curvatures defined by $C_1 = (\frac{1}{R_1})$; $C_2 = (\frac{1}{R_2})$.

R_1 and R_2 = radii of curvature.

κ_c= Bending modulus.

κ_G= Gaussian bending modulus.

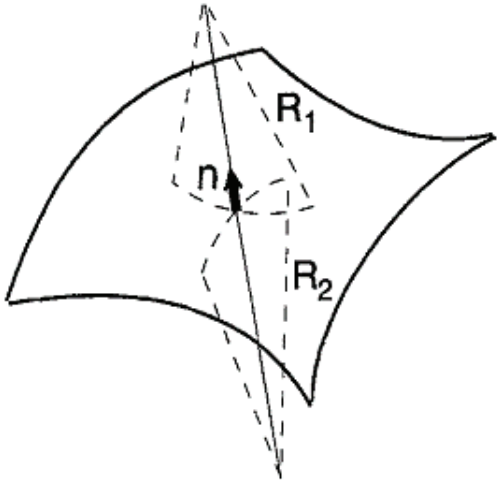

Figure 3.8: Curvature on a 2D surface. The vector $\vec{n}$ denotes the normal vector [5]

In the fluid phase it is a minimization of the energy of curvature that maintains the equilibrium shape of the vesicles. Typical values of phospholipid bilayers are the order of $10^{-19}J$. Typical values of bending modulus are shown in table. 3.2.

Phospholipid	$k_c(10^{-19}J)$	$k_c(k_BT)$	$K(mN/m)$
$diC13:0$	0.56 ± 0.07	14 ± 1.75	239 ± 15
$diC14:0$	0.56 ± 0.06	14 ± 1.5	234 ± 23
$C18:0/1$	0.9 ± 0.06	22.5 ± 1.5	235 ± 15
$diC18:1c9$	0.85 ± 0.1	21.25 ± 2.5	265 ± 18
$diC18:9c9$	1.03 ± 0.11	21.75 ± 2.75	229 ± 12
$diC20:4$	0.44 ± 0.05	11 ± 1.25	250 ± 10

Table 3.2: Bending Modulii of different lipids

Equilibrium shapes of vesicles in a fluid at rest can be computed by minimizing the Helfrich energy by assuming vesicle area A and volume V as constants. This investigation of shape catalogue was proposed by Seifert [21] as shown fig. 3.9. The only parameter controlling the shape of a vesicle, in the absence of an external applied flow, is the reduced volume ([1]).

[1]The important parameter is the volume to area ratio, also called the reduced volume, and defined as $\nu = V/(4\pi/3)R_0^3$ where $R_0 = (V4\pi)^1/2$ is the radius of the sphere with the same surface area as the vesicle of volume V

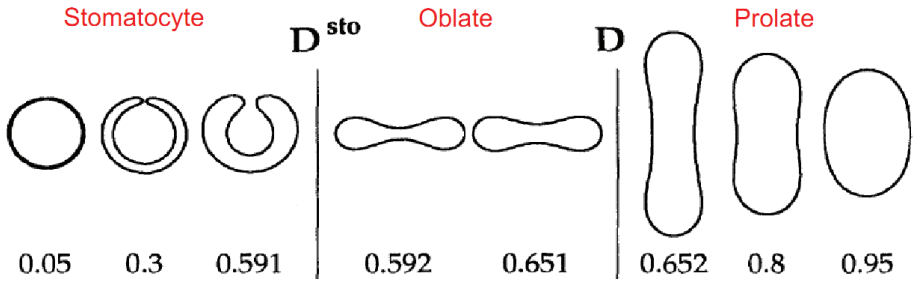

Figure 3.9: Different vesicle equilibrium shapes as a function of its reduced volume

This parameter quantifies the degree of deflation of a vesicle. In fig. 3.9 different vesicle equilibrium shapes as a function of its reduced volume are represented. If we consider a sphere ($\nu = 1$) and deflate it progressively, we first find prolate shapes, which are elongated around the rotation axis, which is vertical in the figure (cigar-like shapes). If we de-swell below $\nu \approx 0.65$, the equilibrium shape is oblate, or discocyte. This kind of shape is the biconcave one assumed by red blood cells. Below $\nu \approx 0.59$ there is a transition towards stomatocytes, the vesicle folds on itself and forms a inside budded shape.

Shear modulus

Lipid bilayers in a fluid state have a zero shear modulus by definition. However, Lipid bilayers that are in crystal phase or gel phase exhibit a limited elastic response followed by surface flow. An experiment on DMPC L'_β phase shows shear modulus of membrane is equal to 10^{-13} N m^{-1} [22].

Viscosity

Lipid bilayer membranes are in liquid phase have a shear viscosity of order 10^{-3} to 10^{-2} Pa.s as reported in the literature [23, 24].

Permeability

Lipid bilayers are semi-permeable. Their chemical and structural limitations allow only a few specific classes of molecules to pass through it. The permeability of membranes to molecules depends on their charge and polarity. Since bilayers form by aggregation of hydrophobic tails, they act as a barrier to most of the substances that are dissolved in water. Permeability of the membranes to polar molecules is very low and particularly very low for large

size polar molecules such as glucose and sucrose. Membranes are highly impermeable to ions and permeable to lipid-soluble molecules like gas molecules such as oxygen (O_2) and carbon dioxide (CO_2). However they are permeable to some polar molecules which are very small and also lipid soluble such as water (H_2O), glycerol ($C_3H_5OH_3$), and ethanol (C_2H_6O).

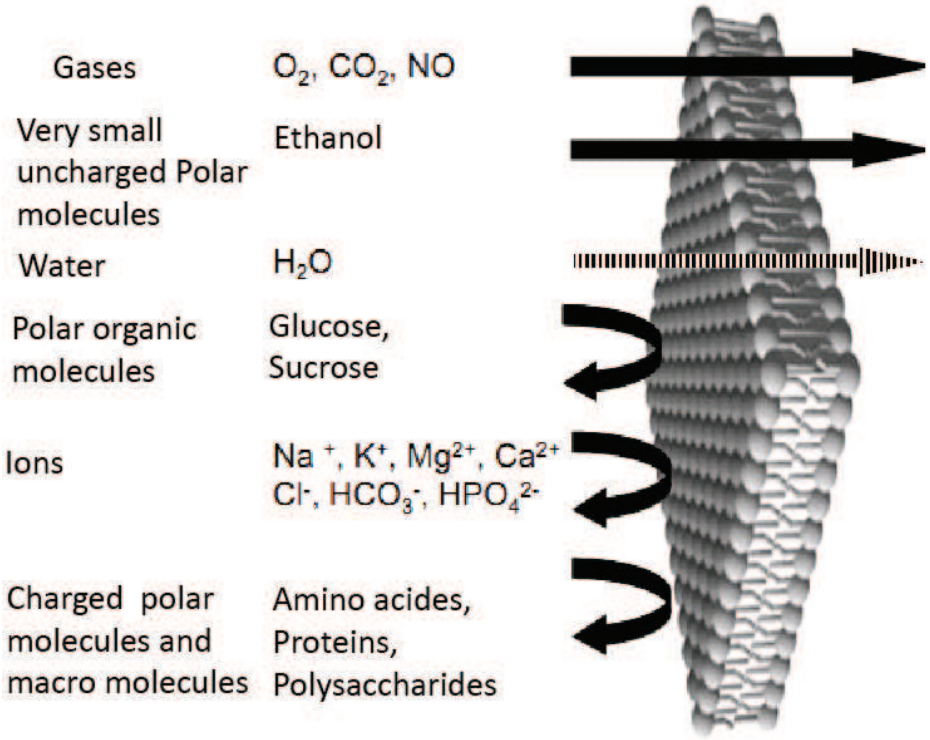

Figure 3.10: Permeability of lipid bilayer membrane

Typical values of lipid bilayer membrane of water permeability are reported between 3×10^{-3} to $27 \times 10^{-3} cm.\sec^{-1}$ in experiments depending on the type of lipid [25], [26].

Tension

If we consider that membrane surface area is non-spherical and at rest. We can define the membrane tension σ mathematically by

$$\sigma = \Delta P \left(\frac{R_1 \times R_2}{R_2 + R_1} \right) \tag{3.3}$$

Where ΔP is the pressure difference between inside and outside of vesicle. R_1 and R_2, are the two local radii of curvature. Experimentally the lysis tension can be measured. Lysis tension is the critical tension at which the membrane ruptures. Membrane tension has been measured by micro pipette aspiration experiment [20] which correspond to maximum extension of surface area before the rupture of envelop. Some quantitative values are represented in table. 3.3.

Phospholipid	σ	*Ref*
$DOPC$	$3mN.m^{-1}$	[25]
$DMPC$	$2-15mN.m^{-1}$	[19]
$DLPC$	$24mN.m^{-1}$	[19]

Table 3.3: Lysis tension of membrane in different lipid

Osmotic Pressure

Osmosis is defined as the movement of water molecules from a region of low solute concentration to a region of higher solute concentration. This concentration difference between interior and exterior of vesicle creates an osmotic pressure π on the membrane.

$$\pi = RTln(C_{in} - C_{out}) \tag{3.4}$$

Where C_{in} and C_{out} are the concentrations of solute inside and outside of membrane. R is the universal gas constant and T is the absolute temperature. Thus osmosis is influenced by the membrane permeability of the vesicle allows the tunability of the vesicle's volume at a constant total surface area, allowing us to deflate it and to obtain various shapes and more deformable objects.

3.2 Red Blood Cell

3.2.1 Blood composition

Blood is a non-homogeneous material formed mainly by a plasma and cells. Whole blood (plasma and cells) exhibits non-Newtonian, viscoelastic fluid properties. Due to its specific flow properties, it can pass through tiny

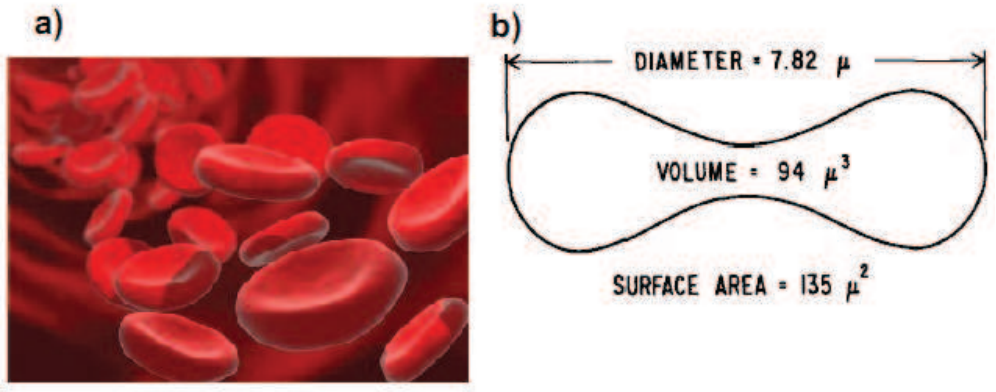

Figure 3.11: a) Healthy red blood cells with its usual discocyte shape [3]. b) Typical dimensions of a healthy red blood cell

capillary blood vessels with a reduced effective viscosity. The average density of whole blood is approximately 1060 kg/m^3. Blood pH is regulated to stay within the narrow range of 6.8 to 7.45 and osmolality of blood is 275295 milliosmoles/kg. The two main components of whole blood and their properties are as following:

(1) **Plasma**: Whole blood contains 54.3% volume of plasma. It is extracellular fluid in which the blood cells are suspended. It consists of 90% water, 8% protein (albumin, globulin, fibrinogen), 0.9% inorganic salts and 1.1% organic salts. Plasma helps to maintain an ideal balance of electrolytes in the blood and tissues of the body and works as transport medium for the cells to carry nourishing and waist elements.

(2) **Cells**: Cellular components of blood consists in 45% volume of erythrocytes (red blood cells) and 1% in volume of leucocytes (white blood cells) and thrombocytes (blood platelets). Red blood cells transport oxygen via haemoglobin components in whole body. White blood cells are part of the immune system. Platelets are cells without nuclei that play a role in blood clotting . They do this by adhering to the walls of blood vessels or by releasing coagulating substances which promote the formation of clots.

3.2.2 Structure and composition of a red blood cell

The shape of a red blood cell is a biconcave disc as shown in fig. 3.11. A red blood cell measures about 6 to 8 micrometers in diameter (average = 7.8 μm) with an average thickness of 2 micrometers (2.5 μm) at the thickest point and less than 1 μm at the center. Although a red blood cell is wider than some capillaries, its flexibility allows it to become distorted as it squeezes through narrow passages and then restores to its original shape. red blood cell can squeeze to pass through a small capillary of diameter 5 μm. In contrast with other living cells, red blood cells do not have a nucleus and organelles and contains a hemoglobin solution. Except external shape and size it possesses some important structural complexities which separate it from other living cells.

3.2.3 Mechanical properties of the red blood cell

A red blood cell consists of a closed membrane enclosing a Newtonian fluid (haemoglobin solution) and it is suspended in blood plasma. Its membrane is composed of three components with the following fractions : 52% of protein (about 100 types of protein), 40% of lipid and 8% of cholesterol. Its lipid bilayer is composed of four types of lipids which are asymmetrically distributed in the membrane. The choline lipids which are uncharged phospholipids are mostly in the outer leaflet of the membrane mainly 30% of phosphatidylcholine (PC) and 25% of sphingomyelin (SM) whereas phosphatidylethanolamine (PE) in (28%) and phosphatidylserine (PS) (14%) which are negatively charge are mainly localized on the inner leaflet [27]. A two-dimensional cytoskeleton network (10nm thick) is attached to the membrane as shown in fig. 3.12(b).

This peripheral protein is referred as cytoskeleton and is composed of three principal components: Spectrin, Actin and protein 4.1. Spectrin is arranged with its six molecules in hexagonal form (fig. 3.12). For the membrane to deform normally, the spectrin network must be able to undergo a conformational rearrangement in which spectrin molecules fold and unfold. Spectrin network is attached to the lipid bilayer by the Ankyrin molecules. Any defect in cohesion between the cytoskeleton and lipid bilayer leads to deformability defects in red blood cell. Without lipid bilayer the cytoskeleton has an area expansion modulus of 9.0 $\pm 3.6 \mu N/m$ and shear modulus (μc) equal to 5.5 $\pm 2.1 \mu N/m$ [28]. red blood cell exhibits a strong shape memory and tends to relax back to its initial shape [29].

As described for phospholipid bilayer in 3.1.2, red blood cell membrane

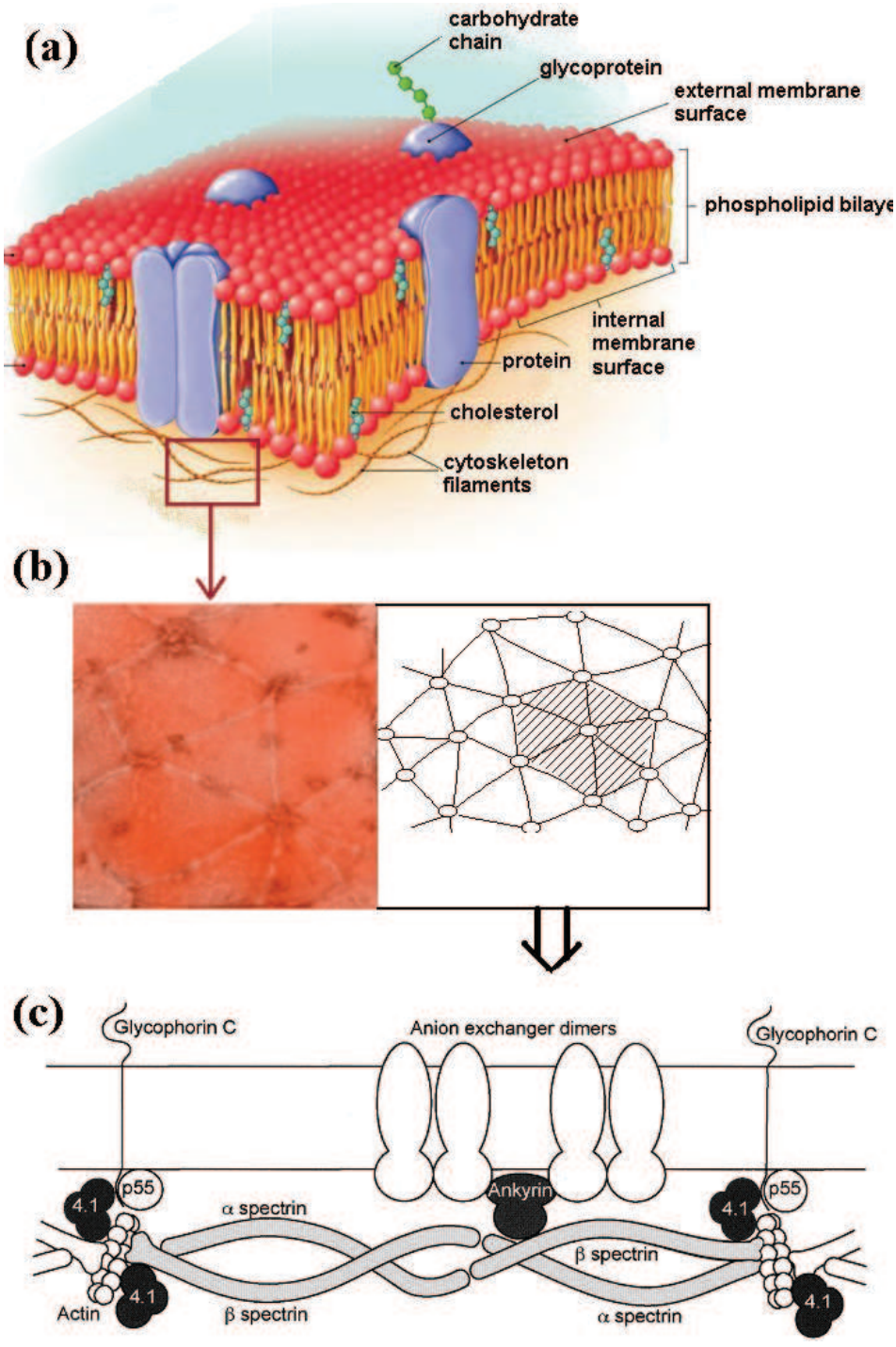

Figure 3.12: (a)Schematic cross-section of red blood cell membrane with cytoskeleton network at the inner layer of membrane (b)snapshot of cytoskeleton (c) structure of spectrin

also exhibits deformations in three independent modes. A "shear" of the membrane without either increasing the surface area or bending at room temperature, $\mu = 6 - 9 \times 10^{-3} mN/m$ [30]. A dilation (isotropic expansion) of the membrane surface without either shearing or bending it, results in area expansion with a modulus K = 450 mN/m at room temperature with a standard deviation of about $\pm 15 - 20\%$ [31]. Erythrocyte's membrane shows bending deformation of order $10^{-19} mN/m$ [30].

An experimental evidence has shown viscoelasticity (η) of red blood cells of the order of $10^{-3} mNs/m$ [32]. The membrane of erythrocytes shows high permeability to water [33] and small molecules [34] similarly lipid bilayers.

3.3 Parameter under study

In the context of the study of hydrodynamic properties of vesicles and red blood cells, few dimensionless parameters are commonly used in many theoretical and experimental studies. These parameters are presented below:

1)**Viscosity contrast, (λ)**:
The viscosity contrast is the ratio between the internal viscosity (η_{in}) and the external viscosity (η_{out}) :

$$\lambda = \frac{\eta_{in}}{\eta_{out}} \tag{3.5}$$

2)**Capillary number**, (Ca):

$$Ca = \frac{\tau_{shape}}{\tau_{flow}} = \frac{\eta_{ext} R_0^3}{\kappa} \dot{\gamma} \tag{3.6}$$

The capillary number, is defined as the ratio between two characteristic time scales, the shearing time, $\tau_{flow} = 1/\dot{\gamma}$, where $\dot{\gamma}$ is the shear rate, and the typical time needed for a vesicle to reach its equilibrium shape after cessation of the flow, $\tau_{shape} = \eta_{ext} R_0^3/\kappa$ where κ is the membrane bending rigidity. Typical values from experimental investigations of vesicles lie roughly in the range of Ca$\sim 1 - 10^3$.

3)**Excess area**, (Δ):

$$\Delta = \frac{A - 4\pi R_0^2}{R_0^2} \tag{3.7}$$

where A is the vesicle area and R_0 is the radius of a sphere having the same volume as the vesicle. $\Delta = 0$ for a sphere, and $\Delta > 0$ for deflated envelopes like human red blood cells, where $\Delta = 5$. The deflation of a vesicle can also be characterized by the reduced volume, ν:

$$\nu = \frac{\text{Volume}}{\text{Volume of sphere of same surface}} = \frac{3V}{4\pi R_0^3} \leq 1 \qquad (3.8)$$

where

$$R_0 = \sqrt{\text{A}/4\pi} \qquad (3.9)$$

The relation between reduced volume (ν) and excess area (Δ) is

$$\Delta = 4\pi(\nu^{-2/3} - 1) \qquad (3.10)$$

For a two-dimensional vesicle (a model often used in theoretical works) the reduced volume is defined as the ratio of the area of the vesicle A to the area of a circle having the same perimeter P as the vesicle:

$$\tau_{2D} = \frac{4\pi A}{P^2} \qquad (3.11)$$

4)**Reynolds number**, (R_e):

This dimensionless number represents the relative importance of inertial and viscous effects in flow, and is defined as:

$$R_e = \frac{\rho L \upsilon}{\eta}$$

where ρ and η are the density and the viscosity of the fluid in motion, respectively, L is the characteristic length of the system and υ the speed of the object. In most situations that are involve in flow at moderate velocities and small scales, the Reynold number is low ($(10^{-5} - 10^{-3})$).

3.4 Visualization of vesicles and red blood cell

Since the objects that we are studying are micron-size (from 5 to 200 μm in diameter), the observations during our experiments require the use of a microscope. We used an inverted basic microscope model IX71/IX51. Several techniques have been used preferentially to fit with the observational needs with the used of bright-field and phase contrast microscopy which are briefly described in this section.

3.4.1 The bright-field microscopy

With a conventional bright-field microscope, light from an incandescence source is directed towards the condenser and passes through the specimen. This light waves project on an object lens, and to the eye through the binocular. Objects are visible only when difference in absorption occurs.

Phase relationships between the surround, diffracted, and particle (S, D, and P) waves in the region of the specimen at the image plane for bright-field microscopy (in the absence of phase contrast optical accessories) are presented in fig. 3.13. The surround and particle waves, whose relative amplitudes determine the amount of specimen contrast, are illustrated as red and green lines (respectively). The wave produced by diffraction from the specimen, which is never directly observed, is depicted as a blue wave of lower amplitude. The surround and diffracted waves recombine through interference to generate the resultant particle wave in the image plane of the microscope. The amplitude of each wave illustrated in fig. 3.13 represents the sum of the electric vectors of the individual component waves.

Relative to the surround wave, the diffracted wave has lower amplitude (because there are fewer diffracted than surround photons at the image point) and is retarded in phase by approximately 90 degrees (a quarter wavelength) through interaction with the specimen. The slight phase shift of 1/20th wavelength exhibited by the resultant particle wave (which arises from interference between the diffracted and surround waves) is typically observed for minute details in a cell, and is related to the optical path length difference. Because the amplitudes of the surround and particle waves are nearly the same, the transparent specimen completely lacks contrast and is almost invisible when superimposed against the bright background.Therefore we need contrast enhancing accessories which is coupled in phase contrast system described in sec. 3.4.2. Different appearance of a cell specimen under two system i.e.

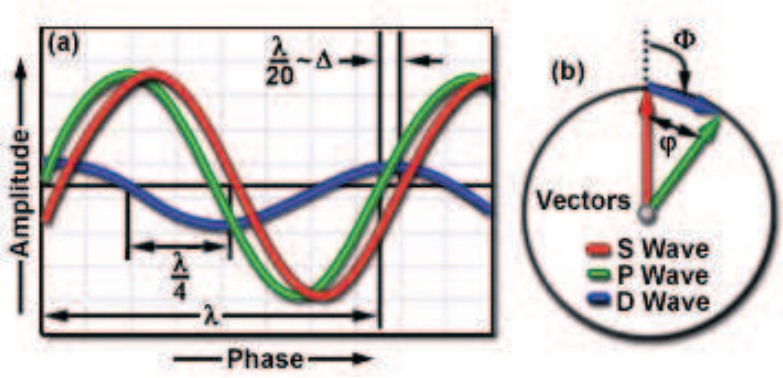

Figure 3.13: Bright field microscope wave phase relationships

bright field and phase contrast is shown in fig. 3.14.

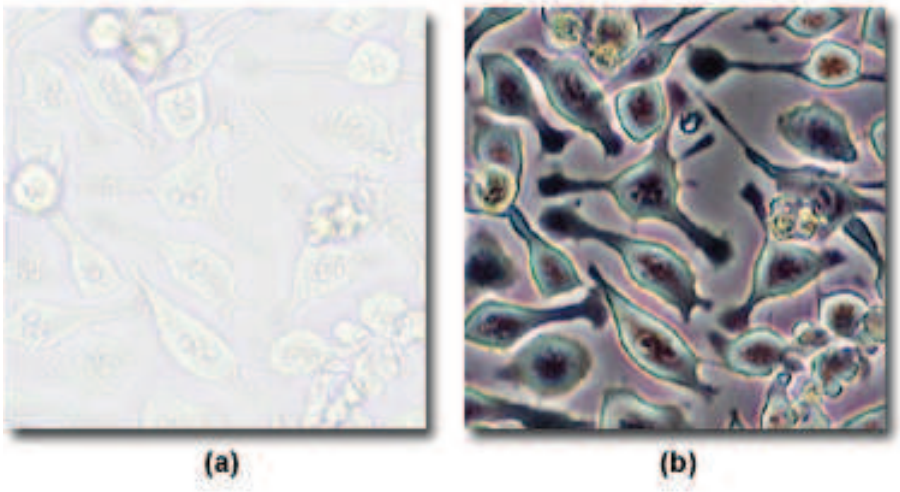

Figure 3.14: Cell specimen in (a)Bright field (b)Phase contrast

3.4.2 Phase contrast microscopy

Phase contrast is contrast-enhancing optical techniques that can be utilized to produce high contrast images of transparent specimens, such as living cells, micro-organisms, thin tissue slices, lithographic patterns, fibres, latex dispersions, glass fragments, and sub cellular particles. Generally, red blood cells are easy to observe in classic transmission microscopy but the study of

vesicle requires the use of phase-contrast microscopy. In effect, the phase contrast technique employs an optical mechanism to translate minute variations in phase into corresponding changes in amplitude, which can be visualized as differences in image contrast.

Principle

An incident wavefront present in an illuminating beam of light gets divided into two components of light waves while passing through a phase specimen. The primary component is an undeviated (or undiffracted; zeroth-order) planar wavefront, commonly referred to as the surround (S)wave, which passes through and around the specimen, but does not interact with it. In addition, second component of wave front deviates or gets diffracted (D) and spherical wavefront produced,These become scattered over a wide arc that passes through the full aperture of the objective. After leaving the specimen plane, surround and diffracted light waves enter the objective front lens element and are subsequently focused at the intermediate image plane where they combine through interference to produce a resultant particle wave referred as a P-wave. The mathematical relationship between the various light waves generated in phase contrast microscopy can be described as:

$$\boldsymbol{P} = \boldsymbol{S} + \boldsymbol{D} \tag{3.12}$$

Detection of the specimen image depends on the relative intensity differences, and therefore on the amplitudes, of the particle and surround (P and S) waves.

Moreover, the intensity of diffracted light altered by the thickness of the specimen through which it passed, therefore if we want to be more precise the argument can be develop as the optical path length (OPL) through an object or space is the product of the refractive index (n) and the thickness (t) of the object or intervening medium as described by [35]:

$$\text{With Optical Path Length}(OPL) = \boldsymbol{n} \times \boldsymbol{t} \tag{3.13}$$

The principle of the phase contrast microscopy is shown in fig. 3.15. Only two specialized accessories are required to convert a brightfield microscope for phase contrast observation. A specially designed annular diaphragm, which is matched in diameter and optically conjugates to an internal phase plate residing in the objective rear focal plane, is placed in the condenser front focal plane which produces a cone of light. This cone is superimposed on a

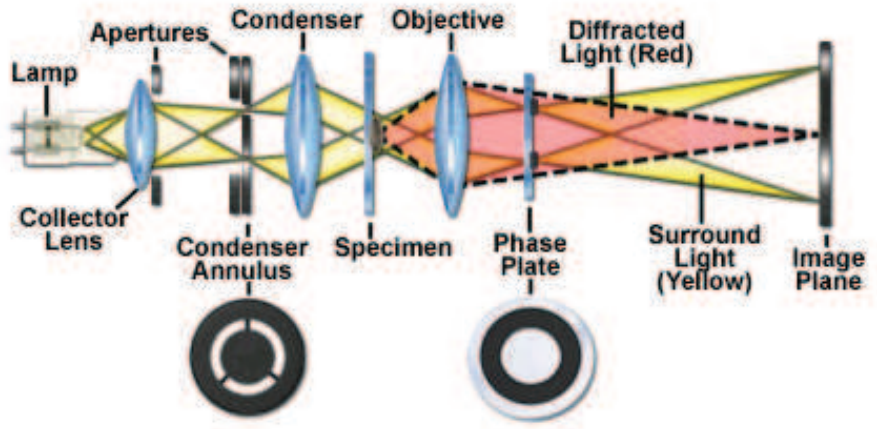

Figure 3.15: Phase Contrast Microscope optical Train

similar sized ring within the objective. The ring in the objective has special optical properties: first of all, it reduces the direct light in intensity, but more importantly, it creates an artificial phase difference of about 1/4 wavelength. As the physical properties of this direct light have changed, interference with the diffracted light occurs, resulting in the phase contrasted image, can see in fig. 3.14.

3.4.3 Camera

In order to make quantitative measurements, all the experiments are recorded with cameras. Two types of cameras, a CCD camera and a high-speed camera have been used depending on the speed of the phenomenon. Once recorded and digitized all the images are analysed using different analysis software. We will describe here the most commonly used cameras.

CCD camera

For relatively slow motion (deflation of vesicles, sedimentation, shear near a plane...), a simple CCD camera (Imaging Source DMK31AF03.AS) has been used. It has good resolution of 1024×768 pixels allows us to capture movie at rate of $30 fps$. The camera has fast refresh rate and minimal noise. The camera is controlled and images are acquired via the IC Capturer software.

High-speed camera

When using microfluidic devices, the objects flow at typical velocities of the order of magnitude of a centimeter per second. The observation of such fast motion requires the use of a high-speed camera. We have used Phantom cameras capable of recording with frame rates up to 10000 fps.

3.4.4 Image analysis

Most of the experimental images require image processing and analysis. The two software were used, **Image J**, a free software developed by NIH registered and a commercial software and **IDL**. With the help of ImageJ we can edit, analyse, process and print up to 32bit images. It can read many graphical formats and convert them in another format if needed. It supports "stack", a series of images that shares a single window and multithreaded, hence time consuming operations can be performed in parallel. IDL is scientific programming language used for data analysis. By programming IDL we can analyse several parameters such as speed of particle, their volume, typical dimensions like radius and axis in case of deformed objects, orientation of cells or deflation of an object.

3.5 Experimental Techniques

The size of our object is a few microns hence to study their dynamics in confined situation we need microchannel with the dimensions of the order of few micron. The system must have some flexibility similar human arteries and veins, reliable and economical too. Therefore we used microfludic devices. A brief introduction about microfludic devices and their manufacturing process is described in the following section.

3.5.1 Microfluidics

Microfluidics are component system of micro to nano scale which allows to manipulate gases, liquid and cells in flow. The system should be capable of manipulating suspensions within cross sectional dimension of order $10 - 100\ \mu$m. Their advantages are manifold: the volumes of fluids within microfluidic channels are generally in the nano-liter to micro-liter in range, fabrication is inexpensive and allows to miniaturize multiplexed devices. Recently, there has been advancement in microfluidic technology which enables to fabricate highly integrated devices that can perform several different func-

tions on the same substrate chip [36, 37].

Fabrication of microfluidics devices

To fabricate a microfluidic device we need a material which must be easy to fabricate, optically transparent and allow an easy control of the flow. To meet these requirements, we use a reticulated polymer named PDMS (Polydimethylsiloxane). The fabrication of microfluidic devices in (Polydimethylsiloxane) PDMS is based on the techniques of soft lithography, and replica molding [38].

PDMS is cheaper than silicon, it is more flexible and it bonds more easily to other material than silicon or glass do. PDMS conforms to the surface of the substrate over a large area and can adjust to surfaces that are non planar, waterproof and permeable to gases. The surface properties of PDMS can easily be changed by exposure of the surface in oxygen plasma. This way PDMS can bond to other materials that have a wide range of free energies.

However, before making a PDMS channel by soft lithography we must first create a master. The master is used to cast the PDMS stamp mold and it is often fabricated with photolithography. To create a master the pattern is drawn with a CAD software. The pattern is then printed on a transparent sheet with a high resolution printer (sufficient to produce structures between 10 and 200 μm) or engraved in a chrome mask (for a better resolution below 10 μm) produced by suppliers of photomasks for contact photolithography.

The first step of soft lithography consists in spin-coating photoresist SU-8 with a homogeneous thickness on a silicon wafer. The speed of the spin-coater sets the homogeneous thickness of this layer of photoresist, controlling the height of the channels. Then, we pre-bake the wafer for several minutes at 65°C and 95°C (the exact time depends on the type of photoresist and the desired thickness) in order to initiate the polymerization of the SU-8. A UV source is used to expose the silicon wafer which is covered with the photomask. Another baking step finishes to cure the photoresist (polymerization of the exposed area). Dissolving away the unilluminated - and so unpolymerized - photoresist leaves a positive relief that serves as a master. The developed pattern can be used as a mold to create the PDMS microfluidic chip.

The PDMS channels are formed by replica molding (ridges on the master appear as valleys in the replica). We mix a solution of silicone elastomer with

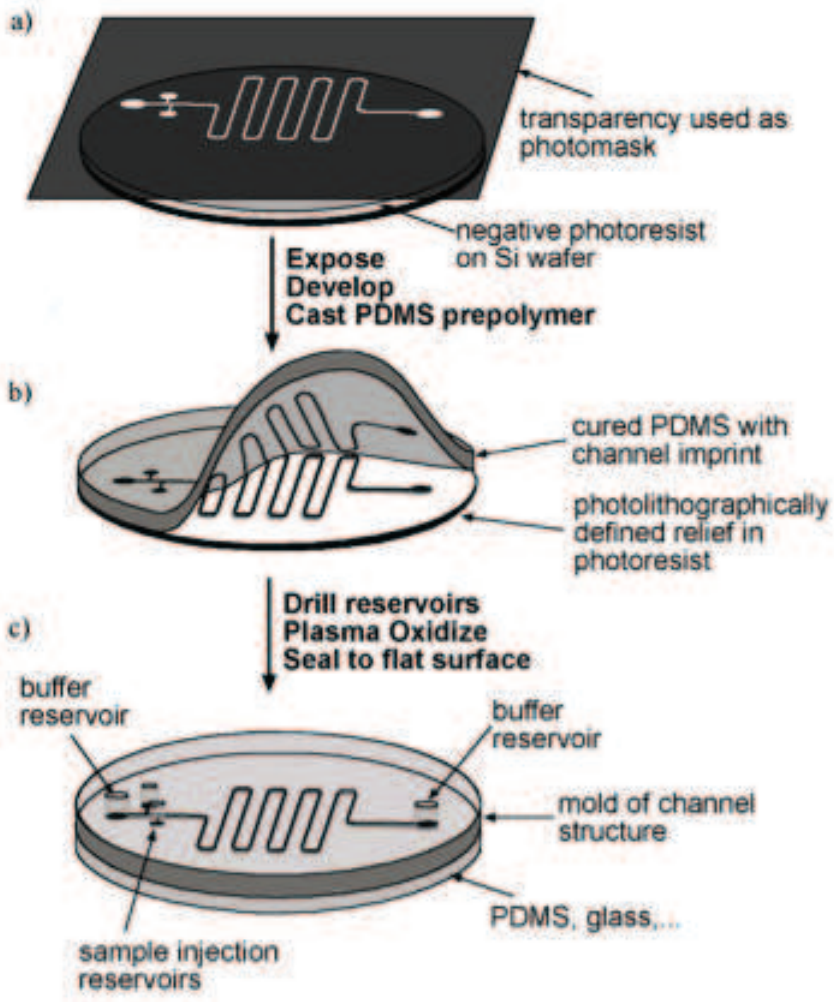

Figure 3.16: Fabrication steps of a PDMS microfluidic device

a curing agent (Sylgard 184 kit silicone elastomer, Dow Corning) in a ratio 9/1 and homogenize the mixture. After pouring the solution into a petri dish over the master, we degas under a vacuum in order to get rid of any bubbles. The whole preparation is cured in an oven at 65°C for 1 hour. The replica is then peeled from the master and access holes for the channels are punched out of the cured layer by using a truncated needle.

The PDMS device can be sealed to a cover glass or to another blank piece of PDMS. To do so, the surfaces of the two units (PDMS and PDMS/glass) are activated by a plasma treatment during 90 seconds in a plasma cleaner (Plasma cleaner PDC-32G, Harrick plasma). Immediately after the treatment, the two pieces are put in contact to let them stick together. The

device is then stored at 65°C over night to allow the strengthening of bonding between the two blocks. [2]

[2]Note:In the case of a PDMS/PDMS device, the preparation of the PDMS is made with an excess space of the curating agent (ratio 5/1) to allow the crosslinking to take place between the two blocks of PDMS.

Chapter 4

Preparation and sorting method of vesicles

Ce chapitre présente notre méthodologie expérimentale pour produire des vésicules. Du fait que l'électroformation produit des échantillons polydisperses, un dispositif dédié au tri de vésicules en fonction de leur taille a été développé pour les études où la monodispersité est requise. Finalement, les performances du dispositif de tri sont caractérisées.

This chapter presents our experimental methodology for producing vesicles. Since electroformation produces polydisperse samples, a device dedicated to the sorting of vesicles according to their size has been developed for studies where monodispersity are required. Finally, the performance of sorting device is characterized.

4.1 Preparation method of vesicles

Since vesicles have many uses, from the modelling of bio-membrane to drug delivery, and other industrial applications, many methods have been developed to produce vesicles with sizes ranging from 30nm to 100μm. According to their size and structure vesicles are classified in the following way:

Multilamellar vesicles (MLV): These vesicles have several layers of lipid bilayers. They have a low trapped volume and unequal distribution of

solutes.

Unilamellar vesicles, with a single lipid bilayer, among which :

Small Unilamellar vesicle (SUV): Typical diameters are within the range 30 to 100nm. They can get by Sonication or Extrusion [39] of aqueous dispersions. Since their diameter is very small, these structures are not appropriate to model cell membrane.

Large Unilamellar vesicle (LUV): Their diameter ranges from 100nm to 1μm. There are two methods to obtain LUVs vesicles. One is Extrusion which was developed by Szoka et al [39] using the method of reverse phase evaporation. Another technique of preparing LUVs is lipid film hydration with liposome breaking in fusion followed by freeze-and-thraw cycle in order to obtain unilamellar structure [39][40].

Giant Unilamellar vesicle (GUV): Their typical diameter ranges from 1 to 100 μm. These GUVs are in the same range of size as biological cells. They are easier to visualize and allow us to play with internal and external solvent concentrations therefore we choose GUVs as model to study hydrodynamic properties of biological membrane. There are two conventional methods to produce GUVs.

The first method is *spontaneous swelling* by gentle hydration introduced by Reeves and Dowben [41]. In this method lipids are hydrated by deionised water and kept for many hours or even days for automatic swelling of dried lipid and form GUVs. In this method GUV size is not larger than 10μm and their suspension is not stable. In addition it produces also negligible amount of multilamellar vesicles. Thus it is not reliable to get the expected range of size and stability.

The second method is the formation of vesicles under an electric field or *electroformation*. This method was introduced by M.I. Angelova [42] and further improved to take into account surface effects under electric fields [43]. We have followed this method of electroformation which is more reliable and produces vesicles of size range $1-100\mu$m in large quantities. Vesicles obtained with this method are of reasonably good size to visualize and allows to vary the concentration of the aqueous internal as well as external medium. The different steps in producing vesicles is briefly described here.

4.1.1 Lipid Solutions

In the preparation of vesicle we have used the following lipids:

DOPC: It is 1, 2-dioleoyl-1-sn-glycerol-3-phosphocholine. This lipid is synthetic ($> 99\%$) and zwitterionic. The schematic molecular diagram is shown in fig. 3.3.

DMPC: Its chemical name is 1, 2-Dimyristoyl-sn-Glycero-3-Phosphocholine. This lipid is neutral. It has two saturated hydrocarbon chains thus melting point is 23°C at gel phase.

Lipids are dissolved in a mixture of chloroform and methanol in $(9 : 1)$ proportion and preserved at temperature of -20°C. Preserved lipid solution can be use for several months.

4.1.2 Electroformation chamber

For production of vesicle we have used electroformation chambers, developed and assembled in our laboratory. This electroformation chamber is easy to manipulate, use and wash after each electroformation. The chamber is composed of two rectangular plastic frames. On each plastic frame an ITO (Indium Tin Oxide) coated glass slide of size 5cm $\times$ 7cm is fixed. The ITO coated glass has high electrical conductivity with excellent transparency. The surface resistance of ITO ranges from 8 to 100 ohm/sqr with an optical transmittance over 85%, which allows us to follow the electroformation process under a microscope during formation.

Before performing the deposition of lipids these ITO glasses are washed with detergent and then rinsed with acetone. After acetone they are rinsed well with deionize water and dried with clean paper and then kept in an oven at 40°C to make sure that chambers are completely dry. These ITO glasses are needed to be changed in case they break otherwise, they can be used for several electroformations.

For making an electric contact between the frames in formation of vesicles, each plastic frame has an blade connector (see figure 4.1). The plastic frame has six holes which are helpful to add it with other frame. The space between two frames is $\approx 0.5mm$. In addition, near each aluminium strip there is one inlet connected with plastic bolt which is used for filling or extracting aqueous solution from the gap. The complete description of the

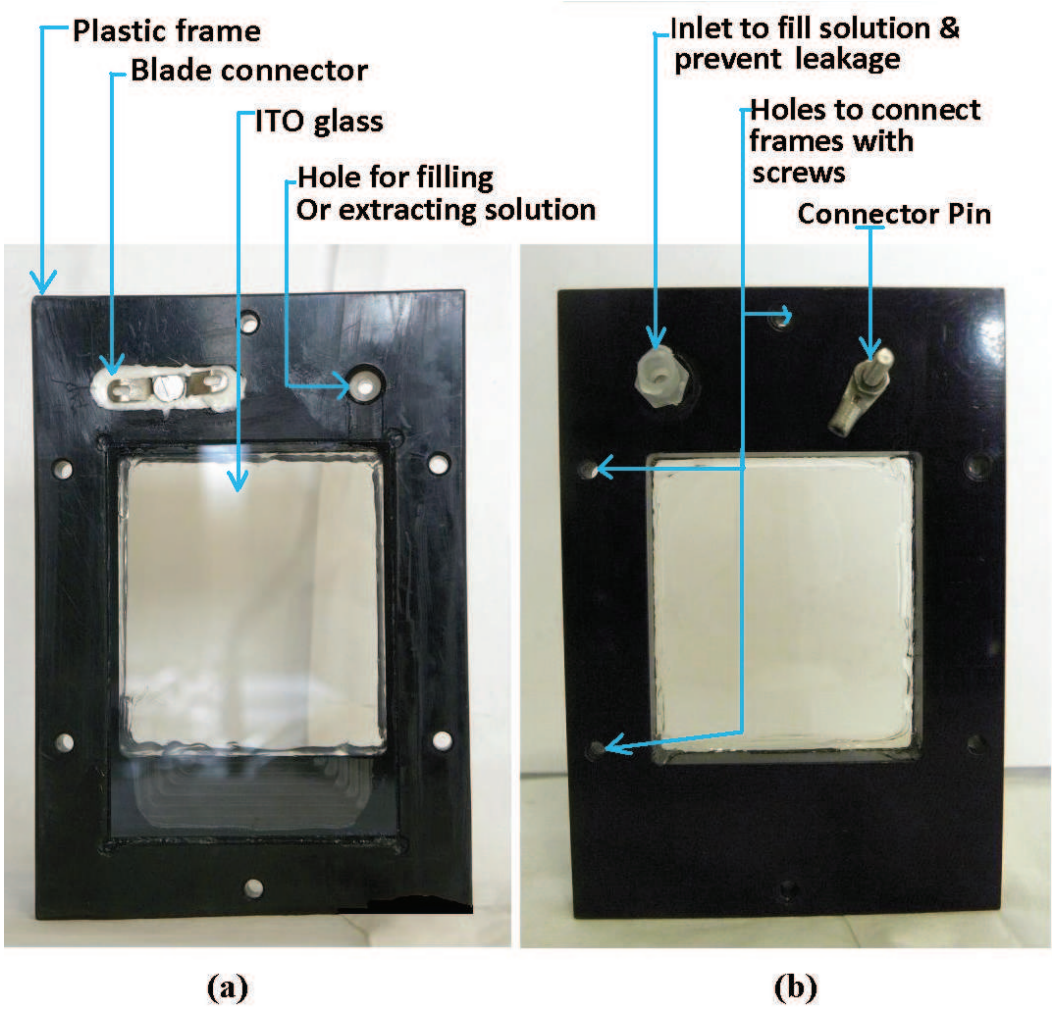

Figure 4.1: Frames of electroformation chamber (a) internal side of frame (b) external side of frame

chamber is shown in fig. 4.1.

4.1.3 Deposition of lipids & filling of chambers

The lipid solution is brought at room temperature before opening the bottle to avoid condensation of water vapour, during the deposition on glass. Approximately 100μl of lipid is deposited with a syringe on ITO glass with the help of a metallic needle. The lipid solution is spread in big zigzags to make sure all the surface of glass is more or less homogeneously covered with lipids. Then two frames of chamber are attached with each other with screws and kept for half an hour under vacuum in order to evaporate the solvent

Figure 4.2: Complete chamber when formation of vesicles takes place

completely.

After deposition of lipids and evaporation of the solvent, the lipid is hydrated by an aqueous solution. In our case we hydrate lipids with sucrose solutions in order to easily generate osmotic pressure in the GUVs by controlling internal and external solute concentrations. The hydrating solution is filled through inlet in the frame (as shown in fig. 4.1). There are two inlets in the electroformation chamber, opposite to each other to fill the hydrating solution. After filling the gap between frames by hydrating solution, these inlets are closed with the help of clamps to prevent leakage. After the end of electroformation, the vesicles samples are extracted from the same inlets with a syringe.

4.1.4 Electroformation

Once the chambers is filled with internal solution, electroformation can be launched by applying tension of few tenths of volt with frequency $\approx$ 10Hz for few hours. The optimal protocol depends on the viscosity of encapsulating fluid. We can change the tension and frequency within a certain range to slightly control the size of vesicles.

If the internal solution has higher viscosity, tension and frequency may have to adapt. For example, when using an optimal electroformation solution of 300mM sucrose in a mixture of 20% glycerol and 80% milipore water, since viscosity is higher, the frequency has to be slightly lowered to get a good resonance of the lipid deposited layers and an optimal swelling. A typical sequence of tension and frequency is presented in tab. 4.1 for an electroformation with the solution mentioned above. The formation of vesicle can be followed by visualizing transparent electroformation ITO glass chambers under microscope. At last, to favour the vesicles to detach from substrate completely, electroformation chamber is kept at very low frequency. After the end of electroformation, we left the cell formation chamber at rest for few minutes to let membrane relax. After a successful formation of vesicle they look like as shown in fig. 4.3. Finally, when vesicles are ready then we extract them from chamber by opening same holes from where we filled internal fluid to swell dry lipid. For getting complete drops of vesicles, at last we gently push syringe to make sure chamber is completely empty.

$Duration(hours)$	$Tension(V)$	$Frequency(Hz)$
1	0.2	10
1	0.4	10
4	0.6	10
1	0.6	4

Table 4.1: Application of tension and frequency in case of $300mM$ sucrose in mixture of 20% glycerol and 80% millipore water as internal solution, in DOPC lipids

4.2 Description of sorting method

4.2.1 Motivation

By following electroformation method one gets polydisperse samples of vesicles ranging from 1-100μm. In some cases, to run an experiment, good quantity and concentration of monodisperse sample is required. For example, in the study of phenomena like shear induced diffusion in flow due to hydrodynamic interaction, monodispersity of concentrated sample is a requisite, especially to make quantitative measurements. In other cases monodisperse samples is not a necessity but removing very small vesicles is helpful (as they exist in big quantity in polydisperse samples). To get rid of smaller vesicle, samples are centrifuged which is not a efficient way to remove very small

vesicles. Therefore a need of reliable sorting method was realized [44], in order to produce monodisperse sample in good concentration.

The sorting of micro particles has been a difficult and challenging task for many years. Several systems have been developed to get quick and precise sorting of a large quantity of particles. For example using laminar flow through diffusive filters to separate red blood cells from plasma, flow passing through arrays of filters to separate DNA molecules, electric field to separate amino acids, proteins and peptides, applying inhomogeneous magnetic field perpendicular to the direction of flow to separate magnetic micro particles from other particles, acoustic forces generated by ultrasonic waves and optical forces in form of optical tweezers to separate micro cells, as described by Pamme [45].

Considering the properties of the vesicles and necessity of a reliable sorting method, we have developed a sorting device based on the principle of

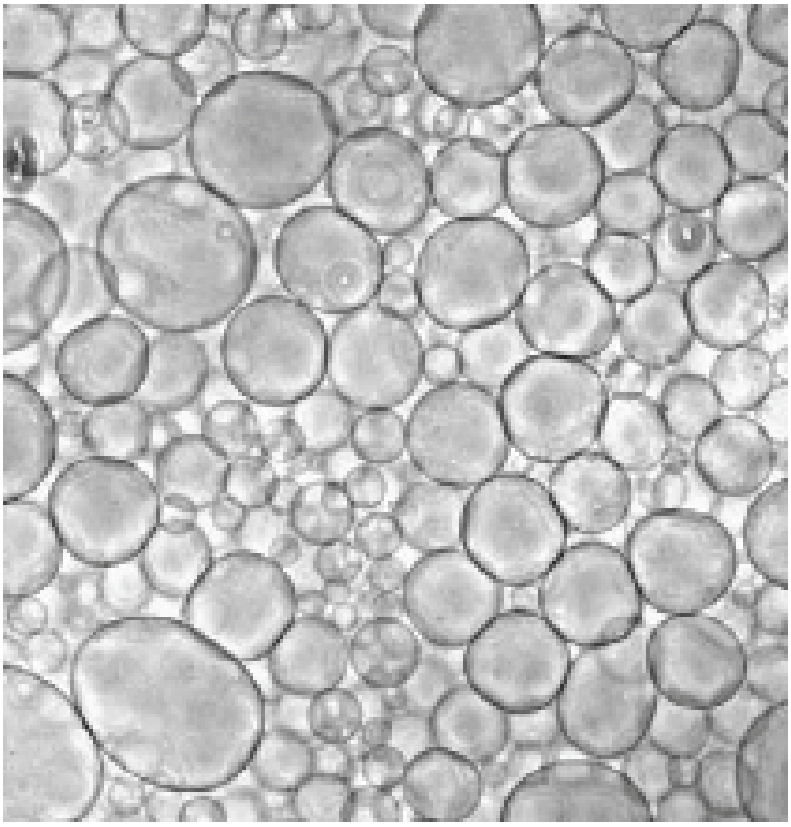

Figure 4.3: Formation of vesicles of in an electroformation chamber ($\approx 100\mu m$ width of image)

pinched flow fractionation (PFF), introduced by Yamada et al in 2004 [46] to separate different sizes. A brief description of the device is presented in next section. 4.2.2. The device we develop is capable to sort vesicles samples of concentration up to 5% whereas in the reference work of Vig and Kristensen [47] the concentration is very low (0.05%). An other work by Maenaka *et al.*, an emulsion is considered with continuous droplet radius distribution between 0 and 30 μm, and a concentration of 5% [48]. In this work the flow rate of the sample is very low ($\approx 300\mu$ l/h) and they are collected in three outlets with overlapping of size around 5μm. In our system we use a sample flow rate of 1-5 ml/h and we can collect our subpopulation sizes in sixteen outlets varying size from 0 to 34μm .

4.2.2 Technical details of sorting device

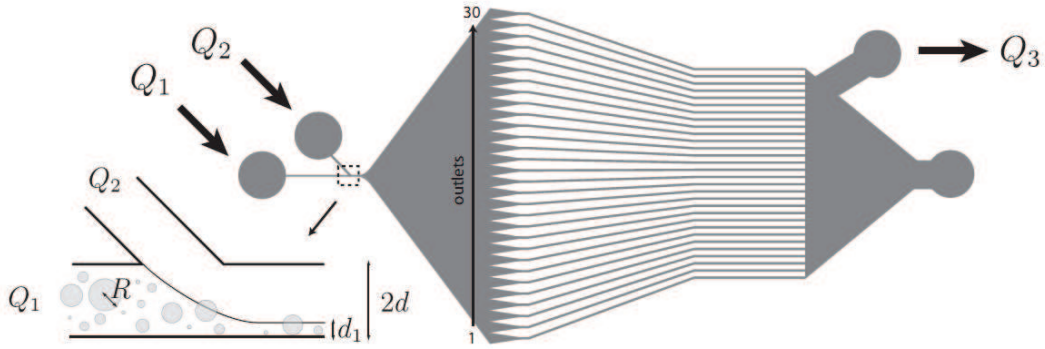

Figure 4.4: Schematic of sorting device

The principle of PFF is simple: the flow of the vesicle sample to be sorted is pushed against a wall by a flow of vesicle free carrier fluid. Due to their finite size, the centres of vesicles are located on the flow streamline which is located at a distance equal to their radii from the wall. Collecting each of these streamlines leads to collecting each subpopulation of the sample. To collect the concentrated samples of subpopulations, two geometrical improvement were mandatory. As most of the pinching fluid will remain particle-free, it is convenient to limit its volume, then the pinching is realized in a channel (the pinched segment). Secondly, collecting effectively subsamples with narrow size distributions clearly requires to increase the lateral distance between the different populations. This is achieved through a broadening of the pinched segment, allowing to add downstream collecting channels.

As at least half of the fluid will remain particle-free, it is convenient to drain it through a single outlet, in order to maximize the space available for

the expansion of particle-charged streamlines [49, 47, 48]. In order to control the destination of sorted particles, they were extracted with the help of microvalves, joined at the outlets of the channel [50]. To improve sorting of micro particles, different geometrical variations were also studied to compare separation efficiency to the expected one [46, 51, 48]. It is also found that the small variations observed are mainly due to channel imperfections, 3D effects or optical errors [52].

The vesicles sample is injected with flow rate Q_1 and pinched by a particle-free fluid with flow rate Q_2 in a segment of width $2d$. The pinched segment whose width $2d$ can be similar to the diameter $2R_{\max}$ of the largest particle to be sorted as shown in fig. 4.4. The typical width of pinching segment is $2d = 70\mu m$ and thickness of the channel is $99\mu m$. The suspension enters then into broad segment where streamlines splits into 30 outlets according to radius of vesicles. By altering flow rate ratio in Q_1/Q_2 we can follow the efficiency of sorting by visualizing under microscope. We were focused on efficiency of sorting rather collecting sorted sample therefore all 30 outlet converged to unique outlet at atmospheric pressure.

Sorted vesicles are collected in the 16 first channels whereas the last 14 channels are vesicle free because of the high flow rate of particle free fluid. The extraction of particle free fluid through a sucking outlet with a flow rate $Q_3 = 0.9(Q_1 + Q_2)$ was considered in order to increase the number of channels containing vesicles. The best place for drainage is a complex issue that depends on geometry of channels.

In each outlet channel the mean radius $< R >_i$ of the vesicles and the standard deviation is measured. The flow rate Q_2 was kept constant to 10 mL/h, and Q_1 was varied between 0.2 ml/h and 10 ml/h. We wish to find the optimum ratio Q_1/Q_2 but this parameter would depend on the chosen width $2d$ (larger d would require larger Q_2 for the same pinching efficiency), which depends itself on the maximum size of the vesicles to be sorted. A more appropriate parameter is the width d_1 occupied in the pinched-segment by the fluid coming from flow rate Q_1. A rough estimation would tell us that d_1 must be of the order of the radius of the smallest vesicle to be sorted. Finally, we used d as the lengthscale of the problem, and the values for d_1 and R are evaluated in d unit.

4.2.3 Performance of the sorting method

In order to study the efficiency of the sorting device, we studied the size distribution of vesicles in different outlet channels by varying width d_1 of vesicle

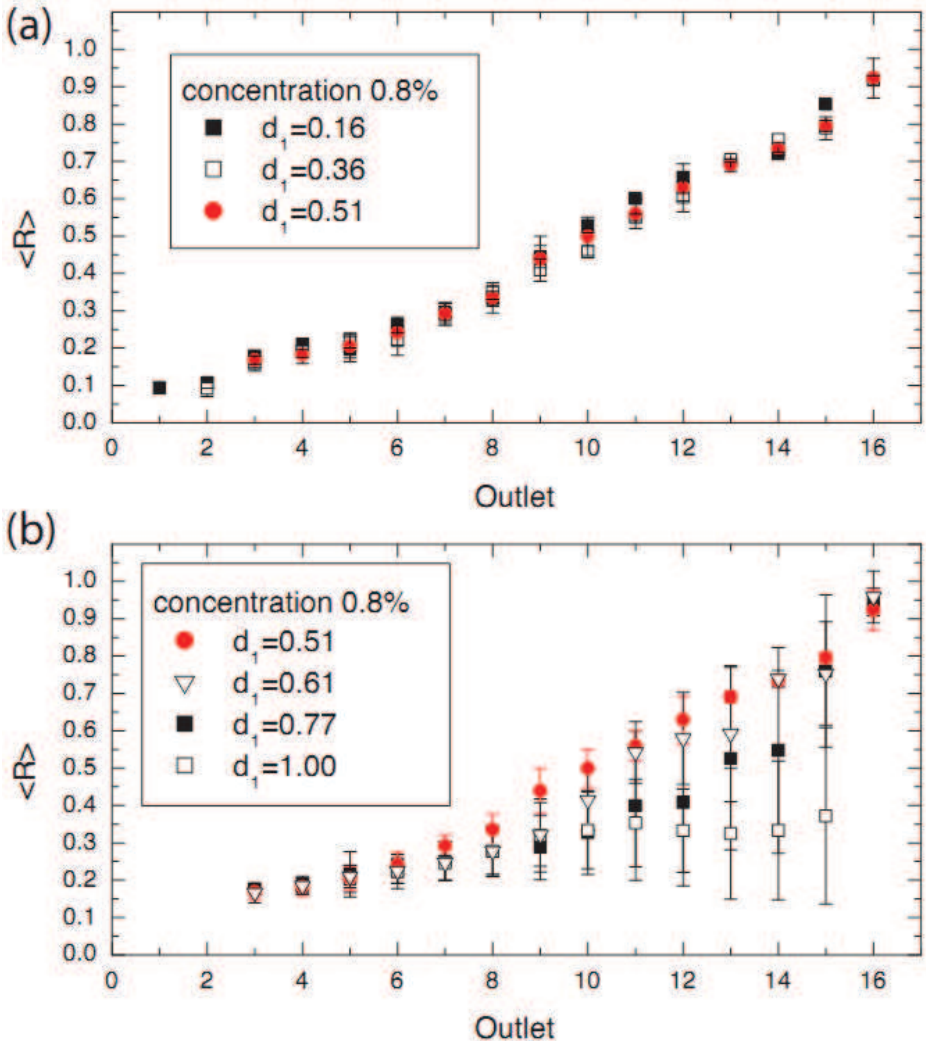

Figure 4.5: Size distribution in the outlet channels for different values of d_1(a) low values of d_1 (b) large values of d_1

suspension as described in fig. 4.4. Figs. 4.5(a,b) shows the mean sizes of the vesicles in the different channels for different values of d_1 between 0.16 ($Q_1 = 0.2$ mL/h) and 1 ($Q_1 = 10$ mL/h). For $d_1 \leq 0.51$, good separation is achieved, with standard deviations of the order of the half distance between two neighbouring mean values. Therefore it can be conclude that sorting does not depend on d_1 and can therefore be considered as optimal.

In addition to this separation, the obtained subsamples have a good monodispersity: the vesicles of radii ranging from 0.05 to 0.97 split into 16 subsamples where the mean radius increases quasi linearly and the standard deviation is roughly constant in the different channels and equal to 0.017 for

$d_1 = 0.16$, 0.021 for $d_1 = 0.36$ and to a still reasonable 0.036 for $d_1 = 0.51$. The monodispersity quality can be estimated by the ratio between the standard deviation and the mean radius, and from channel 1 to channel 16 we find that it goes from 17% to 2% when $d_1 = 0.16$ and from 36% to 4% when $d_1 = 0.51$.

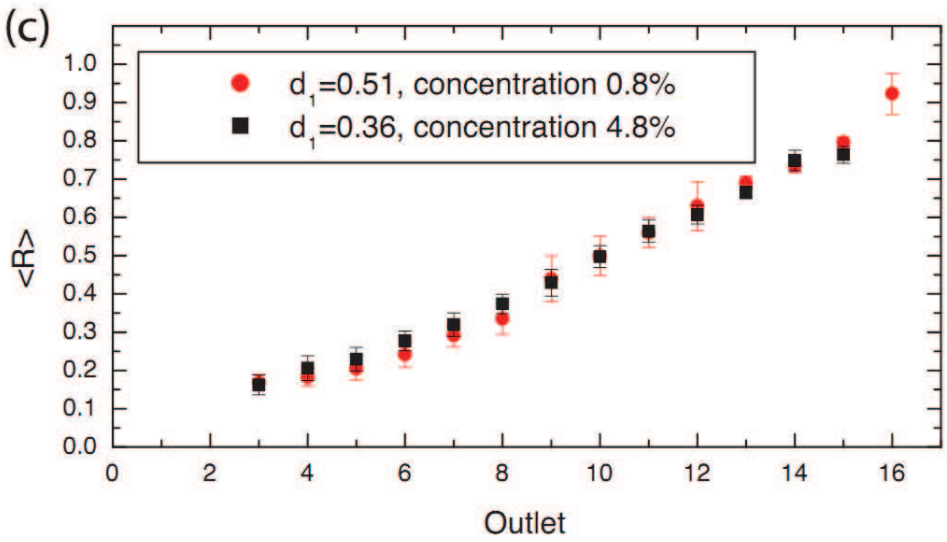

Figure 4.6: Size distribution in the outlet channels for two different concentration

As d_1 is increased even more, the standard deviations increased drastically while the mean radius varies less between the outlets, in particular for high radii, so separation is not achieved. However, for $d_1 = 0.61$, outlets 14 to 16 have narrow standard deviations, as well as outlet 16 for $d_1 = 0.77$: the pinching is strong enough too prevent smaller vesicles from being at the same level as the large vesicles that enter these outlets.

Similarly, for intermediate channels (around channel 10) or for $d_1 = 1$, the population is roughly bidisperse: vesicles of intermediate size are more easily pushed against the wall in the pinched segment than the small ones, that can then enter the same channel as the big ones. This can be seen in Fig. 4.7(b): the narrow distribution of outlet 3 becomes wider in outlet 7 and 10 and two distinct populations appear in outlet 12 and 15. In outlet 16, a rather narrow and monodisperse population is recovered again.

It is remarkable that separation with d_1 around 0.5 is as good as with the more intuitive choice of $d_1 = 0.16$, which is of the same order as the smallest particles considered here (even smaller ones, that enter channel 1, were barely distinguishable). If all the small particles present in the initial

suspension were present in the whole pinched area of width $d_1 = 0.51$, they should be present until channel 10, where $< R >= 0.50$, which is clearly not the case. One must therefore admit that collective effects take place, so that for instance small particles could be pushed against the wall by larger particles.

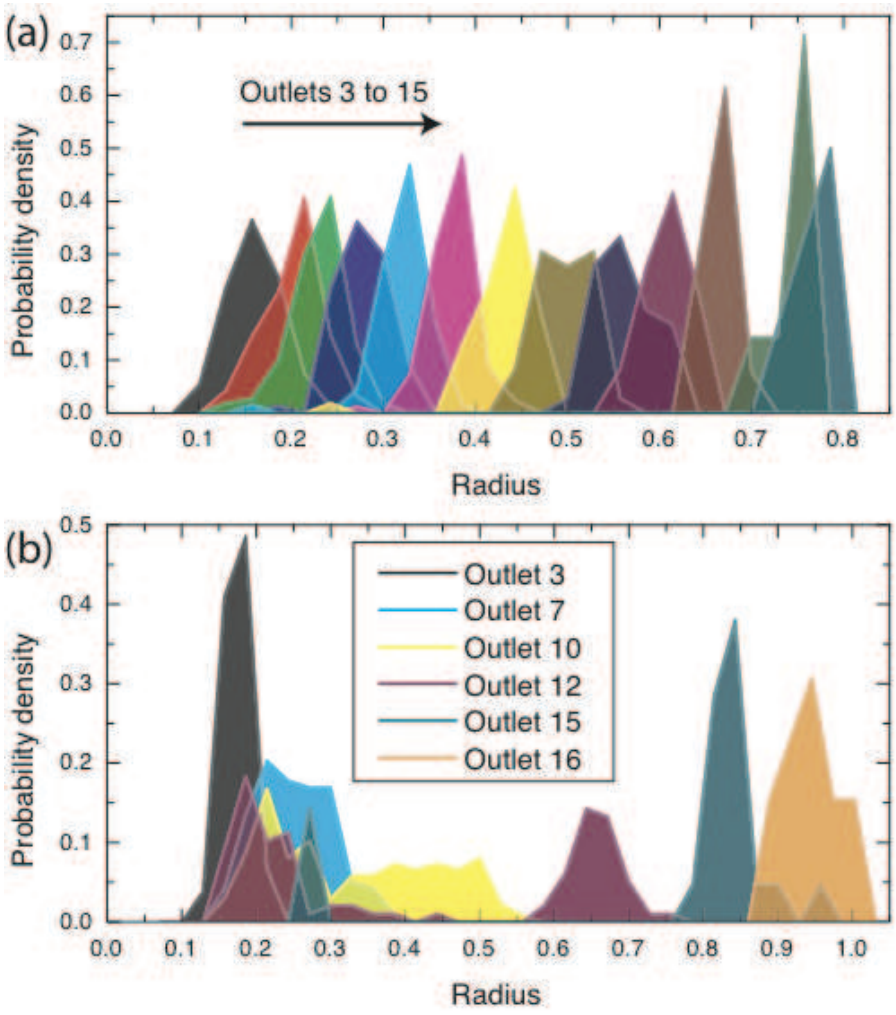

Figure 4.7: Particle distribution in the outlets (a) in the 14 outlets analysed for a concentration of 4.8% and $d_1 = 0.36$ (b) for some selected outlets for a concentration of 0.8% and $d_1 = 0.77$

Finally, as shown in Figs. 4.6 and 4.7(a), good separation and monodispersity are also achieved for a concentration of 4.8%: standard deviations are 0.027, with $d_1 = 0.36$, which is comparable with the more dilute case. The monodispersity quality reaches 3% for the larger particles.

Chapter 5

Dynamics of a deflated vesicle

Ce chapitre présente l'état de l'art sur le comportement de vésicules et globules rouges (en suspension diluée) en réponse à un champ d'écoulement externe. Tout d'abord, nous résumons les faits théoriques et expérimentaux qui sont les fondations de notre travail afin d'avoir une meilleure compréhension du sujet. Puis notre méthodologie expérimentale pour produire des vésicules de forme dégonflée et un exemple de leur réponse en écoulement de cisaillement simple imposé sont présentés en détail.

This section deals with the state of art concerning the behaviour of vesicle and red blood cell (in a dilute suspension) in response to external flow field. First, we summarise briefly theoretical work and experimental evidences that are foundations of our work in order to make better understanding of the subject. Then our experimental methodology in producing deflation shapes of vesicles and an example of their response in imposed simple shear flow is presented in detail.

5.1 Theoretical Background

In most available experimental data on vesicles and red blood cells, and in particular in our experiments R_e is small as compared to unity, and the Stokes approximation (i.e. neglecting inertia) constitutes a good approximation. Hence, if $\mathbf{v}$ denotes the vector velocity field of the fluid, it obeys

$$\eta \Delta \mathbf{v} - \bigtriangledown P + f_{ext} = 0 \tag{5.1}$$

where P is the pressure field. f, represents the membrane force applied on the fluid. For an incompressible fluid the rate change of density is zero. Hence the mass conservation equation is,

$$\bigtriangledown \cdot V = 0 \tag{5.2}$$

As seen in chapter 1, vesicles are endowed with bending elasticity, while their membrane is incompressible. These two effects are also manifested by red blood cells. In addition, red blood cells resist to shear thanks to their cytoskeleton. All these three effect are, a priori, essential ingredients in a modeling that aims to capture the physics of the problem. As the present work is dedicated to experiments, presenting a full modeling would be too much involved. Thus we are going only to introduce some basic modeling that will help understanding the various observations we shall encounter later.

Two basic modes of dynamics that are common to both vesicles and red blood cells are (i) tank-treading -TT (the cell keeps a given steady orientation of its main axis with respect to the flow direction), (ii) tumbling (TB). The transition from TT to TB can be triggered, for example, by a viscosity contrast. The first treatment of these two phenomena is due to Keller and Skalak (KS) [53] in 1982, briefly presented in the next section.

5.1.1 Keller & Skalak's model

KS were motivated by the transition of the tank-treading to tumbling motion that was known for red blood cells. They considered red blood cell membrane as a fluid membrane of fixed ellipsoidal shape of constant surface, encapsulating an incompressible Newtonian liquid. The ellipsoid is subjected to a plane Couette flow (usually also called simple shear flow) of another incompressible Newtonian fluid. The rate of energy dissipation in the membrane is taken to be zero, which is equivalent to assuming that the membrane has no shear viscosity. No shear elasticity was taken into account. Finally, the particle is assumed to be neutrally buoyant. Despite the oversimplification of the model, KS captured some essential features that was confirmed later to hold in more realistic situations; we anticipate, however, that the KS model missed some essential phenomena (caused by the free boundary of the cell), as will be described later.

The KS model is based on two concepts allowing to calculate the movement of an ellipsoidal fluid under shear flow:

1)Equilibrium of moments: the total moment of the system: fluid plus

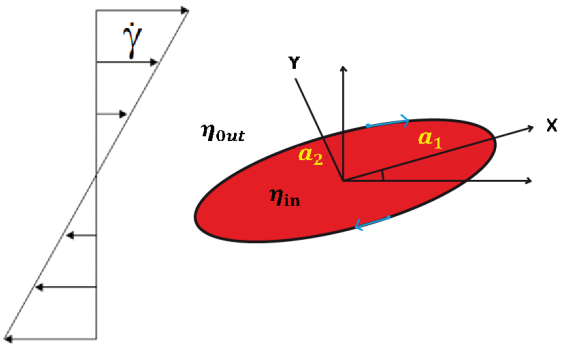

Figure 5.1: Schematic drawing of ellipsoidal membrane in a shear flow

the ellipsoid is equal to zero; for that purpose KS made use of a solution given in 1922 by Jeffery [54] where the flow field around a rigid ellipsoid was known.

2)Energy conservation: the rate of work done by the external fluid is equal to the rate at which the energy is dissipated in the internal fluid.

In addition, KS have assumed a special form of the membrane velocity field (with free parameters to be fixed by energy conservation) in order to preserve local area conservation (local incompressibility). Their postulate did not fulfill the local conservation exactly, but only approximately.

According to the first condition, (consider a membrane-enclosed fluid-filled particle of arbitrary shape immersed in an external flow and particle is neutrally buoyant) no forces are exerted by any external agent. Under these conditions the stress distribution in the internal fluid is such that every volume element of the internal fluid is in equilibrium. In case of equilibrium in internal fluid there will be not any resultant internal force or moment on the membrane. Therefore the resultant force and moment exerted by the external liquid on the membrane must vanish at every instant. This condition establishes the flipping velocity of the particle.

The demand that the rate at which work is done on the particle be equal to the rate at which energy is being dissipated inside the particle, allows to determine the still unknown expression of the amplitude of the tank-treading

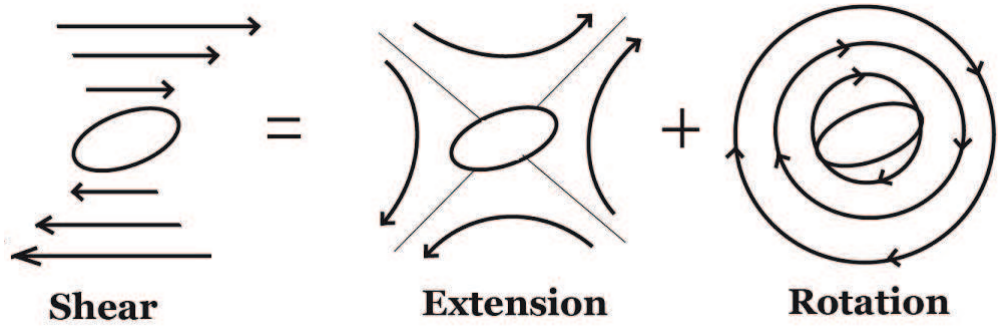

Figure 5.2: Velocity field of vesicle in shear flow is composition of a rotation field and an elongational field

velocity as a function of the orientation angle θ between the direction of flow and the ellipsoid's longest axis:

$$\dot{\theta} = A + B\cos 2\theta \tag{5.3}$$

where

$$A = -\frac{1}{2}\dot{\gamma}, \tag{5.4}$$

$$B = \dot{\gamma}\left[\frac{1}{2} + \frac{C_1}{(C_2 - \lambda)}\right] C_3 \tag{5.5}$$

In above equation, A denotes the mean rotation velocity, which is nothing but the rotation component of the applied shear flow. B is a function of the ellipsoid's aspect ratios and the viscosity contrast. Physically, the term $B\cos\theta$ is a consequence of the elongational part of the shear flow, which applies a torque on the particle, depending on its orientation, as shown in fig. 5.2. C_1, C_2 and C_3 are geometric constants depending on the ratios between the ellipsoid's axes. When shear rate $\dot{\gamma}$ is positive, it may be shown that B is always positive.

There are two types of motions, depending on the ratio -A/B :

1) If $0 < -A/B < 1$, there is a stationary solution where the ellipsoid keeps a constant orientation angle θ^* (which is time independent) and a **tank-treading** motion of the membrane occurs. Actually, as presented

below, despite the nonlinearity of the equation, it has a simple analytical solution. Starting for an arbitrary initial condition, the angle $\theta(t)$ asymptotically approaches a constant value, thus $\lim_{t\to+\infty}\theta(t) = \theta^*$)

$$\theta^* = \frac{1}{2}\arccos(-A/B) \tag{5.6}$$

2) If $-A/B > 1$, the solution for angle $\theta(t)$ is periodic, corresponding to the **flipping or tumbling** motion of the ellipsoid, described by:

$$\theta(t) = arctan\{\frac{A+B}{\sqrt{(A^2-B^2)}}tan[(t-t_0)\pi/T]\}, \tag{5.7}$$

where t_0 is the time at which $\theta = 0$, and T is the period of flipping through an angle π. It is given by:

$$T = \pi(A^2 - B^2)^{-1/2} \tag{5.8}$$

The transition between a flipping (or tumbling) motion and a stationary orientation occurs when B = A and only depends on geometrical parameters (C_1, C_2 and C_3) and on viscosity contrast (λ).

Hence from the above presented model we can conclude that, Keller-Skalak theory [53] predicts two flow regimes: a steady state tank-treading motion where the vesicle assumes a steady-state ellipsoidal shape, and its inclination angle θ remains constant with time. The other is named tumbling regime where the vesicle rotates along the axis perpendicular to the plane flow (the flow vorticity direction), and θ is periodic in time and varies in $[\pi/2, \pi/2]$.

5.1.2 Few numerical & experimental results

Many theoretical, analytical as well as experimental improvements, describing dynamics of vesicles have been done after KS model. Since, the model considered object of fix ellipsoidal shape therefore effect of different deformed shapes on the dynamics was ignored. In improvement of KS-theory, Biben et al. [55] and Beaucourt et al. [56] analyzed the problem in two dimensions (due to computational costs) by considering the shape to be free to evolve. They explored the range of reduced volume 0.747 to 0.987.

They varied the Capillary number between 0.075 and 0.75 and viscosity ratio from 1 to 9. Some quantitative discrepancies that exist between the

KS theory and the numerical results was found. More precisely, the critical viscosity ratios λ_c, was a bit underestimated by the KS theory. Despite this small quantitative difference, and surprisingly, numerical simulations in 2D is quite close to 3D results of the KS-model (for prolate shape).

Moreover, in an experimental study by Kantsler and Steinberg [57], where they considered prolate shape of vesicles, a good agreement with Biben et al. [55] and with Beaucourt et al. [56] was reported.

The transition between the two regimes for a vesicle of fixed ν happens at a critical viscosity ratio λ_c , beyond which the vesicle tumbles. Both tank treading and tumbling regimes were observed experimentally by Mader et al.[58] by varying viscosity ratio and reduced volume. At a certain limit when shear rate is too strong, vesicle gets more deformed. This deformation in shape of the vesicle leads to desynchronisation from the frequency imposed by flow which results in a decrease in tumbling velocity of vesicle. From this quantitative comparison of experiment it has shown that, as long as shear rate (small Ca) is not too strong results agrees with KS-model. Therefore, experimental evidences proves that shear rate (Capillary number) Ca and deformability (reduced volume) ν parameters play an important role in dynamics of vesicles which was underestimated in KS theory.

In a more recent numerical work in 3D by Biben et al. [59] the validity of the KS theory was discussed in greater details. It was shown that the KS theory is valid (i) if the viscosity contrast is large enough, (ii) if the shear rate (or more precisely the capillary number) is small enough; typically the range of validity of the KS theory is confined to $Ca \leq 1$. It was shown that the form $\dot{\theta} = A + B\cos(2 * \theta)$ ceases to be valid for higher Ca. It was reported, however, that the frequency of tumbling times the applied shear rate is quite insensitive to shear rate.

Small deformation theory:

C. Misbah has developed an analytical theory to describe the dynamics of a vesicle subjected to a shear flow in the limit of a small excess area, Δ [60]. This theory highlights certain differences with the model of KS. It led to the appearance of a new regime called vacillating-breathing (VB). In this regime, the main axis makes periodic oscillations with the flow direction, while the shape undergoes breathing-like dynamics. This mode was subsequently reported in experiments [61] (and was also briefly mentioned in the experiment of Mader et al. [58]). Several authors have later confirmed the existence of the VB mode either analytically [62, 63] or numerically [64]

and have provided the phase diagram, similar to the one shown in Figure 5.3.

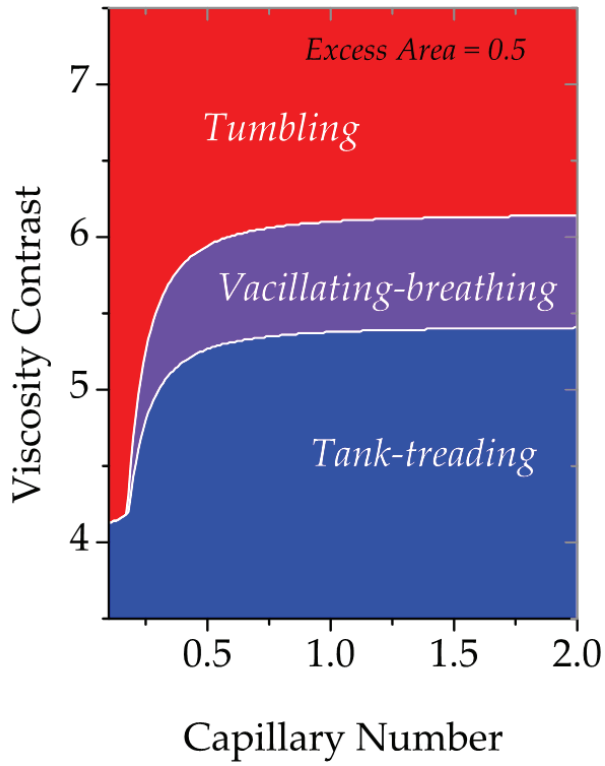

Figure 5.3: Phase diagram showing three kinds of dynamics of a vesicle under shear flow.

More recently Biben et al.[59] have reported on the phase diagram in 3D and have shown, in particular, that the band of the VB mode does not saturate, but rather it widens upon increasing Ca. In addition, it was reported that even for a quasi-spherical regime, the location of the boundaries between the three different regimes in the phase diagram was significantly different from previous analytical calculations which were limited to the quasi-spherical limit [63, 65]. The numerical results of Biben et al. [59] have reported on the fact that higher order harmonics (analytical theories has so far included second order harmonics only) get excited pointing to a nontrivial effect of harmonics higher than two. This numerical simulation triggered a new analytical by Farutin et al.[66] by including the fourth order harmonics. It was shown that this harmonics is important even for a small deviation from a sphere. The confrontation of the analytical results with the numerical ones [66] showed a very good agreement.

5.2 Deflated vesicles in shear flow

Variety in vesicles shapes and transition from one shape to another shape have always been a subject of study for membrane physicists to measure physical parameters of the membrane (energy of curvature, tension, coupling with a gel, adsorption of proteins, etc). Due to the absence of reliable method in producing deflated shapes of vesicles, so far no experimental study on their dynamics has been reported. To compare the dynamical behaviour of deflated shapes with existing regimes such as tank-treading, tumbling and vacillating-breathing (for quasi spherical vesicle), we have put first effort to produce deflated shapes. The dynamical behaviour of deflated shapes can be useful to understand the microscopic properties of the red blood cells in flow, and linking their rheological properties in overall blood flow.

5.2.1 Theoretical background

Dynamics of deflated object :

The first study on dynamics of very deflated shape of 2D vesicle imposed in linear shear flow has been done by Ghigliotti et al. [67], considering viscosity ratio λ (no viscosity difference in internal and external medium) and capillary number Ca, set to unity. Reduced area, τ_{2D}, (corresponding to the 2D model) of vesicle, varied from range of 0.32 to 1 (1 = circle) is shown in fig. 5.4.

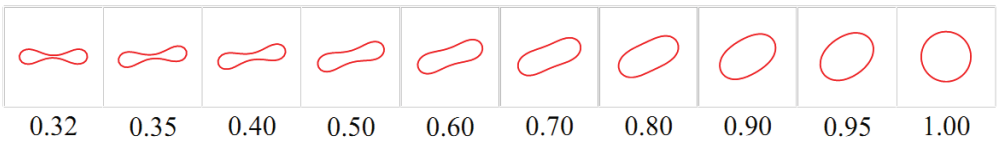

Figure 5.4: Equilibrium shapes for different reduced area

The study shows (fig. 5.5.a) that of a 2D vesicle when reduced area tends to be unity i.e almost spherical (circular in 2D), inclination angle (θ) in tank trading regime tends to be 45°. This is consistent with earlier theoretical predictions. Surprisingly, inclination angle goes to zero for a finite reduced area which is 0.32, even though there is no viscosity contrast.

In addition, tank-treading velocity (v_{tt}) decreases for smaller reduced area of the vesicle, as shown in fig. 5.5.b. This is expected due to fact that as reduced area decreases the vesicle aligns further with the flow. Then torque

due to the imposed flow transfers more to inclination than the tank-treading. The interesting fact is that the vesicles can tumble even without viscosity contrast. The idea is that due to deflation the vesicles assumes a pronounced biconcave-like shape, such that the membrane shows a neck. Upon shearing (with small shear rate), there is a competition between dissipation at the neck (which prevents tank-treading) and the imposed flow that tends to transfer tank-treding to membrane. As a result the vesicle tumbles, up to a certain critical shear where transition to tank-treading is observed. We shall see some preliminary results on deflated vesicles later in this chapter.

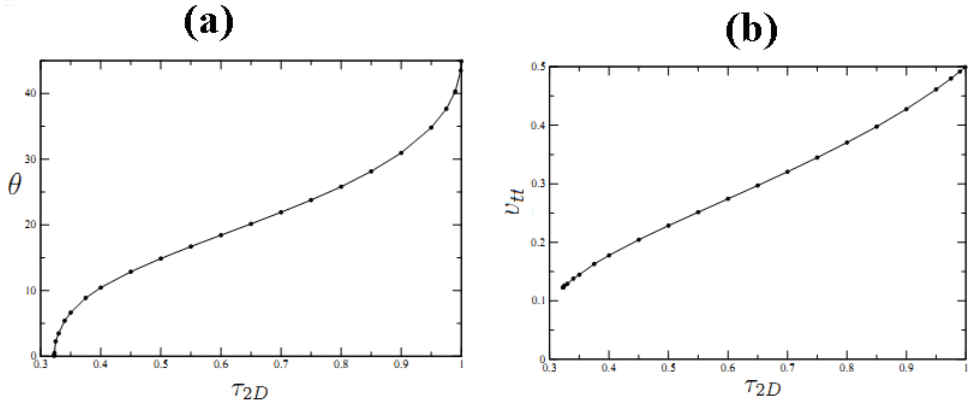

Figure 5.5: (a) Inclination angle (in degrees) of a tank - treading vesicle in a shear flow for Ca = 1 as a function of reduced area τ_{2D}(b)Tank - treading velocity measured in unit of $\dot{\gamma}$ as a function of the reduced area τ_{2D}

Formation of deflated Vesicle:

For producing very deflated vesicles, we chose DMPC lipid, which possess a rich scenario of shape and shape transition with variation of temperature [68][17] due to the difference of area and volume dilatability. Despite the high cholesterol content and the bilayer-cytoskeleton coupling, the bending stiffness of the erythrocyte membrane is equal to about that of DMPC-bilayer [69, 70]. Many experiments on DOPC, DLPC and mixture of these lipids were done to test the reliability of formation of deflated shapes. A few important mechanical properties have already been described in chapter 3 (section:3.1.2) about DMPC and other lipids.

Bilayer coupling model:

When vesicle membrane is a 2D liquid (absence of shear elasticity), and its shape is dictated by the membrane bending energy (see 3.1.2). Under the constraints of constant area and constant enclosed volume, the shape adopted by a vesicle is given the minimum bending energy. In the case where there is no spontaneous curvature (and no area difference between the internal and external monolayer) the shape depends only on the reduced volume (defined in 3.3). For a human red blood cell the reduced volume is of about 0.65. Miminisation of the bending energy under the afore mentioned constraints leads to a discocyte shape [71], which is very reminiscent of that of a red blood cell.

Various experiments (see review [15] for more details) on vesicles have concluded that the above model is not sufficient to account for all the variety of shapes. The first additional ingredient consisted in taking into account a spontaneous curvature (taken to be constant) in the model. Duling and Helfrich [72] took into account the effect of a spontaneous curvature. The model has now two dimensionless parameters: the spontaneous curvature (rescaled by the typical vesicle curvature) and the reduced volume. A catalogue of various shapes in this 2D parameter space has been calculated, as already shown in fig. 3.9 (chapter 3).

Another fact is that when vesicle undergoes deformation, two leaflets of membrane bilayer may respond differently [73]. Later other ingredients were taken into account. Owing from the fact that any change in monolayer may lead different shapes, experimentally it is very complicated to create any difference between monolayers of membrane. Though, in spite of these complications, few deflated shapes have been produced by changing osmotic conditions, the composition of lipid or additional solute in external solution. Indeed, reliable method in formation of controlled shapes could not attempted. Therefore a hypothesis, considering coupling between two monolayer by constancy of the difference between the areas of the two bilayer leaflets has been proposed by Svetina and Zeks [74, 75] which represents a Legendre transformation of the spontaneous curvature model of Helfrich [72].

Due to the fact that lipid exchange (flip-flop) between the inner and outer monolayer is so slow that area difference between two monolayers $\Delta A = A^{ex} - A^{in}$ is fixed. Thus, two constraints, the enclosed volume, V, and the area of the inner monolayer, A^{in} are considered as constant. The basic bending energy reads as

$$G_{el} = 1/2K_c \int (c_1 + c_2)^2 dA^{in} \tag{5.9}$$

where K_c= bending elastic modulus, c_1+c_2= mean curvature. By hypothesis, in equation 5.9 integration can be performed over the inner monolayer only. The contribution to the elasticity due to the area difference can be expressed in terms of the mean curvature as $\Delta A = d\int(c_1 + c_2)dA^{in}$ provided the distance d ($\approx$ 1/2bilayer thickness) between the centers of the monolayers is small ($d \ll [c_1 + c_2]^{-1}$). Different shapes of minimum curvature energy as a function of reduced volume, ν, and reduced area difference, Δa have been calculated by Svetina [75] and Seifert [21]. A phase diagram of vesicles with different shapes is represented in fig. 5.6, where ν and Δa are defined as:

$$\nu = \frac{V}{[(4\pi/3)(A^{in}/4\pi)^{3/2})]}$$

$$\Delta a = \frac{\Delta A}{[8d\pi(A^{in}/4\pi^{13/2})]} \tag{5.10}$$

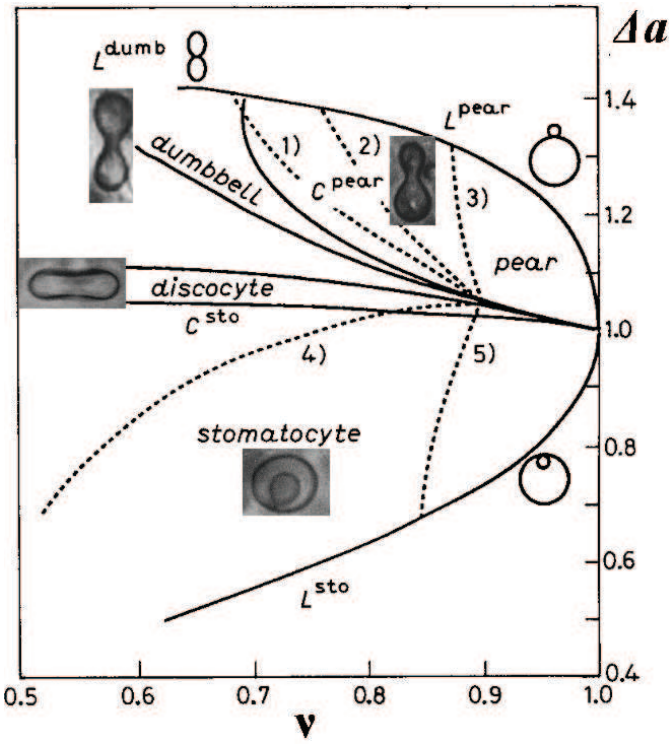

Figure 5.6: Phase diagram of vesicle shapes calculated by the bilayer coupling model shown by continuous lines whereas dashed line shows experimentally observed shapes [76]

By following above hypothesis , an experiment on deflated shapes and transition from one shape to another shape was performed. It was found

that, even a variation of 0.1K/min in temperature resulted in a big transformation in shape [76]. On the basis of temperature effect , to compare theoretical and experimental shapes, Berndl et al proposed a calculation of thermal expansivities between leaflets [76, 68].

Shape change by thermal expansivity:

For explaining shape transition, it is assumed that the thermal expansivities of the inner monolayer, α^{in}, and outer monolayer, α^{ex}, exhibit a small difference, which is denoted by Υ. where α^{in},α^{ex} are defined by,

$$\alpha^{in} \equiv \frac{1}{A^{in}} \frac{dA^{in}}{dT} \tag{5.11}$$

and

$$\alpha^{ex} \equiv \frac{1}{A^{ex}} \frac{dA^{ex}}{dT}$$

with

$$\alpha^{ex} = (1 + \Upsilon)\alpha^{in}$$

By neglecting the small thermal expansivity of the enclosed water volume and assuming that the volume of the bilayer given by $A^{in}d$ is temperature independent, then ν and Δa will depend on the temperature as follows:

$$\Delta a(T) = \frac{A^{ex}(T_o)exp[\Upsilon\alpha^{ex}(T - T_o)] - A^{in}(T_o)}{8d\pi(T_o)(A^{in}(T_o)/4\pi)^{1/2}}.exp[(-3/2)\alpha^{in}]$$

and

$$\nu(T) = \nu(T_o)exp[(-3/2)\alpha^{in}(T - T_o)] \tag{5.12}$$

where $\nu(T_o)$ and $\Delta a(T)$ are the parameters of the initial shape at temperature T $= T_o$. By eliminating $(T - T_o)$ from these equations the change of the reduced area difference can be expressed as a function of ν i.e. $\nu_o \equiv \nu(T_o)$ and $\Delta a_o \equiv \Delta a_o(T_o)$ at T $= T_o$,

$$\Delta a(\nu) = \left(\frac{\nu_o}{\nu}\right)\left[\Delta a_o + b\left(\left(\frac{\nu_o}{\nu}\right)^{2\Upsilon/3} - 1\right)\right] \tag{5.13}$$

with

$$b \equiv \frac{A^{ex}(T_o)}{8d\pi(T_o)(A^{in}(T_o)/4\pi)^{1/2}} \tag{5.14}$$

All four parameters, $\Delta a(T_o)$, $\nu(T_o)$, Υ and b are the main parameters to characterize shape of the vesicle and comparison between theory and experiment. In the ideal case where $\Upsilon = 0$, second term of equation 5.13 drops out and temperature trajectory in the phase diagram would be a simple hyperbola (see fig. 5.6). Whereas for $\Upsilon \neq 0$, the second term of equ. 5.13 contributes and by varying temperature one can get different shapes. For instance, if $A^{ex}(T_o) \simeq A^{in}(T_o) \simeq 100\mu m^2$ and $d \simeq 5nm$, one obtains $b \simeq 900$. Thus an asymmetry of the order of 10^{-3} has a significant effect . As in fig. 5.6, different values of Υ are displayed for the same initial state with $\nu_o = 0.9$ and $\Delta a_o = 1.05$ which corresponds to a prolate ellipsoid. Area difference $\Delta a T_o$ value can be determined by comparison of the experimental and theoretical shapes. $\nu(T_{max})$ is obtained by equation 5.12 and $\Delta a T_{max}$ is fitted to the experimental shape, which finally determines the value of Υ.

An experimental observation of different shapes varying area-to-volume ratio induced by temperature, of DMPC vesicles in millipore water, showed good stability of shapes by Kas and Sackmann [68]. A spherical shape under lateral stress [1] starting from temp $25.3°C$ shows first prolate ellipsoidal, then pear and finally sphere with pointing small vesicle outside by varying temperature until $40.9°C$. Finally a minute change of temperature by $0.1°C$ (i.e. from 40.9 to $41.0°C$) shows sudden outside budded shape. The ellipsoidal and pear shapes in the regime between $27.2°C$ and $41.0°C$ were stable and transition in between shapes were reversible. Discocyte and stomatocyte shapes were found stable at $42.3°C$. By comparison between calculated and observed shapes it was predicted that transition from spherical-to-pear-to-outside budded shape require a positive Υ value, whereas transition of discocyte-stomatocyte would require negative Υ value. An example of sequence of transient shapes of a DMPC vesicle, forming initially a prolate ellipsoid with the volume of $4000\mu m^3$ and area of $1490\mu m^2$ is presented in fig. 5.7. The discocyte shape is stable at T $\geq$ 43.6°C.

5.2.2 Experimental set-up

Preparation method of deflated vesicles :

For the preparation of deflated shape of vesicles, we followed the preparation method described by Kas and Sackmann [68]. This formation method of vesicle involves variations of the excess area-to-volume ratio via temperature change as explained in above section. 5.2.1. To get deflated vesicles, we used this method with electroformation process (presented earlier

[1] Lateral stress: before starting the process of heating to observe transition in shape, vesicles are cooled below the temperature at which they become spherical

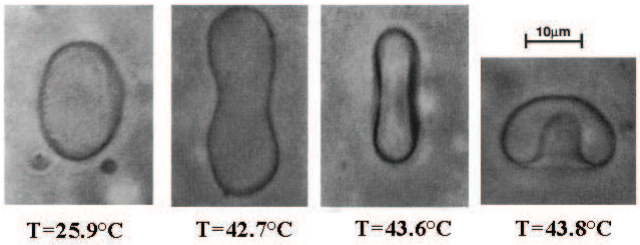

Figure 5.7: Different shapes of DMPC vesicles in millipore water and their transition temperature [68]

in section : 4.1.4). We recall that this method, due Angelova et al. allows a fast processing of vesicle production. Vesicle were obtained from L-α - dimyristoyl-phosphatidylcholine (DMPC), dissolved in solvent made of 9:1 v/v Chloroform methanol at a concentration of 1mg/ml. In case of DMPC vesicle, it exhibits a shape transition temperature of 23.8°C between the gel and L_α state.

200 μl of the solution were spread as a thick layer onto a ITO glass of typical size 5cm $\times 7cm$. After deposition of lipid the solvent is evaporated under vacuum for approx half hour. Dried lipid were swollen in aqueous solution of 250mM sucrose and millipore water. Prepared elctroformation chambers were then connected with an electric tension of 0.28 V and frequency $\approx$ 0.6 Hz and kept in an oven at constant temperature of $\approx$ 40°C for 6 hours or over night to get prolate or oblate shapes. After electroformation we obtained deflated vesicles without needing to dilute the suspension in a hyper osmotic solution, as shown in fig. 5.8. We were able to produce deflated shapes of vesicles of reduced volume ranging from 0.70 to 0.40 see in fig. 5.4, without viscosity contrast.

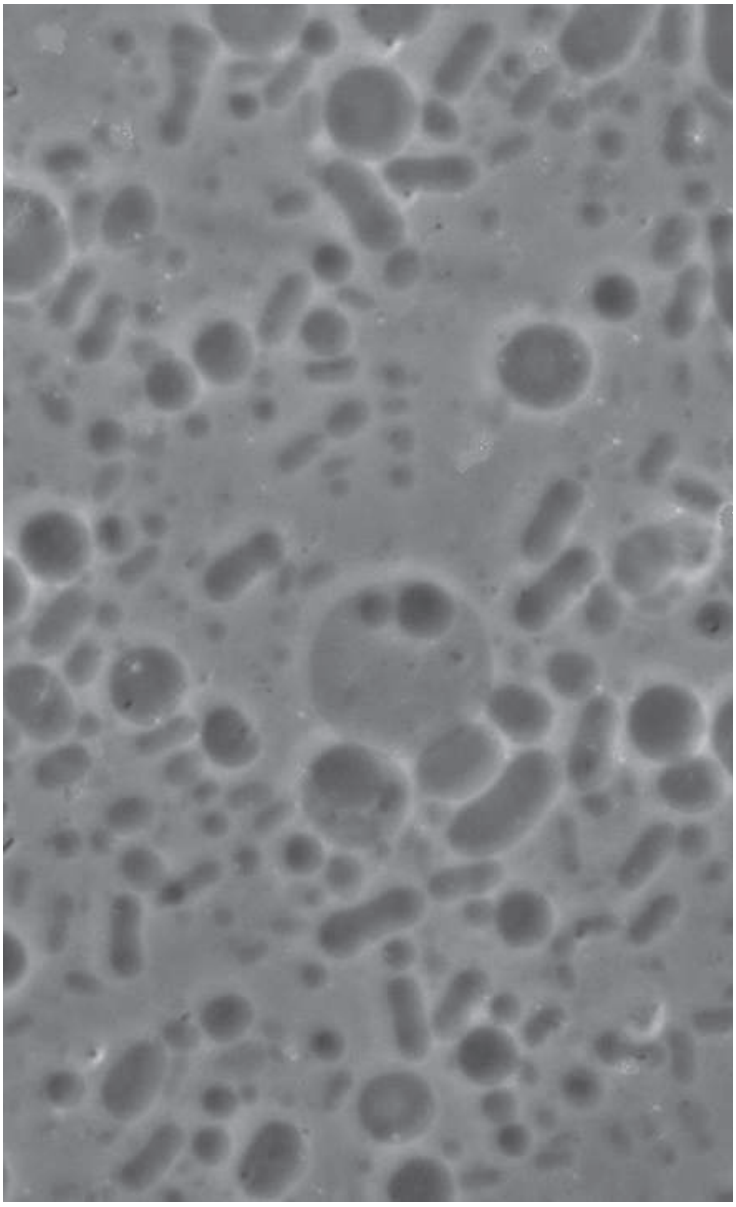

Figure 5.8: Deflated vesicles in dilute suspension

Flow set-up in channel :

A suspension of deflated vesicles was driven through a PDMS micro-channel as described in sect. 3.5.1. Channels of 10 mm length were used. Their cross-section have a typical width of 120 μm and thickness of 100 μm. Deflated vesicles obtained by the process described above were then diluted in external solution of 300mM glucose to achieve a constant of optical index with almost the same viscosity ($\lambda \approx 1$). The inlet and outlet of the channel

were connected to reservoirs, and the flow rate was controlled by varying the height of reservoirs. Deflated vesicles were gently injected at one end of the channel and mixed with carrier fluid (exterior sucrose solution), at a flow rate controlled by reservoir height.

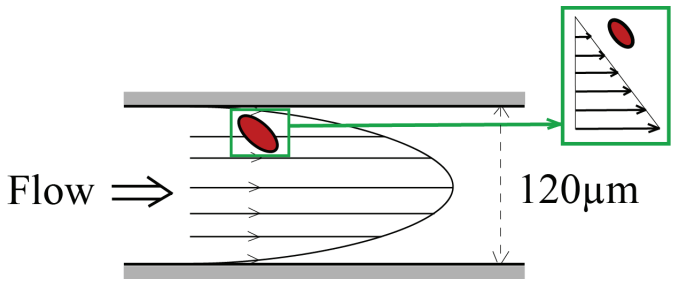

Figure 5.9: Vesicle locally experiencing shear flow in a channel flow

Strictly speaking the shear rate, $\dot{\gamma}$, is not uniform throughout the sample (where a Poiseuille flow is imposed). However, with the provison that the observed vesicle is not at, or close to, the center, the shear rate is merely uniform at the scale of the vesicle size. Explored local shear rates ranged from 1 to 100 s^{-1}, which was locally uniform, as shown in fig. 5.9. The plane of shear flow takes place at X-Y plane, which is the plane under microscope (fig. 5.10).

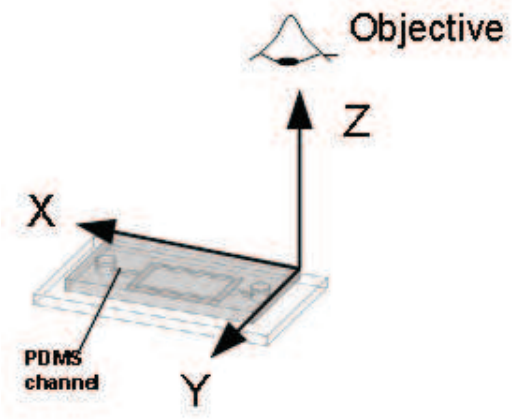

Figure 5.10: Schematic description of shear plane and plane of projection

Measurements of vesicle dynamics were conducted at constant shear flow, near wall region. After achieving expected flow profile, measurement were taken with the help of camera and images were captured at the rate of 7.5

frame per second by using objective 10X of the microscope. Captured images were then treated with the help of IDL software by measuring time, reduced volume by assuming axis-symmetry along the main axis, 2D-surface, orientation angle, horizontal and lateral positions according to width of channel and distance from the wall.

5.2.3 Result and discussion

As described in former theoretical and analytical studies, tumbling motion of quasi-spherical vesicle have been expected only at high viscosity contrast ($\lambda > 1$) when vesicle is elongated in presence of shear rate. Tank-treading and tumbling motions of vesicle at different viscosity ratios were also observed and verified experimentally from Mader et al [58].

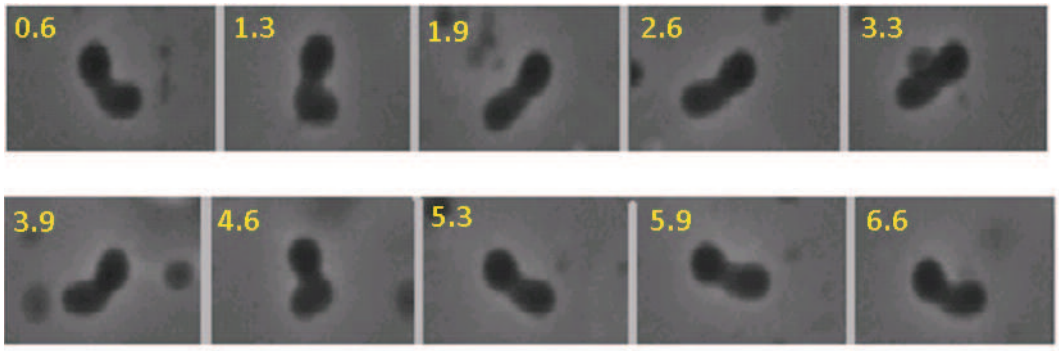

Figure 5.11: Orientation of deflated vesicle. Numbers in fig. show time (second)

Surprisingly, in our study of deflated vesicles shows an average orientation of $\pi/2$ with a vesicle undergoing a combination of tumbling and probably kayaking (or spining) regime without viscosity contrast i.e. $\lambda = 1$. An example of such orientation of deflated vesicle is presented in fig. 5.11. It is observed that the orientation of vesicle angle under linear shear flow exhibits periodic frequency. A graph of the angle θ relatively to flow direction as function of time, t, is presented in fig. 5.12. This experimental result shows that very deflated vesicles may have very different dynamics than quasi-spherical 2D vesicles deformed in shear flow. In some respect our experimental result can be identified quantitatively with numerical results from A. Farutin, shown in fig. 5.13, in a somewhat different situation as far as viscosity ratio is concerned.

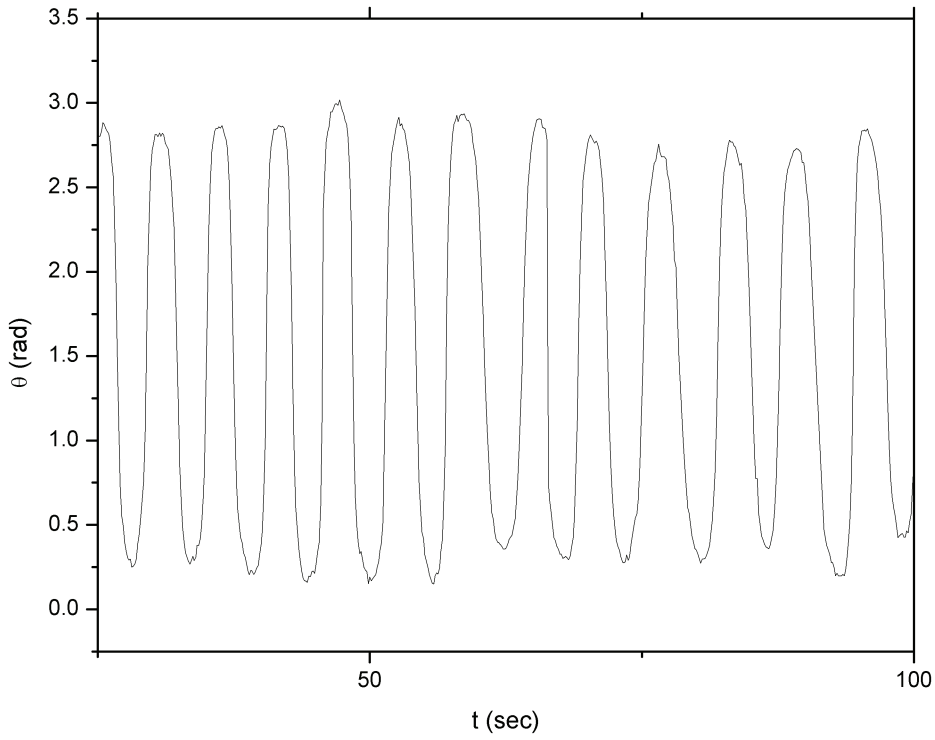

Figure 5.12: Periodic orientation of deflated vesicle (experimentally) of reduced volume ν=0.71 and radius $7\mu m$

In fig 5.13 the projection of the vesicle shape in a plane perpendicular to the main plane of shear is shown. In that situation a qualitatively oscillation around an average $\pi/2$ angle is recovered while the main angle in the plane of shear does not show such an unusual oscillation. This shows that this surprising oscillation may not be necessarily identified with a kayaking motion (which could be less surprising for a highly viscous or rigid object). Instead, one may need to consider the 3D nature of the flow field and suspect that in our case the main plane of shear may not be the X-Y plane but a combination of shear in the X-Y and X-Z plane due to the possible proximity of the bottom channel wall as sedimentation may have occurred.

For hydrodynamic study of stable prolate and oblate shapes, one has to maintain a minimum temperature of $\approx 40^\circ$, as shown in a study from [68]. Due to technical uncertainties, as explained, we were not able to explore other dynamic regimes as described by [67, 63, 59], or more clear quantitative results of tumbling motion or kayaking. Study on dynamics of deflated shapes of vesicle in shear flow is still lacking. This new motion of the highly deflated

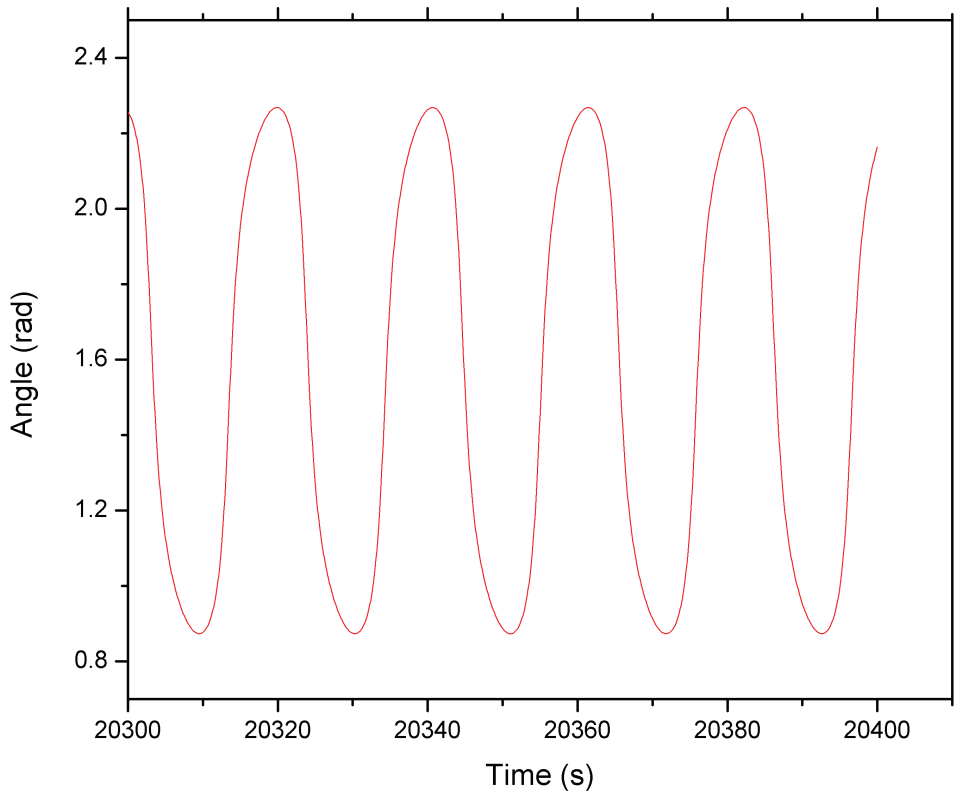

Figure 5.13: Periodic orientation of deflated vesicle (analytical result) at reduced volume around 0.95, capillary number Ca=2 and viscosity contrast λ=11.

vesicles is in qualitative agreement with some theoretical and numerical results obtained in the group, and suggests that the phase diagram of vesicle dynamics in shear flow can be more complex than what is predicted from theories on weaker deflated shapes. More studies are needed in understanding of dynamics of deflated vesicle phenomena and its effect on suspensions and over all impact on rheology which can be helpful to understand blood flow in micro capillaries.

Since the DMPC vesicles were very fragile, it was difficult to make an extensive study of these regimes. Variation of temperature can indeed lead to shape changes or even budding transition. Locally high shear rate can also lead to breakage of vesicles or elongation. As an interesting perspective multicomponent vesicles composed of DMPC in combination with other lipid or cholesterol could produce some stable and robust prolate or oblate shapes.

Chapter 6

Hydrodynamic interaction between two vesicles in shear flow

Dans ce chapitre, le phénomène dinteraction hydrodynamique entre deux vésicules dans un écoulement de cisaillement est décrit. Un dispositif expérimental microfluidique a été concu pour produire des conditions favorables à l'observation des interactions de paires de vésicules, à savoir un jet concentré de la suspension de vésicules dans un canal plus large. Pendant linteraction, une répulsion hydrodynamique a lieu, ce qui augmente la distance latérale (transverse à la direction de l'écoulement) de vésicules. Lintensité de cette répulsion dépend du volume réduit de la vésicule (les sphères ne sont pas déplacées), du contraste de viscosité, et est une fonction décroissante de leur distance initiale dans la direction transverse. Nous mesurons quantitativement cette répulsion et comparons les résultats aux résultats théoriques obtenus dans le groupe. Ces résultats fournissent une base quantitative pour la dérivation des coefficients de diffusion induite par cisaillement dans les suspensions de vésicules.

In this chapter, the phenomenon of hydrodynamic interaction between two vesicles in a shear flow is described. An experimental microfluidic device has been designed to produce favourable conditions to observe pair-interactions of vesicles, namely a focused jet of the vesicle suspension in wider channel. During the interaction, a hydrodynamic repulsion takes place, which increases the lateral (cross-streamwise) distance of vesicles. The intensity of this repulsion depends on vesicle reduced volume (spheres are not displaced), viscosity contrast and is a decreasing function of their initial cross-streamwise

distance. We quantitatively measured this repulsion and compared the results to theoretical results obtained in the group. These results provide a quantitative basis for the derivation of shear-induced diffusion coefficients in sheared vesicle suspensions.

6.1 Introduction

Since the early 70's the interactions between two bodies in flow such as spherical particles, bubbles, drops, or capsules have been the subject of many works. [77, 78]. The effects of hydrodynamic interactions on the motion of bubbles [79, 80], bulk stress and sedimentation velocity [81] have been studied. Even in dilute suspensions, interactions between micro particles affect the rheological behaviour [82]. The phenomenon of interaction in various systems is described below

6.1.1 Statement and review of the problem

We consider two particles of identical size in shear flow. The centers of mass of the two particles are in same plane of shear. The two interacting particles are on different streamlines moving with different velocities. For simplicity we herein assume one vesicle is at the origin of the reference frame ($X = 0$, $Y = 0$) at constant position and an another vesicle follows a trajectory from its initial position X_{in} and Y_{in} ($\mid X_{in} \mid \gg R_0$ where R_0 is the effective radius of the particle).

After travelling a distance X_{in}, the particle meets the other one which is located at the origin and crosses it. During the crossing it is displaced in the Y direction from its initial lateral position and after crossing relaxes towards its final lateral position. Studies on drops and capsules showed that in the limit of dilute suspension spherical objects came back to their initial Y coordinate and initial streamline. In the general case, the particle does not relax to Y_{in} and a net lateral displacement is observed with a final coordinate Y_{fin}, as shown in fig. 6.1.

For spheres, cross-stream lateral displacement is expected to be negligible from symmetry arguments by considering the linearity of the Stokes equation [83]. To break the symmetry of the problem three body interactions are necessary, which are negligible in dilute suspensions.

In other cases when roughness with a relative amplitude of $\approx 4.7 \times 10^{-5}$ is considered, interacting spheres are shifted from their initial streamline and

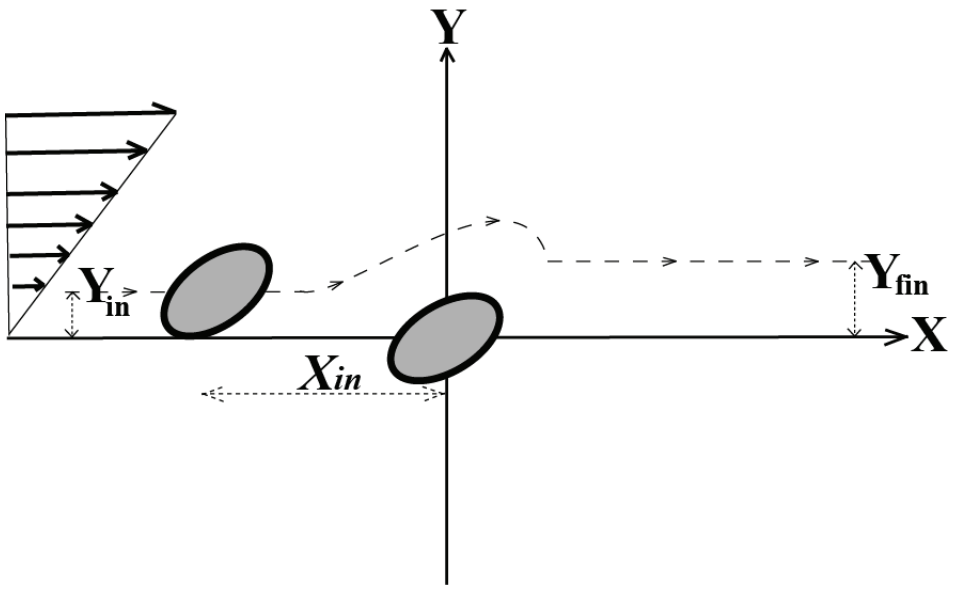

Figure 6.1: Schematic of the relative trajectory between a pair of interacting vesicles

the collision is asymmetric. The amplitude of the net displacement increases with rugosity, as shown from da Cunha and Hinch [83]. For deformable particles such as drops, bubbles, vesicles or cells, the deformation of the particles under shear breaks the fore-aft symmetry of the problem and leads to a repulsion when the trajectory of two deformable particles meet under shear flow.

For example, the deformation of drops is governed by shear rate (or capillary number $Ca = \eta U/\sigma$ where σ is surface tension) and viscosity ratio ($\lambda = \eta_{in}/\eta_{out}$) , and has an influence on the mechanism of interaction. Thanks to their deformability, they can slide over and around each other with reduced dissipation. At moderate value of the capillary number i.e. $Ca > 0$ (~ 0.1 to 0.4) with no viscosity ratio between inside and outside ($\lambda = 1$), drops are largely deformed and spacing between them is minimum as a result cross stream displacement is larger, as shown by Lowenberg and Hinch [84]. When the variation in viscosity contrast is taken into account i.e. as the internal viscosity increases ($\lambda > 2$) the deformation in shape decreases as a result drops behave almost like spherical particles which leads to a reduction in cross-flow displacement.

During the hydrodynamic interaction of capsules, which are bounded by a thin elastic membrane capable of sustaining elastic deformation in shear flow, Lac et al. showed that their trajectory is irreversibly shifted [85]. Buckling of

membranes were also observed during the separation phase of capsules. This theoretical prediction shows qualitative agreement with Loewenberg's drop model but shows membrane mechanics plays a specific role. It was found that the trajectory displacement of a drop was about 30% higher than that of capsules.

Theoretically, it is challenging to study more than two deformable shapes in interaction. Wang, Mauri and Acrivos [86], [87] have shown an effect on cross stream diffusivity by considering the interaction of three spheres whereas Acrivos calculated far field streamline interactions by considering four spheres as two pairs [88].

While there have been many studies on pair interactions of particles, bubbles, drops or capsules, there are actually very few studies reported related to the quantitative study of the objects with membranes having mechanical properties similar to those of living cells.

Apart from the few experimental results reported by Kantsler [89] on the displacement of vesicles during their interaction in shear flow, no quantitative study of this phenomenon and the influence of parameters such as initial relative position and vesicle properties has been performed and many questions remain unanswered.

However, at the scale of a whole suspension in shear flow, direct consequences of hydrodynamic interactions have been observed and quantified : in a shear flow between plates, it has been observed that a vesicle suspension reaches a steady non-uniform distribution due to a balance between lift force that repels vesicles away from walls, and shear-induced diffusion due to repulsion between vesicles during random interactions [90]. Interestingly, a poly-disperse suspension of vesicle is sheared between two plates, the small vesicles interact with large vesicles and are pushed towards the wall: the population of large vesicles is concentrated around the center of the flow while smaller vesicles show a dissipation in their distribution near the center, as shown in fig. 6.2.

As shown by Da Cunha and Hinch [83], in a suspension of deformable particles of size R in a shear flow, a shear-induced diffusion coefficient due to pair interactions can be computed as:

$$D = f_i R^2 \dot{\gamma} \Phi \tag{6.1}$$

where $\dot{\gamma}$ is the shear rate, Φ the volume fraction of particles in the sus-

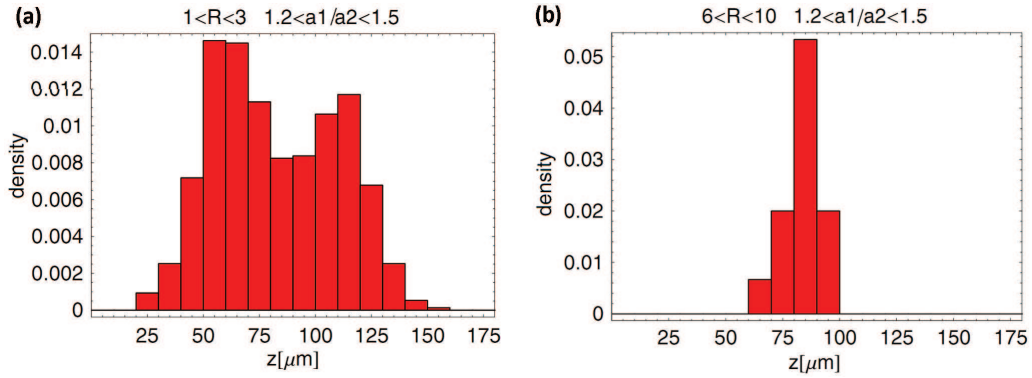

Figure 6.2: Steady distribution of (a) small and (b) large vesicles with no viscosity contrast. z is the distance between two plates that are separated by $180\mu m$, R is the radius of vesicle and a_1/a_2 aspect ratio [90]

pension and f_i is a dimensionless diffusion coefficient which is proportional to the mean square displacement of particles during interactions averaged over all possible initial relative positions, $f_i = f_2$ or f_3 for cross-flow self-diffusion in the direction of velocity gradient or vorticity.

In order to derive the shear induced diffusion coefficient from microscopic interactions, it is therefore necessary to make quantitative measurements of the repulsion of vesicles during pair interactions by varying the initial relative positions, and quantify the effect of parameters such as vesicle size, reduced volume and viscosity ratio.

Ideally, for a complete understanding of the effects measured at the scale of the suspension [90], it would be useful not only to study interactions between identical vesicles, but also between vesicles of different sizes, which could shed light on phenomena such as possible segregation effects in polydisperse suspensions. Such effects are biologically relevant (a segregation between blood cells and platelets is sometimes observed in blood flow in small vessels) and could also be interesting for microfluidic manipulation and separation of cells.

6.2 Preparation and experimental set-up

To achieve a good probability of interaction between vesicles in experiments, an experimental set-up has been designed to produce a narrow layer of concentrated vesicles in a larger shear flow. This set-up is described in section 6.2.1.

6.2.1 Microfluidic flow focusing system

To study the interaction between two vesicles, it is necessary to have a sufficiently high concentration of vesicles to maximize their probability of interactions. If the initial average lateral distance between two interacting vesicles is more than their radius, the possibility of interaction between them is low. On the other hand, if the concentration is too high, the interactions will not be isolated and be perturbed by the presence of many other vesicles, in addition to possible optical problems.

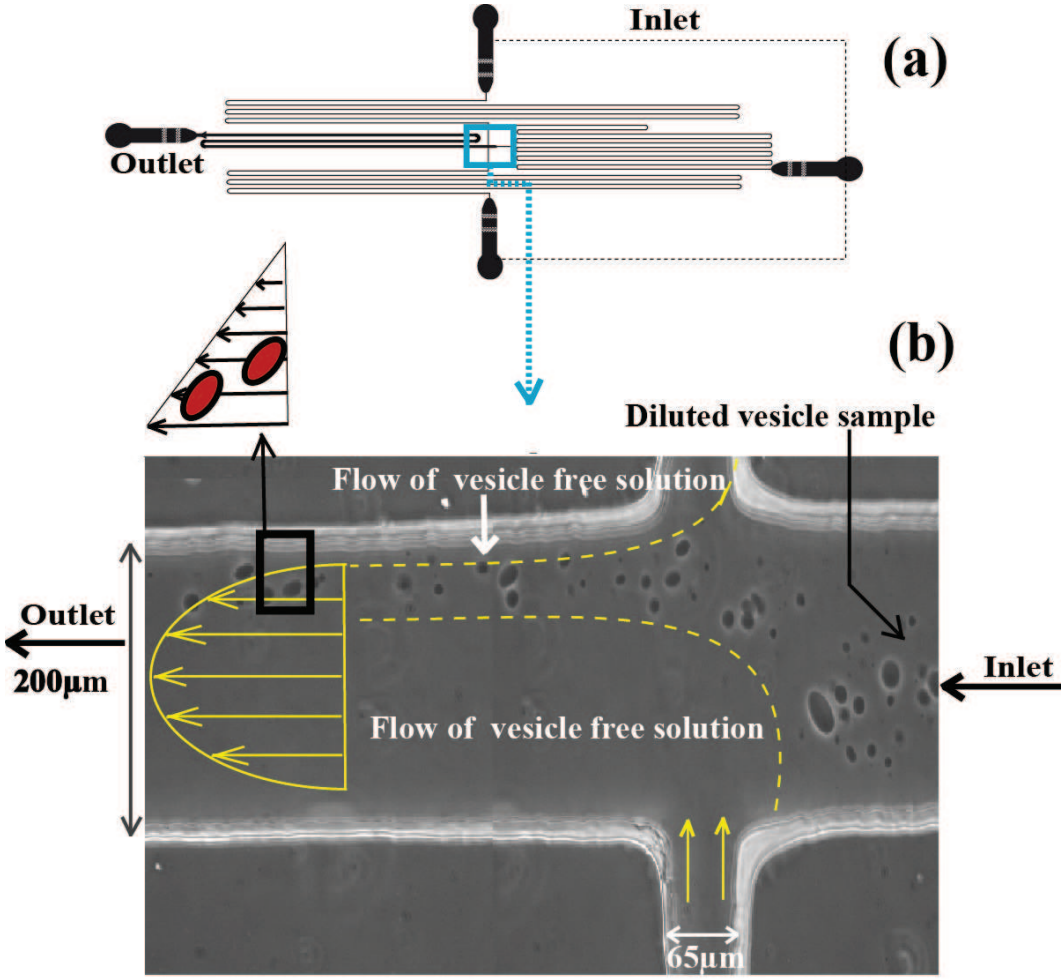

Figure 6.3: (a) Schematic of the microfluidic device used in the experiments: the width of the channel is $100\mu m$ and the overall length is 60mm (b) Vesicles jet in the flow confinement inside the channel

Therefore it was decided to use a focused flow of a vesicle suspension in a larger channel, which has the advantage of producing a locally highly

concentrated suspension and therefore enhance the interaction probability, without having too many parasite interactions. Many tests on micro channels of different geometries were done in order to determine the best geometry of channel. A micro-channel of PDMS elastomer dedicated to the study of interactions has been designed. A geometrical description of the flow profile of vesicles dilute suspensions is presented in fig. 6.3.

The channel has three inlets of typical width 65 μm (1/3 of the width of the main channel where the observation is made) and length 200 mm each and an outlet of width 200 μm and length 65 mm. The choice of length for these channels has been dictated by the need to precisely control the different flow rates by gravity (the pressure at each inlet is imposed by hydrostatic pressure). The common region where the three inlets meet and the confinement of vesicle takes place, is shown in fig. 6.3. A narrow inlet which is parallel to outlet(shown right side of the channel) carries the vesicles suspension while two other narrow inlets which are in the perpendicular direction bring vesicle-free fluid at a higher flow rate on each side of the vesicle suspension jet and pinch it. The lateral position of the vesicle suspension in the interaction channel (e.g at center of channel or near the upper or lower wall) can be adjusted by varying the relative pressure of two branches of vesicle-free fluid. The typical thickness of the channel where the interaction is observed is $\approx 100\mu m$.

6.2.2 Flow set-up :

A nearly 2D Poiseuille flow with a parabolic velocity profile across the thickness of channel is achieved in the configuration shown in figure. 6.3. When two vesicles of identical size are in flow, they must be in two different streamlines to overcome each other, as illustrated by the inset of fig. 6.3. The flow of inlets and the outlet were controlled by varying the height of reservoirs with the help of a computer controlled motorized elevator, as shown in figure. 6.4.

The height of the elevator was varied of a typical order of magnitude ≈100-200mm. When internal and external viscosities are identical ($\lambda = 1$) the density difference is 0.02 g/l which leads to sedimentation velocity 92μm/sec for a vesicle of size 20μm. To prevent sedimentation that would bring vesicles out of the observation plane approximately at the middle of the channel's thickness (X-Z plane), the X direction is oriented parallel to gravity. The microscope is tilted and the microscope stage is vertical. A picture of the tilted microscope and a close-up of the interaction channel mounted on a home-made stainless steel holder keeping the chamber horizontal is shown

in figure. 6.4.

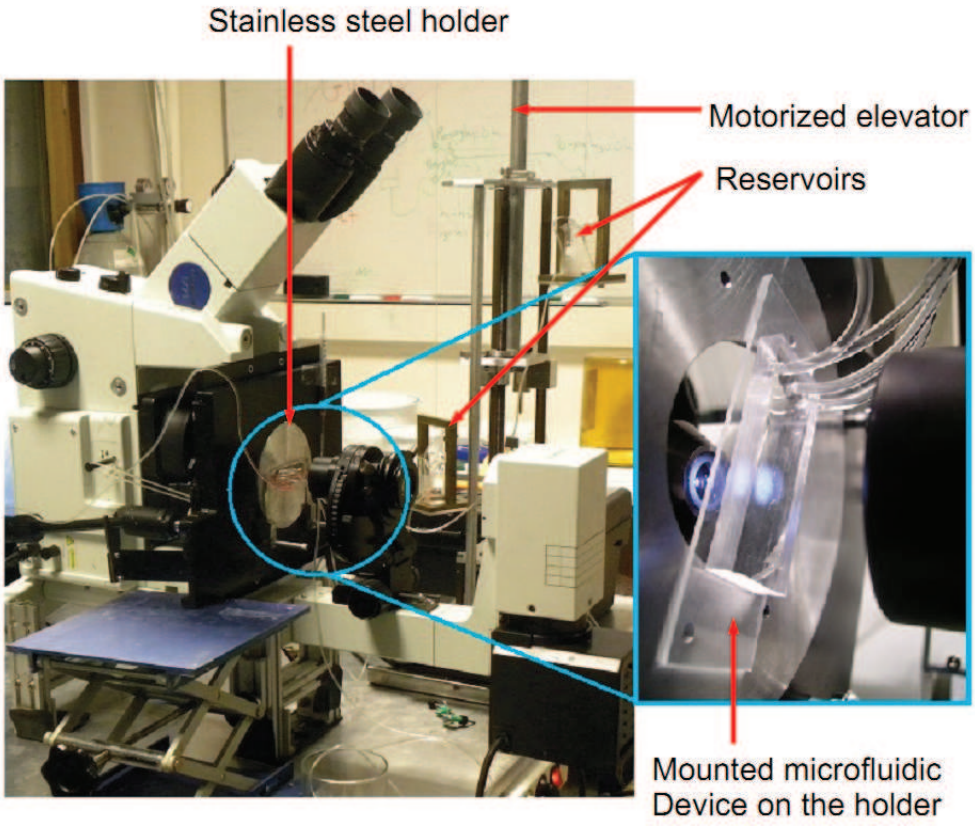

Figure 6.4: Experimental set up: the tilted microscope allows an observation perpendicular to gravity.

6.2.3 Sample preparation :

For the preparation of vesicles we used the electroformation method as described in chapter 4(sec. 4.1.4). To study vesicles without viscosity contrast ($\lambda \simeq 1$), vesicles were swollen in an internal solution of 300mM sucrose and mixture of 20% glycerol and 80% ultrapure water, and they were suspended in an external solution of 370mM glucose and mixture of 20% glycerol and 80% deionized water. Observations were made by diluting the vesicles sample in ratio 1:3 in external solution. Three different viscosity contrasts were also studied, a brief description of their respective viscosities and compositions is presented in tables 6.1, 6.2 and 6.3.

Solution	$\lambda = 1$	Viscosity (m Pa.s)
IS	300mM sucrose + (20%glycerol + 80% water)	2.2
ES	370mM glucose + (20%glycerol + 80% water)	2.2

Table 6.1: Measured viscosities of internal solution (IS) and external solution (ES) at T = 23°C

Solution	$\lambda = 3.8$	Viscosity (m Pa.s)
IS	100mM sucrose + 3.3%dextran	4.2
ES	115mM glucose	1.1

Table 6.2: Measured viscosities of internal solution (IS) and external solution (ES) at T = 23°C

Solution	$\lambda = 0.28$	Viscosity (m Pa.s)
IS	300mM sucrose	1.1
ES	316mM glucose + 3% dextran	4.0

Table 6.3: Measured viscosities of internal solution (IS) and external solution (ES) at T = 23°C

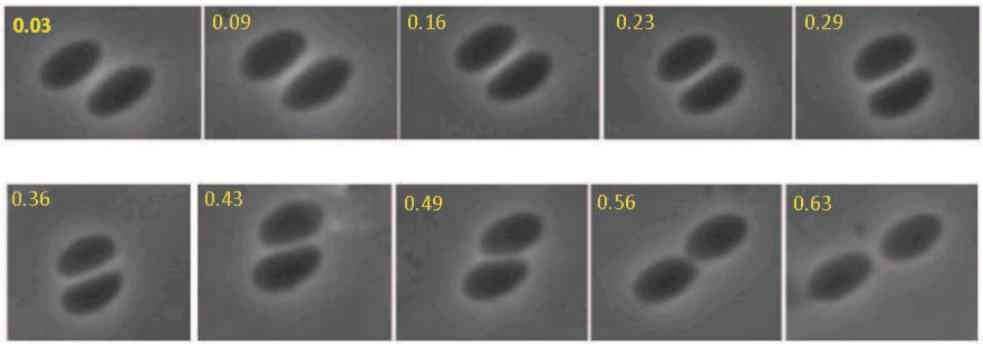

Figure 6.5: Snapshots of interacting vesicle pairs with λ= 1 and ν= 0.89 with radius typically 10 μm. Typical time between first and last image is 0.6s

6.3 Results and discussions

The trajectories, and especially the lateral displacement of a vesicle pair during hydrodynamic interaction was studied by varying the reduced volume and viscosity contrast. The reduced volume typically varies between 0.65 and 0.99 in experiments without viscosity contrast ($\lambda \approx 1$). An example of

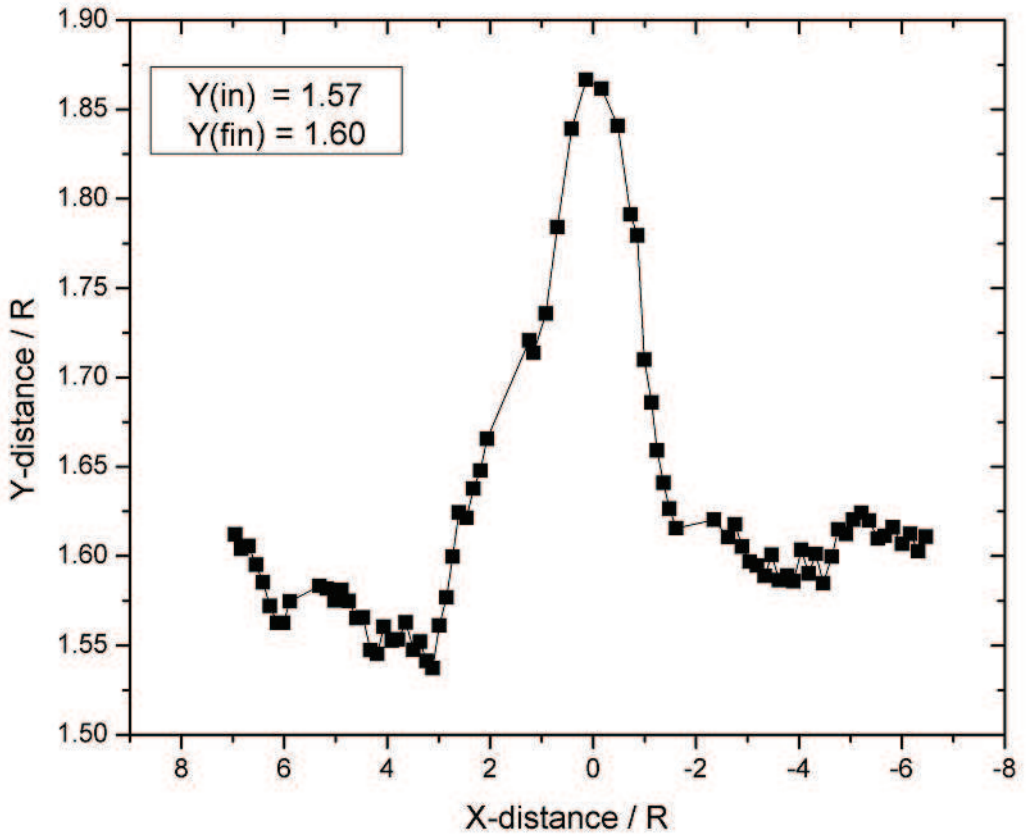

Figure 6.6: Relative trajectory of the two interacting quasi-spherical vesicles : Y-position shows the lateral difference between two deformed vesicles. The average reduced volume of the interacting vesicle pair is ν= 0.980 and typical radius=8.40 μ m

such an interaction is presented in fig. 6.5, with two vesicles of identical size.

When two spherical (and thus non-deformable) vesicles of identical size interact, after interaction they relax to their initial streamlines as if no interaction had occured. In fig. 6.7 lateral displacement between two quasi-spherical vesicles of reduced volume $\nu \approx 1$, after interaction is shown. If one compares the initial lateral position and final lateral position, the difference between them ($Y_{in} - Y_{fin}$) is 0.168 which is negligible in comparison with deformed shapes (6.7) and shows nearly no effect of interaction.

On the other hand, in the case of a pair of deflated vesicles of identical size an irreversible lateral displacement is observed. A pair of vesicles with a reduced volume of about 0.780 shows a significant displacement from initial streamlines, as shown in fig. 6.6. The difference $Y_{ini} - Y_{fin} \approx 4.35$ microns

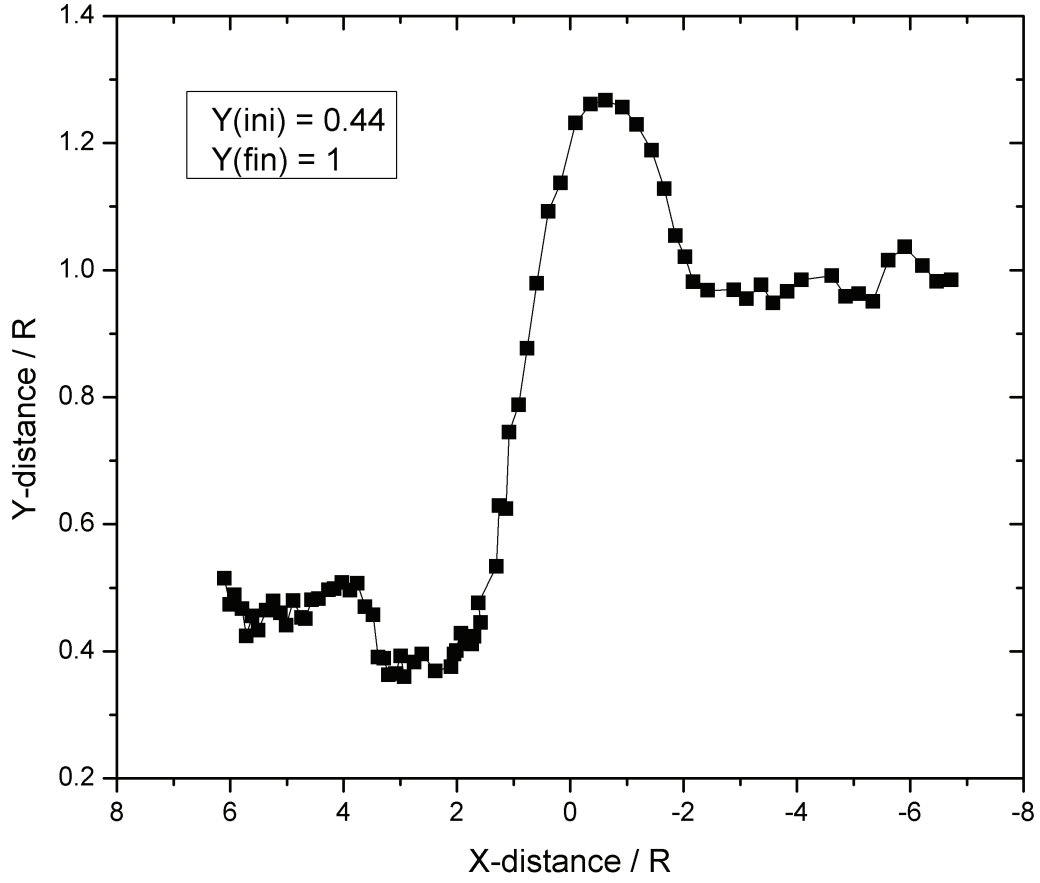

Figure 6.7: Relative trajectory of two interacting deformed vesicles : Y-position shows the lateral difference between two deformed vesicles. The average reduced volume of the interacting vesicles pair is $\nu = 0.780$ and typical radius=7.25 μm

is significantly higher than the case shown in 6.7. Quantitative results with many pairs of deformed and non-deformed shapes of vesicles of various size and reduced volumes are presented below.

The experimental relative trajectories of vesicles can be compared to the results of numerical simulations made in the group by Pierre-Yves Gires using a boundary integral method (Fig. 6.8). Qualitatively similar trajectories were found, by varying the capillary number from 10 to 100. In both the experimental and numerical cases, the lateral distance is maximum when the two vesicles are at the same X coordinate, then relaxes to a lower value which, for deflated vesicles, is still greater than the distance before interaction.

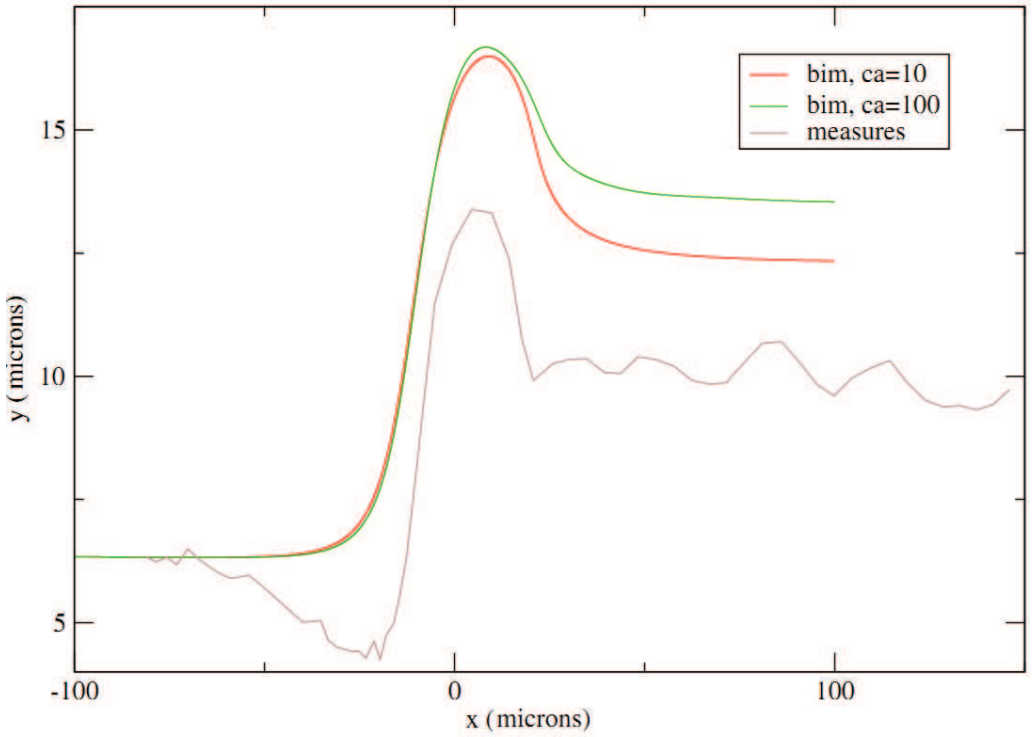

Figure 6.8: Lateral trajectory displacement of interacting vesicles(numerically): change in position in lateral distance vs X-direction between them. capillary number=10 (red line), at capillary number= 100 (green line), experimental measurements (pink line) of a vesicles pair of $\nu = 0.94$ and typical radius=9.28 μ m

When the shear rate is low (or the capillary number Ca is low), the shape of vesicles stays close to their equilibrium shape and they are less expected to deform during the different phases of the interaction. On the other hand, at high shear rate they experience larger variations of hydrodynamic stresses during the phase where their distance is smallest: strong shear and extensional stresses are experienced during this phase. From the numerical study shown in fig. 6.8, it is found that at low capillary number ($Ca = 10$), the net lateral displacement after interaction is smaller than at higher capillary number ($Ca = 100$) for the same vesicles.

In fig. 6.8, a comparison is made with an experimental trajectory. While the amplitude of the displacement is lower in the experiment due to the 3D

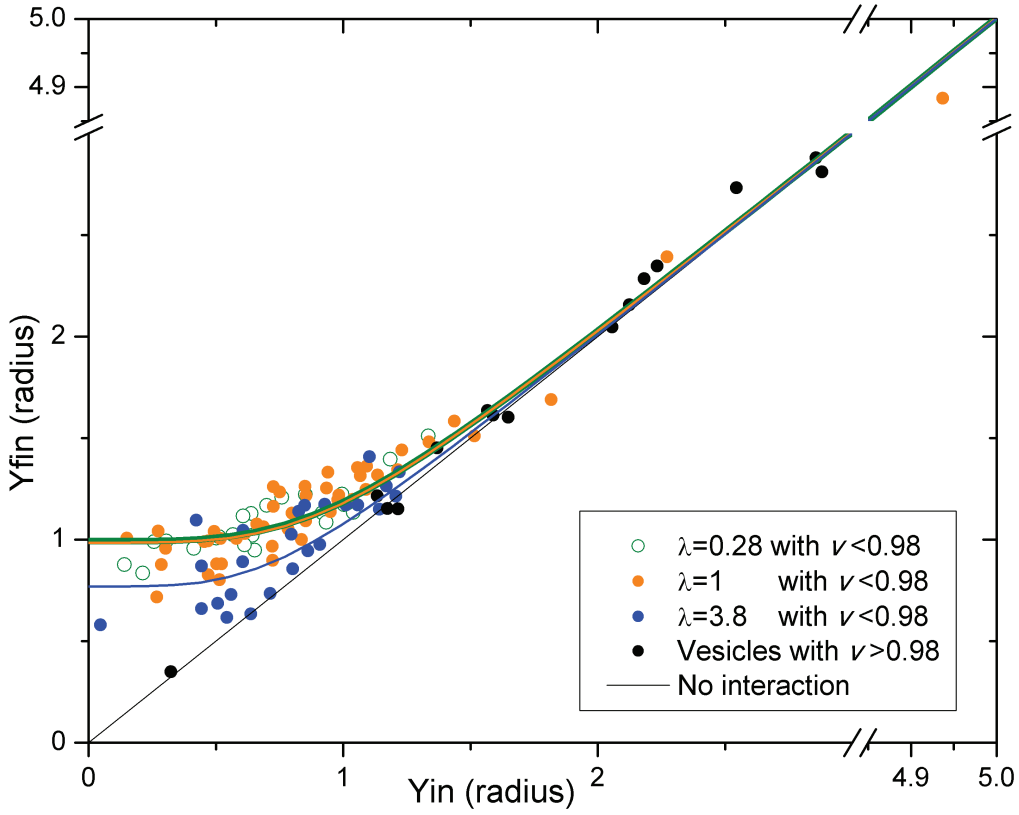

Figure 6.9: Relative lateral displacement of interacting pairs of identical vesicles. The diagonal line presents no interaction. black spheres - vesicle pair of reduced volume ≈ 1, orange spheres - vesicle pair with no viscosity contrast, blue spheres - when viscosity contrast is 3.8 whereas green spheres - when viscosity contrast is 0.28. Full lines show fits to equation 6.4

nature of simulations, the overall behaviour is the same. This experimental study on the trajectory vesicles (as well as its numerical counterpart) shows qualitative similarities with former studies on the interaction of drops and capsules [84, 85].

We made a systematic study of the influence of the initial lateral distance Y_{ini} of vesicles on the interaction by varying vesicle size, reduced volume and viscosity contrast. As expected, since the perturbation of the flow decreases like $1/r$ in Stokes flow, the lateral displacement of a vesicle pair during the interaction is a decreasing function of their initial distance in the direction transverse to the flow.

All the experimental results are shown in Fig. 6.9 where the final distance

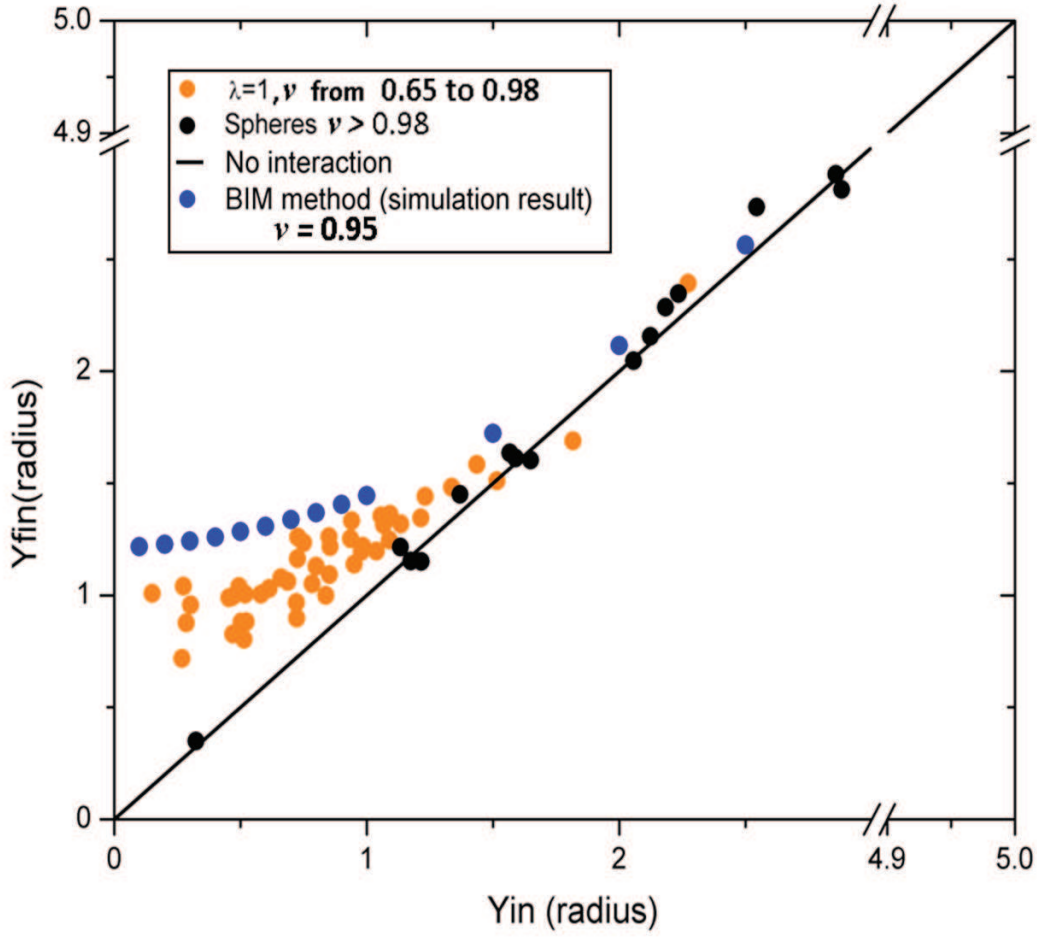

Figure 6.10: Relative lateral displacement of interacting vesicle pair (numerical result)at $\lambda = 1$, (orange spheres) experimental measurements and (blue spheres) Boundary Integral method

Y_{fin} is plotted versus initial distance Y_{ini} for different values of the viscosity ratio λ. The quasi-spherical vesicles with reduced volume $\nu > 0.98$ are also highlighted in black and show no net displacement within experimental error, whatever the initial distance.

A general feature is that the effect of the interaction becomes negligible when the initial Y_{in} distance between vesicles is bigger than their diameter, as shown by the alignment of data points with the straight black line in fig. 6.9, and significant repulsion takes place when the lateral distance is shorter, with a relative displacement which can be as high as one vesicle radius.

For each series, the data is rather scattered due to the variation of re-

duced volume between different vesicle pairs. However except for the two sub population $\nu \leq 0.98$ and $\nu \geq 0.98$ no quantitative result on this influence of this parameter could be extracted from the data, due to the experimental errors. Intuitively, and by analogy to what is observed and computed for the lift of vesicles in shear flow near a wall ([91]), one expects more deflated vesicles to be more displaced, at least for $\lambda = 1$.

Note that part of the scattering in the data could also be due to imperfections in the co-planarity of the two vesicles in the same plane of shear: a small mismatch leads to a decrease in the intensity of interaction. A weak effect of the viscosity ratio is observed in the results: on average when λ increases, the repulsion between vesicles decreases slightly. This is coherent with the effect of viscosity ratio on other phenomena of lift and lateral displacement of vesicles in flow [92] . This is a consequence of the lower inclination angle of a vesicle in tank-treading motion in shear flow, which decreases the asymmetry at the source of these related drift phenomena.

The numerical results obtained by the boundary integral method are in nearly quantitative agreement with the experiment as shown in fig. 6.10.

Note that an analytical result obtained by an asymptotic expansion of vesicle shape around a sphere is shown in this figure. While there is qualitative agreement, there are quantitative differences for small initial distances of vesicles due to the fact that the interaction between vesicles is computed with a perturbative approach.

We can suggest the following empirical relation between initial and final lateral position by following the model proposed by P. Olla [93] and confirmed by Callens et al [94]. For the lift of a vesicle near a wall:

$$\frac{dy}{dt} = \frac{lR^3\dot{\gamma}}{y^2} \tag{6.2}$$

where l is a constant that depends on viscosity contrast and reduced volume , $\dot{\gamma} = V_x/y$ and $V_x = \mathrm{dx/dt}$, thus equation 6.2 becomes

$$y^3 dy = lR^3 dx \tag{6.3}$$

if we integrate eq. 6.3 along the trajectory, we get

$$\frac{1}{4}[y_{fin}^4 - y_{ini}^4] = lR^3 x$$

where x is the distance covered by one vesicle when it interact with the other. This distance scales with the diameter of vesicle, we will get

$$\frac{y_{fin}^4}{R^4} - \frac{y_{ini}^4}{R^4} = L$$

By replacing $\frac{y_{fin}^4}{R^4} = Y_{fin}$ and $\frac{y_{ini}^4}{R^4} = Y_{ini}$, we get an empirical law as given by,

$$Y_{fin} = \sqrt[4]{Y_{in}^4 + L} \tag{6.4}$$

$L^{1/4}$ is the maximum displacement obtained when vesicles are initially very close and is related with diffusion coefficient. The fit of experimental measurement of different viscosity by this law is shown in fig. 6.9. Such a correlation is essential for the derivation of a shear induced diffusion coefficient which is related to the integral of the square of the displacement $(Y_{fin} - Y_{in})^2 = (\Delta Y)^2$ over all possible initial configurations.

In this study, we concentrated on a pair of vesicles in the same plane of shear. For completeness, one would need to also study the effect of misalignment in the third dimension Z_{in}. This is a challenging task from the experimental point of view, but it can certainly be studied numerically.

For a first estimation of the diffusion coefficient, one could assume that the lateral displacement $(Y_{fin} - Y_{in}) = \Delta Y$ decreases with Z_{in} as it decreases with Y_{in}. In this case function $\Delta Y(Y, Z)$ becomes

$$\Delta Y(Y, Z) = \frac{f_L(Z) f_L(Y)}{\sqrt[4]{L}}$$

where $f_L(Y)$ and $f_L(Y)$ can be defined from equation 6.4, as following $f_L(Y) = \sqrt[4]{Y^4 + L} - Y$; $f_L(Z) = \sqrt[4]{Z^4 + L} - Z$.

The dimensionless diffusion coefficient can be analytically calculated from the equation proposed by Lowenberg [84], given by

$$f_2 = \frac{3}{2\pi\sqrt[4]{L}} \int_0^\infty \int_0^\infty Y(\sqrt[4]{Y^4 + L} - Y)^2 (\sqrt[4]{Z^4 + L} - Z)^2 dY dZ \tag{6.5}$$

By substituting $u = \frac{Y}{\sqrt[4]{L}}$ and $v = \frac{Z}{\sqrt[4]{L}}$ in equation (6.5) one gets,

$$f_2 = \frac{3L}{2\pi} \int_0^\infty u(\sqrt[4]{u^4 + 1} - u)^2 du \int_0^\infty (\sqrt[4]{v^4 + 1} - v)^2 dv \tag{6.6}$$

The numerical evaluation of equation (6.6) shows that f_2 is proportional to L by factor of 0.019. In the study of drops, the coefficient f_2 is found to be equal to 0.02 for λ= 1 and in the limit of low Ca [84]. On the other hand, the

diffusion coefficient of vesicles under shear and lift force is shown to be equal to 0.1 [90]. In our case, the determination of f_2 of two interacting vesicles in dilute suspension is of different order of magnitude than the former work on vesicles. The calculated value are presented in tab. 6.4. On the contrary, they show good agreement with the study on drops. The discrepancy with the value found for vesicles in [90] could be due to the rough estimate we made for the variations of Y_{in} in the z direction.

Viscosity contrast	L by fit	calculated value of f_2
$\lambda = 1$	0.94	0.017
$\lambda = 3.8$	0.35	0.006
$\lambda = 0.28$	0.97	0.018

Table 6.4: f_2 values

At the microscopic level, hydrodynamic interaction between two particles in shear flow leads to a repulsion. On the other hand, at the scale of whole suspension, the statistical effect of interactions between particles in shear flow leads to shear induced diffusion, which is studied quantitatively for a particular flow geometry in the next chapter.

CHAPTER 6. HYDRODYNAMIC INTERACTION BETWEEN TWO VESICLES IN SHEAR FLOW

Chapter 7

Shear induced diffusion of RBCs in Poiseuille flow

Nous étudions la diffusion induite par cisaillement d'un nuage de globules rouges injecté dans un écoulement en canal. L'équation d'advection-diffusion non linéaire est établie pour ce problème, et une analyse théorique de quelques cas limites est présentée. Nous montrons qu'en fonction des conditions, la longueur caractéristique de diffusion peut varier comme $x^{1/3}$ ou $x^{1/2}$ où x est la distance parcourue. Une étude expérimentale est réalisée, et alors qu'une loi de puissance pour la dépendance spatiale est généralement trouvée, une grande gamme d'exposants apparaît, ce qui suggère une superposition d'effets de la diffusion dans différ ents plans de l'écoulement et éventuellement un rôle des interactions à 3 corps dans les situations localement concentrées. Finalement, ceci devrait conduire à un moyen simple de mesurer les coefficients de diffusion induite par cisaillement.

We study the shear induced diffusion of a focused cloud of red blood cells injected in a channel flow. The non-linear advection-diffusion for this problem is establish and a theoretical analysis of a few limit cases is presented. We show that depending on the conditions, the characteristic diffusion lengths can vary like $x^{1/3}$ or $x^{1/2}$ where x is downstream distance. An experimental study is performed, and while a power-law for the space-dependency is generally found, a wide range of exponents is found, suggesting an interplay between diffusions in different planes and possibly an influence of 3-body interactions for locally concentrated suspensions. Ultimately, this should provide a way to measure shear induced diffusion coefficients in a simple way.

7.1 Introduction

In blood, the distribution of cells is non-uniform due to several phenomena for example the formation of clots or thrombi caused by the displacement of platelets towards the wall. The non-uniform distribution of cells (mainly vesicles) in shear flow is due to the interactions among neighbouring cells and lift forces exerted from walls as shown in microgravity experiment by Podgorski *et al* [90] for vesicles. In this study it is found that a steady distribution takes place with a well defined concentration profile that depends on vesicle properties (size, reduced volume and viscosity ratio). The distribution of large vesicles are concentrated at center of flow while small vesicles are pushed away from the center due to interaction with large vesicles.

The effect of interactions between vesicles in dilute suspension, is described in detail in chapter 6. Motivated by the fact that the difference in size of vesicles affects the distribution in overall suspension, it is therefore of great importance to study the diffusive behaviour of red blood cells or monodisperse suspensions of vesicles, induced by interactions. To obtain monodisperse and concentrated sample of vesicles is hard task and self-diffusivity of red blood cells in flow has rarely been studied, so far. It is also motivating to study the phenomena in geometries and flows that are different from the one studied on microgravity experiments [90]. Indeed this kind of diffusion is non-linear and therefore its quantitative features should strongly depend on detail of the flow. For all these reasons, we chose to investigate the diffusivity of a jet of red blood cells initially confined in a Poiseuille flow in a channel by measuring the widening of the red blood cells suspension when travelling downstream.

7.2 Theoretical background

The dispersion of RBCs in the blood flow can be studied by the determination of the diffusion coefficient. According to Fick's law, diffusion flux is given by:

$$\vec{J} = -D\vec{\nabla}\Phi,$$

where, $\vec{J}$ is the flux per unit area, $\vec{\nabla}\Phi$ is the rate of change of concentration and D is the diffusion coefficient depending on nature of the substance.

As we concentrated our study to determine the diffusion coefficient of particles under flow, we explain few examples of diffusion in order to make better understanding of the subject.

7.3 The advection-diffusion equation

In case of 2D flows of diffusing particles, we consider that, the particles of volume fraction $\Phi(x, y, t)$ are flowing in x direction which is also the flow direction. Suppose the suspension velocity is $v(y)$ and particles are flowing with the same velocity. Then x-component of particle diffusion is negligible as compared to the advection. Due to the advection x-direction, the amount of particles in a small volume around (x, y), the volume in particles $\Phi(x, y, t)dxdydz$ varies whereas the diffusion occurs in a perpendicular direction of the flow. We get the following conservation equation.

$$\begin{aligned}\frac{\partial \Phi}{\partial t} dxdydz = {} & v(y)dydz\,\Phi(x, y, t) - v(y)dydz\,\Phi(x + dx, y, t) \text{ (advection)} \\ & + \big[- D(x, y, t)\frac{\partial \Phi(x, y, t)}{\partial y} dxdz \\ & - \big(- D(x, y + dy, t)\frac{\partial \Phi(x, y + dy, t)}{\partial y} dxdz\big)\big] \text{ (diffusion)}, \quad (7.1)\end{aligned}$$

which simplifies into

$$\frac{\partial \Phi(x, y, t)}{\partial t} = -v(y)\frac{\partial \Phi(x, y, t)}{\partial x} + \frac{\partial}{\partial y}\big(D(x, y, t)\frac{\partial \Phi(x, y, t)}{\partial y}\big). \quad (7.2)$$

The above solution cannot be further simplified. In the general case a few approaches have been attempted to calculate the diffusion coefficients of concentrated suspension in flow for different limit case, which are described in the following section.

Note that the equation above is already a simplified one, as we do not taken into account effects due to gradients of shear rate. We expect concentration gradients to be the main motivation for diffusion, because of the peculiar experiment we consider.

7.4 Thermal diffusion

In thermal diffusion, D is constant. Let us consider an experiment, for instance, a rectangular channel of high aspect ratio. At the inlet of the channel

constant initial condition is imposed in such a way that fluid velocity v does not depend on y. If one observes evolution of the stationary distribution of particles along the channel, the corresponding equation can be written as :

$$v\frac{\partial \Phi}{\partial x} = D\frac{\partial^2 \Phi}{\partial y^2} \tag{7.3}$$

The above equation can be solved with Fourier series depending on initial condition. For instance, the following solution describes the widening of a Gaussian particle distribution,

$$\Phi(x,y) = \frac{\Phi_0}{\sqrt{4\pi Dx/v}} \exp\big[-vy^2/(4Dx)\big]$$

We can see from the solution that the width scales as $x^{1/2}$ and amplitude scales as $x^{-1/2}$. From the scaling of the width one can identify the relevant parameter as $yx^{-1/2}$. Therefore in order to work with dimensionless parameters, we define $\eta = y(Dx/v)^{-1/2}$ where, D/v has the dimension of a distance and is the typical length-scale of the problem. A similar solution was shown by Taylor [95], in a Poiseuille flow when velocity profile v was not homogeneous. In his study, determination of the diffusion coefficient depends on other parameters of the problem.

7.5 Shear-induced diffusion

Shear-induced diffusion has been studied at two different levels: self-diffusion of individual particles and collective process of gradient diffusion. The present work is particularly concerned with shear-induced diffusion due to hydrodynamic interactions on the particle level.

The diffusion of RBCs from the flow of concentrated suspension is influenced by microscopic interaction among them as described by the following example. When a concentrated suspension of particles is subjected to shear flow, individual particles tend to follow the flow of their streamlines. On their way they encounter particles of neighbouring streamlines with different velocities.

In fig 7.1 a concentrated suspension of particles in simple shear flow is depicted. A marked particle which is following its trajectory (shown with dotted line in fig. 7.1), meets the neighbouring particles. The neighbouring particles bounce on the marked particle and divert it from its initial trajectory. Consecutive interactions with particles leads to irreversible displacement. At

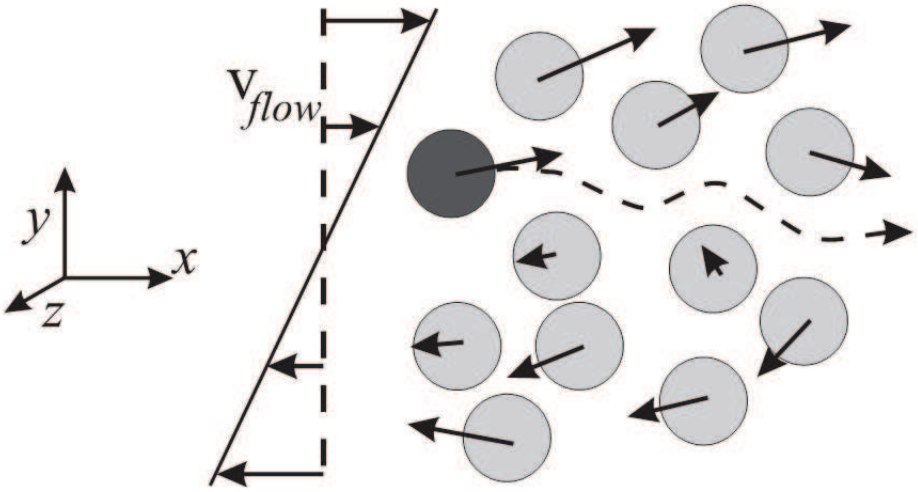

Figure 7.1: Schematic picture of a concentrated suspension under shear flow

the macroscopic scale, several interactions among the neighbouring particles result in migration of particles in perpendicular direction of suspension flow. In this case, the diffusion coefficient D depends on the rate of interaction of two particles which is proportional to $\dot{\gamma}\Phi$. Furthermore, if the interaction takes place between three particles at same time the diffusion coefficient is proportional to Φ^2. This kind of diffusion is applicable in the concentrated suspension of particles and is a function of space and time.

The first study on the shear-induced diffusion of spheres and disklike particles in Couette flow by lateral migration was experimentally done by Eckstein et al [96]. The diffusion coefficient D was calculated by using the random walk theory when the velocity profile was linear and concentration (Φ) was uniform. It is predicted that diffusivity of spherical and disklike particles, made up of polystyrene, are same and depend on $D/R^2\dot{\gamma} \approx 0.025$. An other study on the diffusion coefficient of drops by considering pair wise interactions between identical drops was numerically done by Lowenberg [84]. On the assumption that emulsion is diluted ($\Phi = \frac{4}{3}\pi a^3 n$ where n is the number density of drops) and monodisperse, the diffusion coefficient is given by,

$$D = f_\alpha \Phi \dot{\gamma} R^2 \tag{7.4}$$

where $\alpha = 2$ or 3 for cross-flow self-diffusion in velocity gradient or vorticity direction. In drops, collision is irreversible and diffusivity is significant and depends strongly on viscosity ratio.

7.5.1 One particular case

Collisions between two spherical particles result in no net displacement but diffusion can occur when three spherical particles meet. A comparison between spherical particles and platelike clay particles by Rusconi and Stone [97] shows that diffusion is significant in platelike clay particles even at very low volume fraction Φ. The shear flow observation was made in a channel of large length (y-direction) and reduced thickness (z-direction). Under this condition the velocity v of flow does not depend on y and shear plane takes place in xz-direction, thus diffusion occurs in perpendicular direction of xz-plane i.e. in y-direction. At the inlets of the channel, constant initial conditions are imposed which leads to the time-independent equation, given by,

$$\frac{\partial \Phi}{\partial x} = K\dot{\gamma}\frac{\partial}{\partial y}\big(\Phi\frac{\partial \Phi}{\partial y}\big), \tag{7.5}$$

where K is defined by $D = vK\dot{\gamma}\Phi$. Here $K\dot{\gamma}\Phi$ has the dimension of a distance, and thus can be associated with x and y. In addition, this parameter is also function of an unknown volume fraction Φ. In the experiment of Rusconi and Stone, the main channel has two inlets, of which one is injected by particles of concentration Φ_0 and the other is being injected with particle free fluid. The spreading of the particles in the direction transverse to the flow direction give rise to shear induced diffusivity. To modelize the experiment, Rusconi and Stone suggested that the concentration was constant at the wall (implicitly meaning that it is a sourse of particles). The concentration of particles spreading with $\Phi = \Phi_0$ at one side and $\Phi = 0$ on the other side, by varying x. In this case, one can consider $A = K\dot{\gamma}\Phi_0$ and build dimensionless parameter $\eta = y(Ax)^{-}1/2$. Hence the solution can be found in the form of $\Phi(x, y) = \Psi(\eta)$. We have,

$$\frac{\partial \Phi}{\partial x} = \frac{\partial \Psi}{\partial \eta}\frac{\partial \eta}{\partial x} = -\frac{\eta x^{-1}}{2}\frac{\partial \Psi}{\partial \eta} \tag{7.6}$$

$$\frac{\partial}{\partial y}\big(\Phi\frac{\partial \Phi}{\partial y}\big) = \frac{\partial}{\partial y}\big(\Psi\frac{\partial \Psi}{\partial \eta}\frac{\partial \eta}{\partial y}\big) = ... = (Ax)^{-1}\frac{\partial}{\partial \eta}\big(\Psi\frac{\partial \Psi}{\partial \eta}\big). \tag{7.7}$$

In equation 7.5, the x^{-1} terms disappear, and one gets an equation for Ψ as a function of η: $-\Phi_0\eta\Psi' = 2\big(\Psi\Psi'\big)'$. This indicates the possibility for self-similar solution for Φ with a typical width scaling as $x^{-1/2}$, which is confirmed by the experiments [97].

7.5.2 More general case

We consider the case of time-independent distribution. This case also indirectly includes the one of the time-evolution of an initially x independent distribution. It is typically the case for a suspension under shear (either in a plane-plane shear chamber or in a Couette apparatus), where one can start with an initially homogeneous suspension or with a sedimented suspension on the bottom plate of the plate-plate shear chamber. In that case $\frac{\partial \Phi}{\partial x} = 0$ and equation 7.2 is the same as the time-independent equation 7.2 with constant v.

We consider now the general case where v can be written under the form $v \propto y^\nu$, and D scales as $\dot{\gamma}\Phi^m$, where $m = 0, 1, 2$ and $\dot{\gamma} \propto y^\delta$. As we want to focus only on exponents here, we will not take into account here the fact that $|\dot{\gamma}|$ must be considered instead of $\dot{\gamma}$. We also neglect any wall effect. Equation 7.2 becomes

$$y^\nu \frac{\partial \Phi}{\partial x} = A \frac{\partial}{\partial y}\big(y^\delta \Phi^m \frac{\partial \Phi}{\partial y}\big), \tag{7.8}$$

where A is a constant. We wish to find self-similar solutions of this equation and will therefore consider the variable $\eta = yx^{-\alpha}$, which means that we expect the typical width to increase as x^α.

Rusconi and Stone looked for solutions under the form $\Phi(x, y) = \Psi(\eta)$. However, this kind of solution will lead to a solution with fixed amplitude Φ_0, which is relevant in the case of the presence of a source, as they assumed, but not in the more common case of the spreading of an initial given amount of particles. In which case, if the width increases as x^α, particles volume conservation implies that the amplitude should decrease as $x^{-\alpha}$. We shall therefore look for solutions under the form $\Phi(x, y) = x^{-\alpha}\Psi(\eta)$.

Equation 7.8 becomes:

$$-\alpha\, x^{\nu\alpha-\alpha-1}\, \eta^\nu(\Psi + \eta\Psi') = x^{-m\alpha-3\alpha+\delta\alpha}\left(\delta\eta^{\delta-1}\Psi^m\Psi' + \eta^\delta(\Psi^m\Psi')'\right), \tag{7.9}$$

which leads to an equation for Ψ as a function of η if:

$$\alpha = \frac{1}{\nu + m - \delta + 2}. \tag{7.10}$$

For thermal diffusion in a flow of homogeneous velocity v, one has $\nu = m = \delta = 0$, therefore $\alpha = 1/2$ is the good choice, which corresponds indeed

to the Gaussian solution already evoked. Note that, in this particular case, if one looks for solutions under the form $\Phi(x, y) = \Psi(\eta)$ (spreading of a source), one finds also $\alpha = 1/2$.

On the contrary, in the case of the experiment by Rusconi and Stone, we find a different solutions according to the form chosen for Φ. In their experiment, we have $\nu = \delta = 0$ and $m = 1$, so $\alpha = 1/3$. The $x^{1/3}$ widening is therefore the expected behaviour once the finiteness of the available amount of particles is felt, in particular, for large x. One sees here that the necessity to have particle collision to get diffusion leads to slower diffusion (subdiffusion) by comparison with the thermal case.

In the case of the time-evolution of a suspension in a shear chamber, it is equivalent to consider the stationary equation with homogeneous v, so one has $\nu = \delta = 0$ and $m = 1$, so $\alpha = 1/3$. This was observed in parabolic flight experiments, when considering the cloud of lifting vesicles [90].

In the present study, we are concerned with the diffusive behaviour of the concentrated suspension of RBCs. Such a suspension will be introduced continuously in a microfluidic channel of section $2d \times 2h$ in the yz plane and flow in the x direction. The initial cluster will have a given initial width and initial position in the y direction, while it will be invariant in the third direction (across the channel thickness). We shall restrict ourselves to cases where the RBCs will not touch the walls, so that the above theoretical considerations are valid. As v scales as 1-$(y/d)^2$, there are two powers of y so the proposed scalings do not work. We shall then make simulations of equation 7.9 in order to seek for possible simplifications.

7.5.3 Detailed solutions for shear-induced diffusion under Poiseuille flow

We re-introduce the physical constants in the problem. Equation 7.2 becomes, in the stationnary case:

$$v_0(1 - y^2/d^2)\frac{\partial \Phi}{\partial x} = fR^2\frac{\partial}{\partial y}\big(|\dot{\gamma}|\Phi\frac{\partial \Phi}{\partial y}\big). \tag{7.11}$$

f is a dimensionless factor which depends on the details of the pair interaction, R is the typical particle size.

Considering the dimensionless y position $y^* = y/d$ and concentration $\Phi^* = \Phi/\Phi_0$, we get:

$$v_0(1-y^{*2})\frac{\partial \Phi^*}{\partial x} = \frac{fR^2\Phi_0}{d^2}\frac{\partial}{\partial y^*}\big(|\dot{\gamma}|\Phi^*\frac{\partial \Phi^*}{\partial y^*}\big). \tag{7.12}$$

There are two subcases: the main shear contribution is due to in-plane shear, or to out of plane shear, in which case we shall consider a constant mean effective shear rate.

In the latter case, we consider $\frac{v_0 d^2}{fR^2\Phi_0|\dot{\gamma}|}$ as the x scale. Otherwise, we have $|\dot{\gamma}| = 2v_0|y|/d^2 = 2v_0|y^*|/d$. The x scale is then given by $\frac{d^3}{2fR^2\Phi_0}$.

In both cases, we get the dimensionless equation, with $\delta = 0$ or 1:

$$(1-y^{*2})\frac{\partial \Phi^*}{\partial x^*} = \frac{\partial}{\partial y^*}\big(|y^*|^\delta\Phi^*\frac{\partial \Phi^*}{\partial y^*}\big). \tag{7.13}$$

We shall now drop the stars.

In case of homogeneous flow velocity, we have seen then that self-solution $\Phi(x,y) = x^{-\alpha}\Psi(\eta)$, where $\eta = yx^{-\alpha}$, exists providing $\alpha = 1/(3-\delta)$. Due to the $(1-y^2)$ term, it is more difficult to find self-similar solutions.

7.5.4 Contribution of in-plane shear

Equation 7.13 was numerically solved with Mathematica using the method of lines: the equations are discretized in the y direction, which results in a system of differential equations of the first order for the functions of x $\Phi(x, y_i)$. This method is efficient in that case where an initial condition $\Phi(0,y)$ is prescribed and diffuses as it flows in the x direction.

In figure 7.2, the concentration profiles are shown for different x positions for an initial condition $\Phi(0,y) = e^{-400y^2}$ (centered cluster). One sees clearly a convergence towards a universal triangular profile. As shown on figure 7.3, the amplitude exhibits a clear power-law as a function of x with an exponent A, which is found to be very close from -0.5. As seen on figure 7.4, the power-law behaviour of the width is less clear. If one looks at the local exponent by considering the local slope in the log-log plot of the width as a function of x, one finds that this exponent stabilizes around 0.5 and increases then slightly as the cluster spreads and occupies a significant law of channel width.

The 1/2 exponent is the one that is expected from the theory with homogeneous v. As the cluster spreads, the y^2 contribution in the velocity becomes non negligible compared to 1, and the approximation of homogeneous v becomes less relevant. However, we can see in figure 7.1 that the self-similar triangles are present even for wide distribution. This triangle solution is confirmed theoretically for homogeneous v:

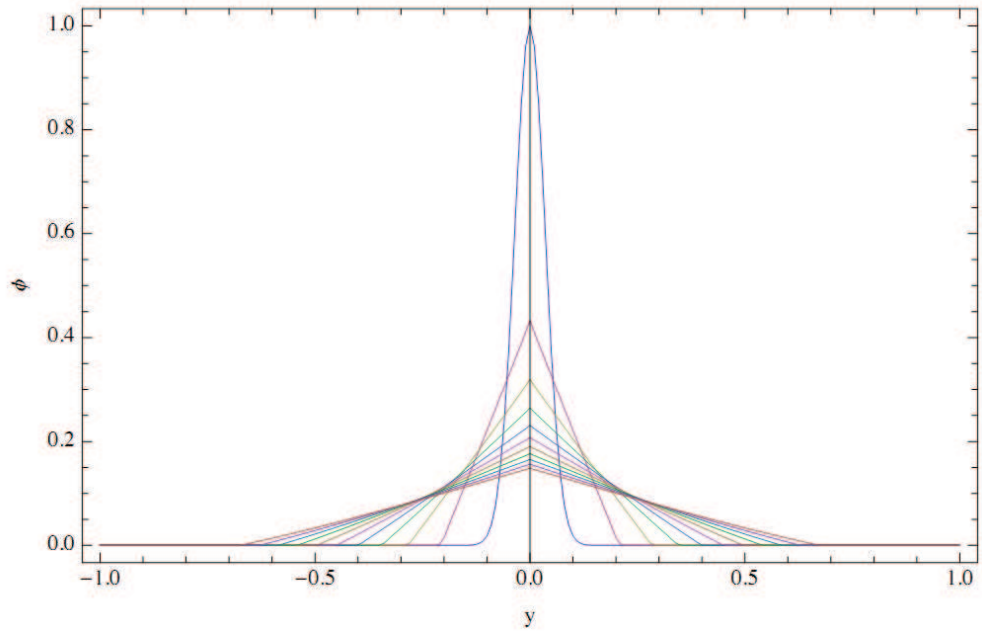

Figure 7.2: Concentration profiles from the numerical resolution of equation 7.13, for $x = 0$ to 2 by 0.2 steps, with centered initial condition.

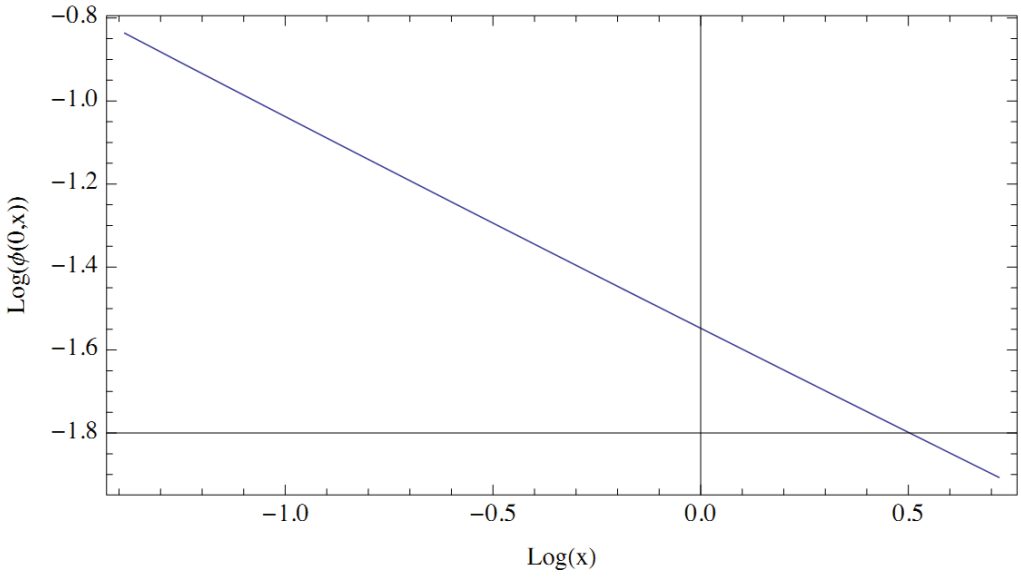

Figure 7.3: Log-log plot of distribution amplitudes as a function of x. The distributions are those of fig. 7.2. A fit gives $\Phi(0, x) = 0.21(x + 0.03)^{-0.494}$.

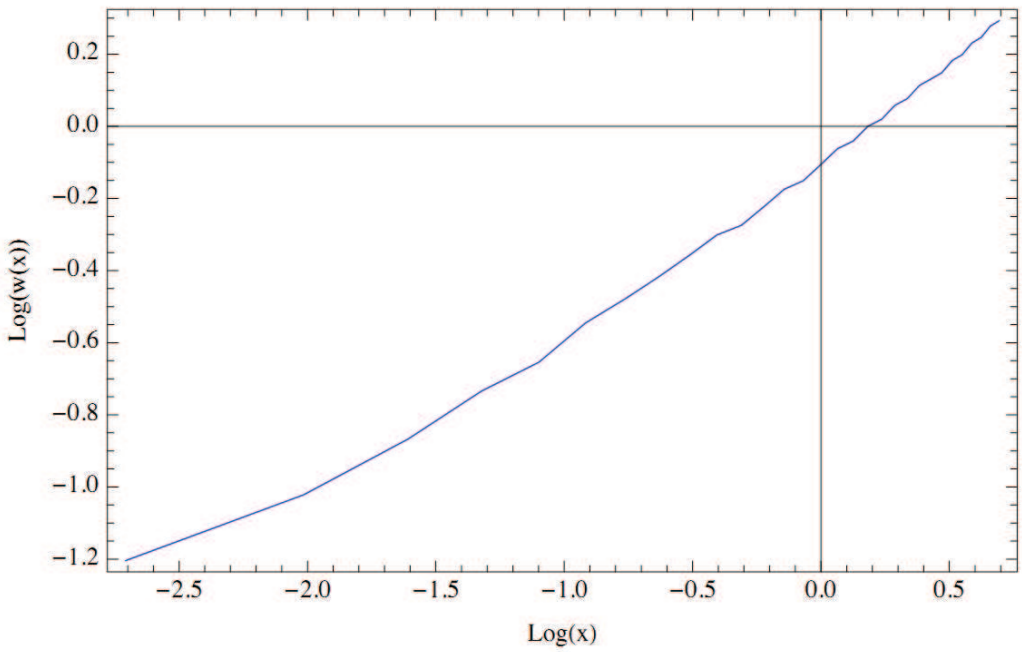

Figure 7.4: Log-log plot of distribution widths as a function of x. The distributions are those of fig. 7.2.

If $\delta = 1$, equation 7.13 gives the following equation for Ψ (see also eq.

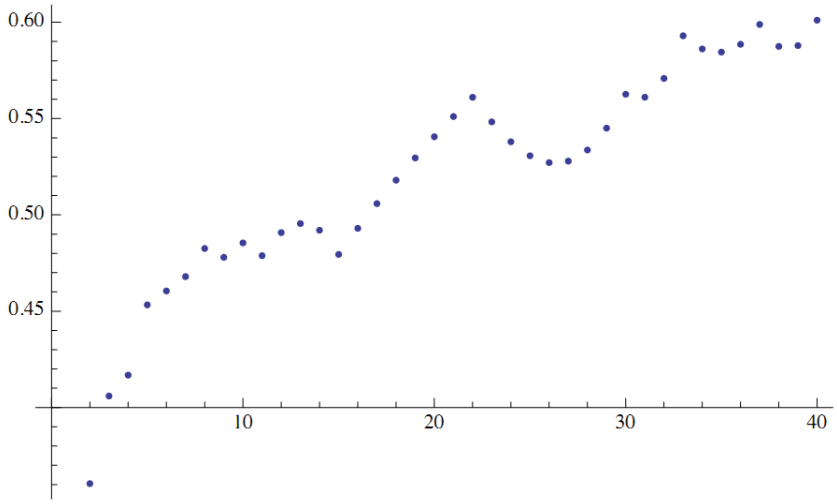

Figure 7.5: Sliding average of the exponent (averaged over an interval of 0.4 in x) for the distribution width as a function of x. The distributions are those of fig. 7.2.

7.9):

$$\Psi + \eta\Psi' + 2H(\eta)\Psi\Psi' + 2|\eta|(\Psi\Psi')' = 0, \tag{7.14}$$

where $H(\eta)$ is the sign of η: 1 if $\eta > 0$ and -1 if $\eta < 0$. In the $\eta > 0$ domain, solutions under the form $\Psi = a\eta + b$ exist, under the conditions $b/2 + ab = 0$ and $a(1 + 2a) = 0$. This leads to 2 families of solution : the null function and the more interesting $\Psi = -\eta/2 + b$, where b is free. If $\eta < 0$, one gets the solution $\Psi = \eta/2 + b$. There is no other polynomial solutions of higher order.

If the cluster is initially centered ($y_0 = 0$), a centered triangle-shaped distribution would be compatible with this family of solutions. We can hope that other centered distribution would converge towards this solution, as seen in the simulations.

Back to the initial function Φ, one gets, in the $y > 0$ space, the following form, for which we consider that at $x = y = 0$, the maximal concentration is 1 and the initial width is not 0, therefore one should consider $x + x_0$ instead of x, where $-x_0$ is the hypothetic initial position where the width was 0:

$$\Phi(x, y) = (x + x_0)^{-1/2}(-y(x + x_0)^{-1/2}/2 + x_0^{1/2}) \tag{7.15}$$

as long as it is positive, and 0 otherwise.

Back to the initial units, the concentration is then given by:

$$\Phi(x, y) = \Phi_0 \frac{\sqrt{a_x}}{\sqrt{x + x_0}}(-\frac{y}{2d}\frac{\sqrt{a_x}}{\sqrt{x + x_0}} + \frac{\sqrt{x_0}}{\sqrt{a_x}}), \tag{7.16}$$

where $a_x = \frac{d^3}{2fR^2\Phi_0}$ is the x-scale. The distribution becomes 0 at $y = 2\frac{d}{a_x}\sqrt{x + x_0}\sqrt{x_0}$, which is also the width at half-height of the whole distribution. $2x_0\frac{d}{a_x}$ is therefore the initial width at half-height $2w_0$ of the distribution. The half-width at half-height is finally given by :

$$w(x) = w_0\sqrt{1 + \frac{2fR^2\Phi_0}{d^2}\frac{x}{w_0}} \tag{7.17}$$

It seems difficult to build easily non-centered solutions. In that case, we can consider the local problem, still with homogeneous velocity, which is justified by the above consideration, and a shear rate which is constant in the vicinity of the considered center of the initial cluster. We are thus in the same situation as the case of diffusion due to out of plane shear, that is $\delta = 0$, therefore $\alpha = 1/3$. Simulations with non-centered initial distribution and diffusion due to in-plane shear show effectively a $x^{1/3}$ broadening with a

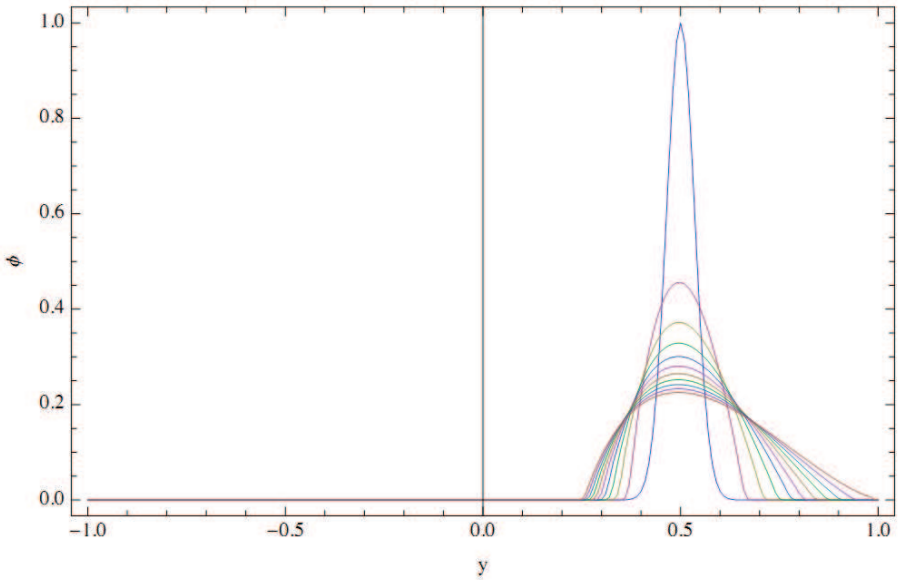

Figure 7.6: Concentration profiles from the numerical resolution of equation 7.13, for $x = 0$ to 2 by 0.2 steps; with off-centered initial condition.

parabolic profile before flow asymmetry plays a role:

In figure 7.6, the concentration profiles are shown for different x positions for an initial condition $\Phi(0, y) = e^{-400(y-0.5)^2}$ (off-centered cluster). The profiles are symmetric in a first time, before diffusion becomes more important close to the walls. As shown on figure 7.7, the amplitude exhibits a power-law as a function of x, which is found to be very close to an exponent -0.33. Again, as seen on figure 7.8, the power-law behaviour of the width is less clear but the exponent is close to $1/3$ before increasing slightly.

7.5.5 Contribution of out-of-plane shear or of in-plane shear on off-centered cluster

If $\delta = 0$, equation 7.13 gives the following equation for Ψ (see also eq. 7.9):

$$\Psi + \eta\Psi' + 3\Psi'^2 + 3\Psi\Psi'' = 0, \tag{7.18}$$

Polynomial solutions can be found, under the form $\Psi(\eta) = 0$ or $\Psi(\eta) = -\frac{1}{6}\eta^2 + b$, where b is free. We get the parabolic profile seen in the simulations (fig. 7.7).

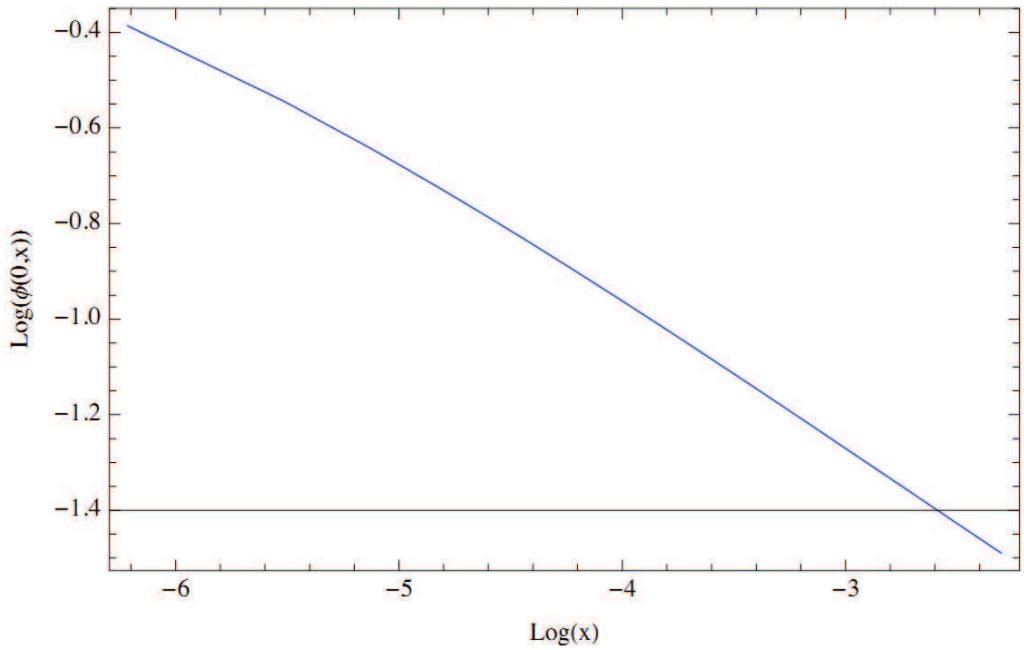

Figure 7.7: Log-log plot of distribution amplitudes as a function of x. The distributions are those of figure 7.6. A fit gives $\Phi(0, x) = 0.11(x{+}0.001)^{-0.322}$.

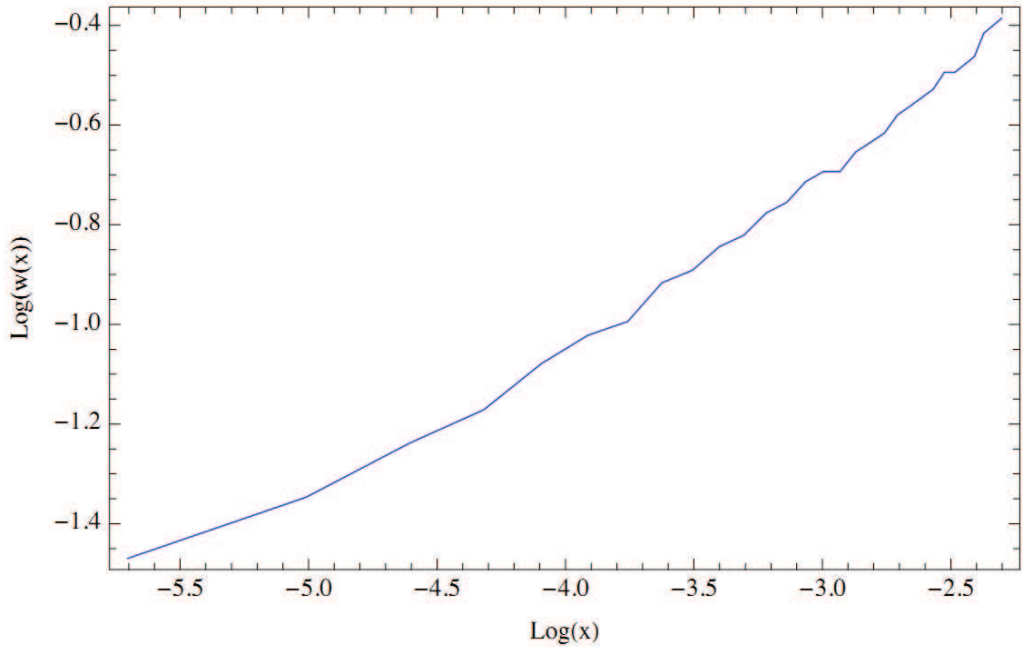

Figure 7.8: Log-log plot of distribution widths as a function of x. The distributions are those of figure 7.6.

We get for Φ: $\Phi(x,y) = (x+x_0)^{-1/3}(-y^2(x+x_0)^{-2/3}/6 + x_0^{1/3})$ if positive, and 0 otherwise. Back to the initial units, we find

$$\Phi(x,y) = \Phi_0 \frac{{a_x}^{1/3}}{(x+x_0)^{1/3}}\left(-\frac{y^2}{6d^2}\frac{a_x^{2/3}}{(x+x_0)^{2/3}} + \frac{x_0^{1/3}}{{a_x}^{1/3}}\right), \tag{7.19}$$

where $a_x = \frac{v_0 d^2}{f R^2 \Phi_0 |\dot{\gamma}|}$ is the x-scale.

Solving $\Phi(x,y) = \Phi(x,0)/2$, we find that the half-width at half-height is given by :

$$w(x) = \sqrt{3}d\,\frac{(x+x_0)^{1/3}\,x_0^{1/6}}{a_x^{1/2}} = w_0\Big(1 + \frac{3fR^2\Phi_0|\dot{\gamma}|}{v_0}\frac{x}{w_0^2}\Big)^{1/3} \tag{7.20}$$

Note that $|\dot{\gamma}|$ is proportional to v_0, so the result is v_0-independent in reality. In case we consider the diffusion due to in-plane shear, and if y_0 is the location of the center of the distribution, we have $v_0 = v_{\max}(1 - y_0^2/d^2)$, where $v_{\max}$ is the fluid maximum velocity, and $|\dot{\gamma}| = 2v_{\max}|y_0|/d^2$.

If the diffusion is due to out-of-plane shear, if the velocity profile in the xz plane of thickness $2h$ is the parabolic, $|\dot{\gamma}|$ is the mean value $(2h)^{-1}|\int_{-h}^{h} 2v_0 z/h^2\, dz = v_0/h$. In particular, $w(x)$ will not depend on the lateral position y_0 of the diffusing cluster.

Conclusion

In the two subcases considered in the preceding subsections, the half-width can finally be written as

$$w(x) = w_0(1+ax)^{\alpha}, \tag{7.21}$$

with the following values for a and α:

$$a = \begin{cases} 2f_2R^2\Phi_0\frac{1}{w_0 d^2} & \text{for centered cluster due to in-plane shear} \\ 6f_2R^2\Phi_0\frac{|y_0|}{w_0^2(d^2-y_0^2)} & \text{for off-centered cluster due to in-plane shear} \\ 3f_3R^2\Phi_0\frac{1}{w_0^2 h} & \text{for cluster at any location due to out-of-plane shear} \end{cases} \tag{7.22}$$

$$\alpha = \begin{cases} 1/2 & \text{for centered cluster due to in-plane shear} \\ 1/3 & \text{for off-centered cluster due to in-plane shear} \\ 1/3 & \text{for cluster at any location due to out-of-plane shear} \end{cases} \tag{7.23}$$

These approximations are valid for not too wide clusters, for which we can consider only the leading order of advection velocity and shear rate.

7.6 Arrangement of the work

7.6.1 Sample preparation

The blood sample used in the experiments was collected from a healthy donor and provided by EFS Grenoble. In order to prevent their aggregation over long times and their adhesion on the non-treated surfaces, we remove the plasma from the whole blood solution by washing the cells thrice in an aqueous solution of Phosphate Buffer Saline (PBS) and Bovine Serum Albumin (BSA), purchased from Sigma. After gentle centrifugation, this model cellular solution was dispersed into the suspending media chosen for the experiment. In order to test the effect of the viscosity of the surrounding fluid, several suspending media were prepared by dissolving dextran at a molecular weight from 15000 to 2×10^6 in the PBS and BSA buffer. The viscosities of the solutions were measured and varied with respect to the concentration of dextran added. Although dextran is known to facilitate aggregation of blood cells, no aggregates were observed during the time of our experiments in the range of dextran concentration we used. Two type of external suspension were used in the experiment:

1) A solution of PBS and BSA of measured viscosity 1 m Pa.s.

2) A mixture of 10% dextran of molecular weight 15000 + 5% dextran of molecular weight 450000 in PBS and BSA solution of measured viscosity 20 m Pa.s.

7.6.2 Device and flow set-up :

To study the diffusion behaviour of RBCs in simple shear flow, we used a microfluidic device of the same geometry as explained in chapter 6(section 6.2.1). To study the diffusive behaviour of the cluster we used concentrated sample of RBCs. When RBCs cluster is injected in the channel, by pinching the suspension between two auxiliary flow a high hydrostatic pressure from the two sides of the channel is needed. Therefore, to pinch the RBCs cluster in such a way that their flow can be adjusted at any expected lateral position of the channel and shear rate can be controlled, we modified the length of the channel.

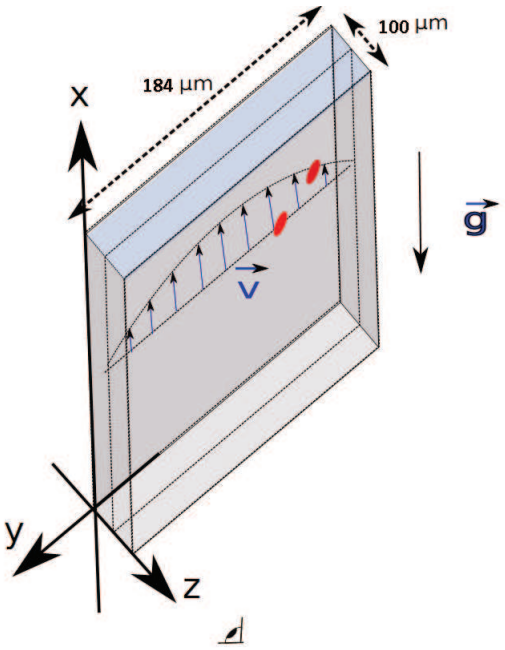

Figure 7.9: Schematic of shear and projection plane

We designed channels with a very long length, 200mm, with a series of turns of radius of curvature of 400 μm, of typical width 184μm whereas the side channels were reduced in length and directly connected to the inlets in order to maximise hydrodynamic pressure. To prevent sedimentation direction of flow was kept vertical as shown in fig. 7.9. The flow of RBCs was followed in X-direction to whereas lateral position of flow was in Y-direction and plane of projection in Z-direction, as shown in fig. 7.9. The cluster width are measured by considering the intensity profile in the Y direction as a rough measure of concentration. The cluster flow at different Y position along X direction in downstream flow is shown in fig. 7.10 and 7.11.

7.7 Results and discussions:

In figure 7.12, we show the x variations of half-widths of centered clusters of RBCs with no dextran in the outer solution, for varying initial widths. Fits with law $w(x) = w_0(1 + ax)^\alpha$, with (a, α) as fitting parameters give good results. α is found to be 0.35 if averaged on all the experiments, with a standard deviation of 0.09. No clear variation of α with w_0 is seen, so the α variations are probably due to low numbers of points on each curve.

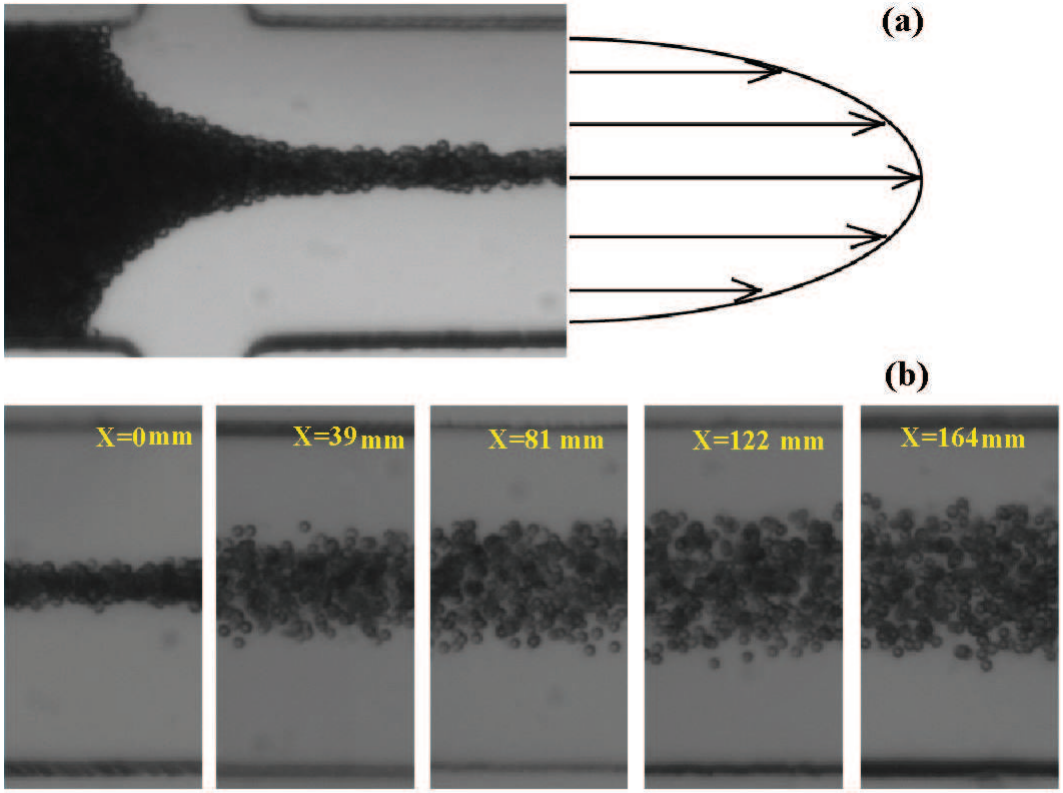

Figure 7.10: Snapshot of (a) pinching flow of red blood cells at the center of channel with initial lateral width Y_0 =0 (b) evolution of a red blood cell cluster along X (shown at different positions of the channel) and initial half-width 11.2 microns.

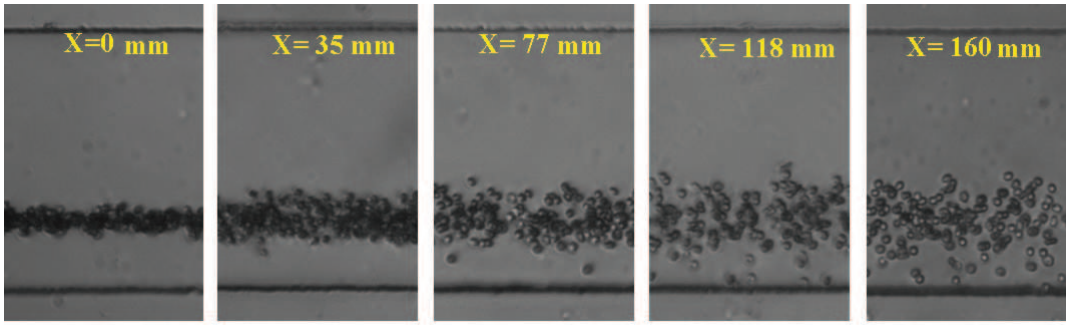

Figure 7.11: Snapshot of evolution of cluster initially off-center along X, the lateral position Y_0 is -41 microns and the channel half-width is 92 microns

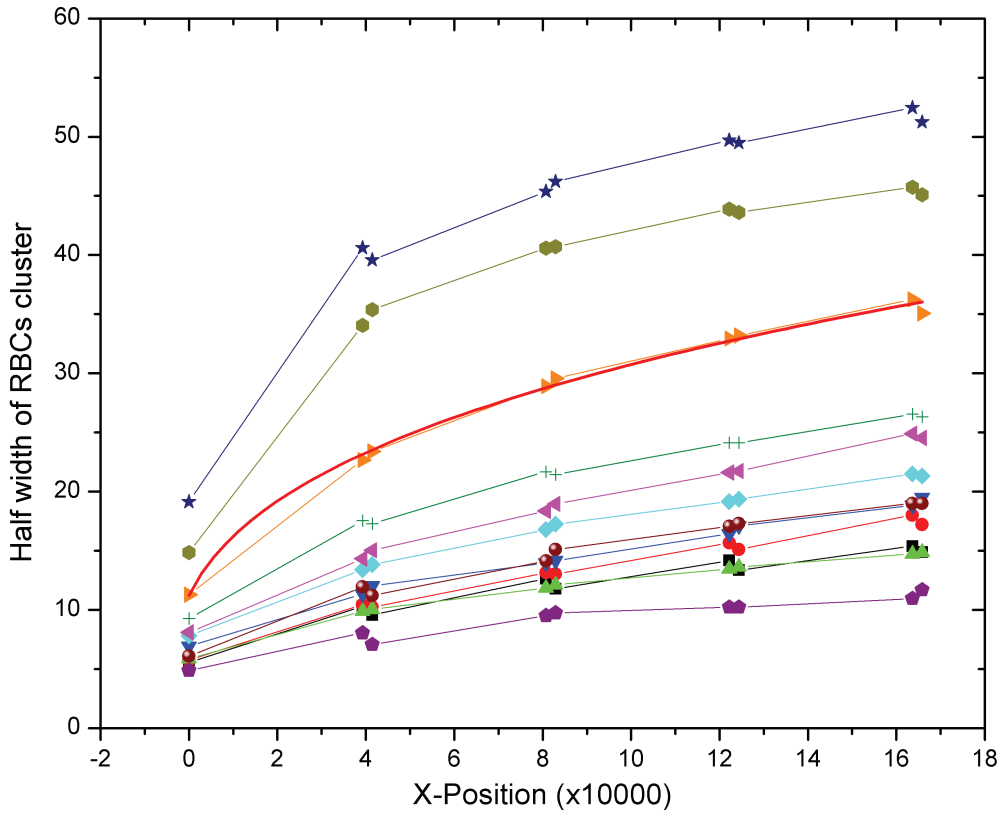

Figure 7.12: Variation of the widths of red blood cells clusters. Full line corresponds to the fit with $w(x) = w_0(1 + ax)^\alpha$. Distances are in microns

We retain that the spreading is subdiffusive, with an exponent not far from 1/3. This indicates that y-diffusion due to shear in the z direction is predominant, otherwise we would get diffusion with exponent 1/2. This is not a complete surprise, since the thickness is the half of the width: more important shear takes place in the z direction.

In order to make the difference between the out-of-plane shear and the in-plane shear contribution, it is convenient to vary the initial lateral position of the cluster. For this, we consider narrow initial clusters, in order to be close to the theory that is limited to the leading order for velocity and shear. One can see on figure 7.13, that diffusion increases when initial lateral position $|y_0|$ increases, which indicates that contribution of in-plane shear must also be taken into account, since pure out-of-plane contribution implies that a does not depend on y_0, as given by equation 7.22. If we assume that diffusive flows due to out-of-plane and in-plane shears can be added, one can see that a is the sum of the two expressions given for a in equation 7.22 for

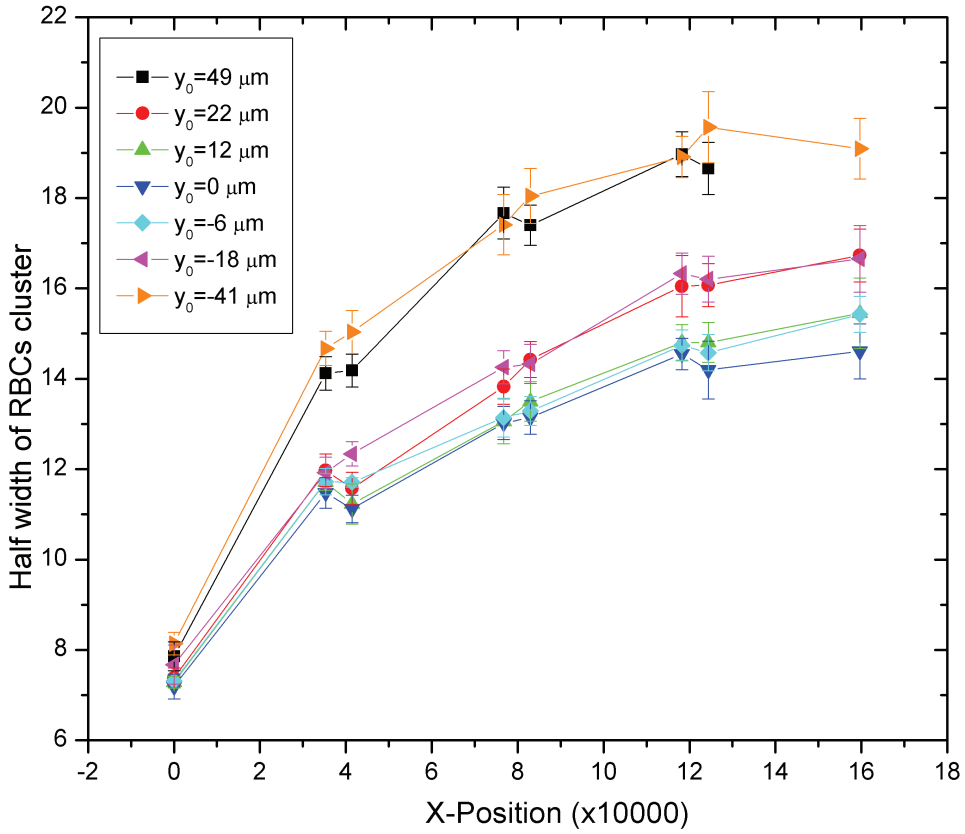

Figure 7.13: Variation of the width of red blood cell clusters at different lateral position of channel and distances are in microns

these two cases :

$$w_0^2 a = 3 f_3 R^2 \Phi_0 \frac{1}{h} + 6 f_2 R^2 \Phi_0 \frac{1}{d} \frac{|y_0|/d}{1-(y_0/d)^2)} \tag{7.24}$$

Fits with law $w(x) = w_0(1+ax)^\alpha$ of clusters of initial half-width $7.6 \pm 0.2\mu$m yield $\alpha = 0.24 \pm 0.04$, while we get $\alpha = 0.28 \pm 0.04$ for clusters of initial half-width $5.7 \pm 0.5\mu$m. These exponents slightly lower than $1/3$ might be reminiscences of 3-body interactions, which are expected to lead to lower exponent, from equation 7.10. In order to discuss the variations of a values, and since we made a 2-parameter fit on curves with a limited number of points, we choose to fix α to $1/3$ and make a 1-parameter fit. The results are shown on figure 7.14, where a is plotted as a function $\frac{|y_0|/d}{1-(y_0/d)^2)}$.

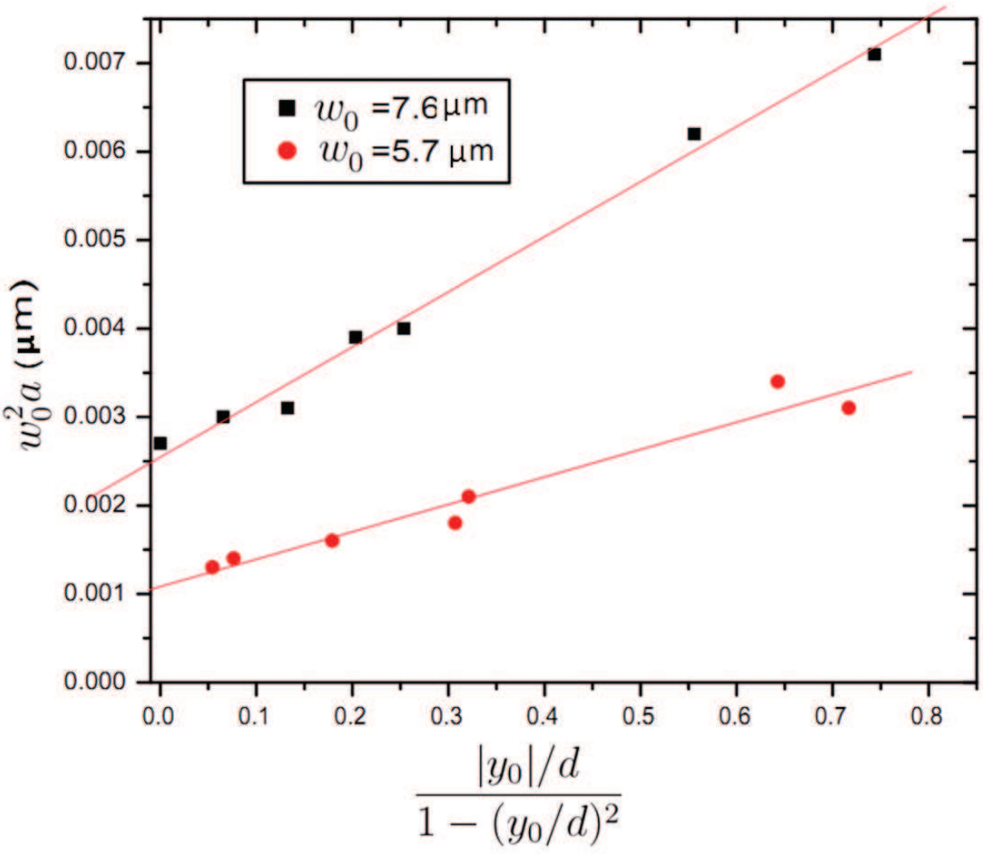

Figure 7.14: Evaluation of a for two different widths of red blood cells cluster, corresponding to fig 7.13

In agreement with equation , we find an affine dependency

$$a = a_0 + a_1 \frac{|y_0|/d}{1-(y_0/d)^2)}, \tag{7.25}$$

the slope giving a_1 the in-plane contribution and the value at origin giving the out-of-plane contribution.

In order to compute f_2 and f_3, we consider the mean volume of RBCs $V \simeq 90\mu$ m and find $R = \sqrt[3]{3V/(4\pi)} \simeq 2.8\mu$m. Φ_0 is estimated around 0.5, which leads to $f_2 = \frac{da_1}{6R^2\Phi_0} \simeq 0.002$ and $f_3 = \frac{ha_0}{3R^2\Phi_0} \simeq 0.001$ for $w_0 = 7.6$. For $w_0 = 5.7$, we find $f_2 \simeq 0.001$ and $f_3 \simeq 0.0005$. The variations between the two experiments can be due to uncontrolled dilution in the initial cluster as it is pinched, or to subtle interplay with the 3-body effect. However, the ratio f_2/f_3, which should be Φ_0 independent, is the same in the two experiments, and the values for f_2 of f_3 are in the good order of magnitude. Note that they are rather important even though the RBCs are in tumbling and not

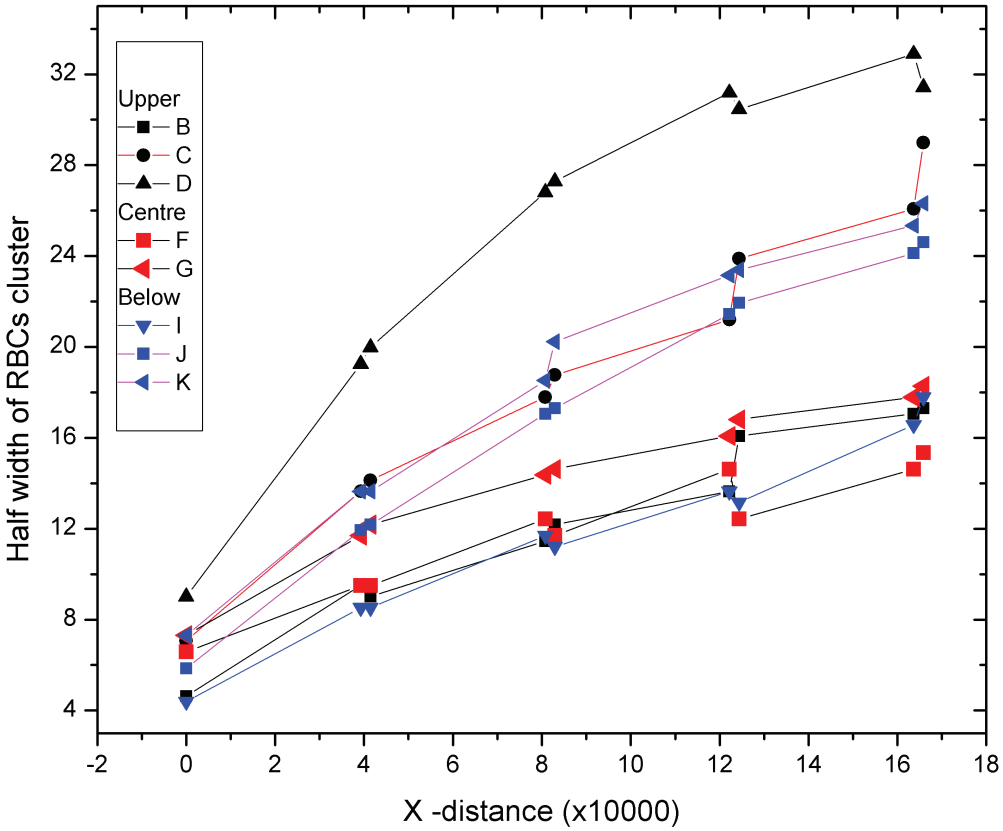

Figure 7.15: Variation of RBCs cluster width at different lateral position of channel with viscosity of outer fluid 20 m Pa.s. Distances are in microns

tank-treading regime.

To our knowledge, there have been only one determination of f_3 in the literature and none of f_2 for red blood cells. In [98], the diffusion coefficient D is determined from the random walk of a red blood cell in a channel much larger than thick. D is found to be proportional to the flow velocity v_0 : $D \simeq 0.6 v_0$, where D is given in $\mu m^2.s^{-1}$ and v_0 in $\mu m.s^{-1}$. We found that the diffusion coefficient D due to out-of-plane shear can be written as $D = f_3 \Phi_0 R^2 v_0 / h = a_0 / 3 v_0$, which gives, in the same units, $D = 0.08 v_0$ for the experiment where $w_0 = 7.6 \mu m$. We thus find a diffusion coefficient one order of magnitude lower.

When considering an outer solution with dextran, the results are less clear. On figure 7.15 are shown some $w(x)$ variations for three initial lateral positions. In this case, we find that centered clusters diffuse with an expo-

nent $\alpha = 0.38 \pm 0.04$ while superdiffusive behaviour is found for off-centered clusters with $\alpha = 0.62 \pm 0.08$. Even though the dynamics of RBCs is close to tank-treading in that case, we don't expect this to be the main reason for this unexpected behavious, since the general scalings for diffusive flows do not depend on the microscopic dynamics but through a multiplicative constant.

In summary, we have found a variety of regimes due to a subtle interplay between several effects : shear in the y and z directions and probably three body effects. A natural extension of this work should probably be a systematic explanation of the influence of the expectation of the channel's cross section (to vary relative importance of the shear in the two planes), and to make reliable measurements of the local concentration of blood cells in the cluster.

CHAPTER 7. SHEAR INDUCED DIFFUSION OF RBCS IN POISEUILLE FLOW

Chapter 8

Conclusion & Perspective

In this section, the obtained results are summarized and some concluding remarks are outlined.

8.1 Conclusion & major outcomes

Along the present thesis we explored the dynamics of red blood cells and lipid vesicles hydrodynamically interacting with each other.

As a preliminary study, in order to make comparisons between both systems, we first tried to study the dynamics of highly deflated vesicles having shapes similar to the one of red blood cells. These vesicles were produced by using DMPC as membrane lipids in an electroformation process run at a temperature higher than the one of the gel-liquid transition. Concave oblate and prolate shapes of vesicles were produced. Finally, the first study on highly deflated vesicles under flow was performed. It showed different dynamics than the one of quasi-spherical vesicles. In particular, tumbling-like motion was exhibited despite the absence of viscosity contrast. However, stability under flow of these vesicles appeared to be a crucial issue, which prevented us from running an exhaustive set of experiments.

When two deformable particles cross each other under flow, their trajectories are generally such that their final lateral distance is larger than the initial one. As a consequence, shearing a suspension of such particles will lead to their diffusion transversally to the flow direction. The corresponding diffusion coefficient can be derived from the knowledge of the trajectories of the particles as they interact.

We measured the net cross-flow displacement due to the collision between two identical vesicles under shear flow. This displacement was found to be a

decreasing function of the initial lateral separation, with a maximum value of the order of the vesicles radius for vesicles lying on almost the same streamline. On the contrary, vesicles separated by more than two radii showed no important deviation from their unperturbed trajectories. In addition, the displacement was shown to decrease slightly with increasing viscosity contrast. On the contrary, we found no significant dependency on the reduced volume, except for quasi-spherical vesicles, for which no important drift was found, as expected. We proposed an empirical model to describe the variations of the displacement with the initial lateral position and calculated the diffusion coefficient resulting from this interaction, which was found to be of the same order of magnitude as the one found in the literature for drops.

The next step was to measure diffusion of a vesicle suspension under shear flow, in order to check the accuracy of our experiments and calculations based on the basic event of pair interaction. To do so, we optimized a sorting technique named Pinched Flow Fractionation in order to produce a monodisperse population of vesicles. We showed that, in comparison with other techniques proposed in the literature, this technique is a fast, simple and efficient way to create subpopulations of similar sizes out of a very polydisperse sample. Such sorted samples will be studied under simple shear flow in microgravity conditions in order to prevent screening by sedimentation effects. These conditions will be obtained by setting the experiment in a sounding rocket, whose launching is scheduled for February 2012.

For this thesis, we focused on a second experimental set-up allowing to get rid of such undesired sedimentation effects, namely a microfluidic channel parallel to the gravity direction. As this set-up requires a continuous supply of concentrated enough vesicles, it appeared to be unadapted to the study of our monodisperse samples, which are highly diluted as they are produced.

Therefore, we chose to study the diffusion of red blood cells, which are available in large quantities and of same sizes. Jets of these cells were focused at the inlet of a channel and their broadening was studied as a function of their initial width and lateral position. As transverse movement only occurs when two particles meet, the corresponding diffusion coefficient is proportional to the concentration, which leads to non-linear advection-diffusion equations. Self-similar solutions of these equations were found under some hypothesis that were validated by numerical resolution of the full equations. Subdiffusion with exponent 1/3 instead of the classical 1/2 was predicted and confirmed by the experiments, which allowed us, in addition, to make the first estimate of the diffusion coefficient of red blood cells under shear flow, be it shear in the diffusion plane or orthogonal to it.

8.2 Perspective

The perspectives opened by our work are the following:

The new motions observed for highly deflated vesicles suggest that the phase diagram of vesicle dynamics in shear flow can be more complex than what is predicted from theories on weakly deflated shapes. More studies are needed to understand such a dynamics and its effect on the rheology of a suspension. The ultimate goal is to allow quantitative comparisons between red blood cells and vesicles of similar shapes, in order to characterize the role of the cytoskeleton. It is thus of the great importance in the future to find a stable and reliable method for producing highly deflated vesicles.

As already mentioned, sorted vesicles will be used to determine the diffusion coefficients under simple shear flow, which will allow direct comparisons with the value tabulated from the study of pair interaction. The latter should be enriched in a very near future by numerical simulations based on boundary integral method (thesis of Pierre-Yves Gires). When vesicles are placed in the same shear plane, the simulations showed quantitative agreement with the experiments. Varying the initial distance in the third direction, thus exploring the whole initial position space, will allow us to compute directly the diffusion coefficient without any simplifying hypothesis.

In a second time, diffusion experiments with red blood cells will allow to determine more precisely the ideal conditions for a reliable study, and will will make it possible to run experiments with sorted samples in an efficient and time-saving manner.

The diffusion experiments with red blood cells were run in a channel of fixed aspect ratio, where effects due to in-plane and out-of-plane shear were superimposed. The next step is to vary this aspect ratio, in order to study separately both effects and measure them with more accuracy. In a second time, the parameters governing the dynamics of red blood cells, such as viscosity contrast and capillary number, could be varied in order to study their effect on diffusion. In addition, studying pair interaction of red blood cells could support these diffusion measurements.

In a channel, this diffusion will be counterbalanced by wall effects, that tend to push cells towards the center. Unlike for vesicles, there have been very few studies aiming at quantifying that lift forces due to walls and their consequences on the spatial distribution of cells across the channel, although this non-homogeneous distribution is commonly identified as the cause of the dependency of blood effective viscosity on channel diameter.

Another perspective is to focus more precisely on situations of biological and medical interest, such as the platelet-RBC segregation, or the diffusion of cells in the presence of plasma proteins, that promote cell aggregation. Diffusion and lift forces are also influenced by cell mechanical properties: pathological cells will then have different behaviour, with possible consequences on their distribution and on blood viscosity, which remain widely unexplored.

Chapter 9

Conclusion & Perspectives (français)

Dans cette section, nous résumons nos principaux résultats et dressons les perspectives de notre travail.

9.1 Conclusion & apports principaux

Dans cette thèse, nous avons étudié la dynamique de globules rouges et de vésicules lipidiques en interaction hydrodynamique.

Afin de pouvoir mieux comparer ces deux systèmes, nous avons dans un premier temps essayé d'étudier la dynamique de vésicules très dégonflées, aux formes semblables à celles des globules. Ces vésicules ont été obtenues à partir de DMPC comme constituant de la membrane et électroformées à une température supérieure à la température de transition gel-liquide. Nous avons pu ainsi obtenir des formes oblates et prolates concaves. La première étude expérimentale sur des vésicules fortement dégonflées soumises à un écoulement de cisaillement a alors pu être initiée, ce qui a permis de mettre en valeur un comportement dynamique bien différent de celui prévu pour des vésicules quasi-sphériques. En particulier, un mouvement semblable à un mouvement de bascule a été observé, malgré l'absence de contraste de viscosité. Toutefois, la faible stabilité mécanique de ces vésicules lorsqu'elles sont soumises ! à une contrainte ne nous a pas permis de poursuivre vers une étude plus exhaustive.

Quand deux particules déformables se rencontrent sous écoulement, il en résulte généralement un déplacement accroissant leur séparation latérale. En conséquence, cisailler une suspension constituée de telles particules conduira

à leur diffusion transversalement à l'écoulement. Les coefficients de diffusion associés peuvent être directement calculés à partir de l'information sur les trajectoires des particules lors de l'interaction.

Nous avons mesuré le déplacement transverse de deux vésicules identiques sous cisaillement dû à leur collision. Ce déplacement est une fonction décroissante de la distance latérale initiale, avec une valeur maximale de l'ordre d'une rayon pour des vésicules situées quasiment sur la même ligne de courant. Au contraire, des vésicules situées à une distance supérieure à deux rayons ne sont pas déviées de manières significative lors de la colllision. Par ailleurs, nous avons montré que le déplacement décroît légèrement lorsque le contraste de viscosité augmente. En revanche, nous n'avons pas trouvé de dépendance significative de ce déplacement avec le dégonflement des vésicules, à l'exception des vésicules presque sphériques, pour lesquelles aucun déplacement n'est attendu ni observé. Nous avons proposé une loi empirique permettant de décrire l'évolution du déplacement final en fonction de la position latérale initiale et avons calculé le coefficient décrivant la diffusion résultant de cette interaction. Il est du même ordre de grandeur que celui proposé dans la littérature pour des gouttes.

L'étape suivante était de mesurer effectivement la diffusion dans une suspension cisaillée, afin de vérifier l'exactitude de notre calcul basé sur l'événement élémentaire que constitue l'interaction entre vésicules. A cet effet, nous avons optimisé une technique de tri basée sur le confinement hydrodynamique de la suspension à trier afin de produire une suspension de vésicules monodisperse en tailles. Nous avons montré que, en comparaison d'autres techniques proposées dans la littérature, celle-ci est particulièrement simple, rapide, et efficace. Les échantillons produits seront en particulier étudiés sous cisaillement simple en condition de microgravité afin de s'affranchir de la sédimentation, qui écrante les effets hydrodynamiques. Ces conditions seront obtenues grâce à l'installation de l'expérience dans une fusée sonde, dont le lancement est programmé pour février 2012.

Pour cette thèse, nous nous sommes focalisés sur un second dispositif expérimental, qui permet également de ne pas être dérangé par les effets de la gravité, à savoir un canal microfluidique vertical. Cependant, l'utilisation de ce dispositif nécessite une alimentation continue en vésicules raisonnablement concentrées, et nous a paru dans un premier temps inadapté pour étudier nos échantillons triés, qui sont relativement dilués une fois produits.

Par conséquent, nous avons choisi d'étudier la diffusion de globules rouges, objets disponibles en grandes quantités et de tailles similaires. Des jets de

cellules ont été focalisés à l'entrée d'un canal et leur élargissement a été étudié en fonction de leur largeur initiale et de leur positition latérale. Les déplacements latéraux n'ayant lieu que grâce à la rencontre de deux cellules, le coefficient de diffusion est proportionnel à la concentration, ce qui conduit à des équations d'advection-diffusion non linéaires. Des solutions autosimilaires de ces équations ont été trouvées sous certains hypothèses simplificatrices qui ont été validées par des résolutions numériques des équations complètes. Une sous-diffusion caractérisée par un exposant 1/3 (et non 1/2 comme en diffusion classique) a pu être mise en valeur et confirmée par les expériences. De plus, nous avons pu estimer pour la premi! ere fois les coefficients de diffusion de globules rouges sous cisaillement, que ce soit pour un cisaillement dans le plan de diffusion ou hors du plan.

9.2 Perspectives

Les perspectives que nous pouvons tirer de notre travail sont les suivantes :

Les nouveaux mouvements que nous avons pu observer pour des vésicules très dégonflées suggèrent que le diagramme de phase de la dynamique de vésicule sous écoulement est sans doute plus complexe que celui connu pour les vésicules faiblement dégonflées. Des études supplémentaires seraient nécessaires pour aller plus loin et comprendre l'effet de ces régimes sur la rhéologie d'une suspension. Le but final d'une telle étude pourrait être de faire une comparaison quantitative entre globules rouges et vésicules de même forme, afin de mesurer le rôle du cytosquelette. Il serait donc important de trouver une méthode fiable permettant de produire des vésicules fortement dégonflées et mécaniquement stables sous écoulement.

Ainsi que nous l'avons déjà signalé, les vésicules triées seront bientôt utilisées pour déterminer les coefficients de diffusion sous cisaillement simple, ce qui nous permettra de réaliser une comparaison avec nos calculs directs. Ces derniers pourront, dans un futur proche, être affinés grâce aux simulations numériques basées sur la méthode intégrale réalisées par Pierre-Yves Gires dans le cadre de sa thèse. Lorsque les vésicules sont placées dans le même plan de cisaillement, les simulations sont en accord avec les expériences. En variant la distance intiiale dans la troisème direction, et en explorant ainsi la totalité de l'espace des positions initiales, nous pourrons alors calculer plus précisément le coefficient de diffusion, sans hypothèse simplificatrice.

Dans un second temps, les expériences de diffusion sur globules vont nous permettre de déterminer les conditions idéales permettant d'obtenir rapidement des résultats à partir de l'expérience en canal, ce qui nous permettra

alors de mener efficacement des expériences avec ces échantillons triés.

Les expériences de diffusion de globules rouges ont été menées dans un canal de rapport d'aspect donné, où les effets du cisaillement dans le plan et du cisaillement hors du plan de diffusion se combinaient. La prochaine étape est naturellement de varier ce rapport d'aspect, afin de découpler ces deux phénomènes et mesurer de manière plus précise les coefficients associés. Dans un second temps, les paramètres contrôlant la dynamique des globules, tels le rapport de viscosité où le nombre capillaire, pourront être modifiés afin de quantifier leur effet sur la diffusion. En complément, une étude directe de l'interaction de paire entre globules pourraient enrichir ces mesures.

Dans un canal, cette diffusion sera équilibrée par les effets de paroi, qui tendent à faire migrer les vésicules vers le centre. Contrairement au cas des vésicules, il y a à ce jour très peu d'études quantifiant ces forces de portance et leurs conséquences sur la distribution finale des cellules dans le canal, bien que cette distribution inhomogène soit identifiée depuis longtemps comme la cause principale de la dépendance de la viscosité effective du sang envers le diamètre d'un canal.

Une autre perspective de ce travail est de s'intéresser à des situations d'intérêt biological ou médical, comme la ségrégation entre globules et plaquettes, ou la diffusion de cellules en présence de protéines du plasma, qui ont tendance à favoriser l'aggrégation des cellules. La diffusion comme les effets de paroi sont également influencés par les propriétés mécaniques des cellules : les cellules pathologiques auront ainsi un comportement différent, avec des conséquences possibles sur leur distribution et sur la viscosité du sang. Tout ceci reste un sujet largement inexploré par la physique.

Bibliography

[1] J. L.M. Poiseuille. "recherches sur les causes du mouvement du sang dans les vaisseaux capillaires.". *Ann. Sci. Nat., Series 2 (Zool. Biol. Animale)*, 5:111–115., 1836.

[2] R. Fåhræus and T. Linqvist. The viscosity of the blood in narrow capillary tube. *Am. J. Physiol.*, 96:562–568, 1931.

[3] R. Guibert, C. Fonta, and F. Plouraboue. A New Approach to Model Confined Suspensions Flows in Complex Networks: Application to Blood Flow. *Transport Porous Med.*, 83:171–194, 2010.

[4] K. Svanes and B. W. Zweifach. Variations in small blood vessel hematocrits produced in hypothermic rats by micro-occlusion. *Microvasc. Res.*, 1:210–220, 1968.

[5] T. M. Fischer, M. Stöhr-Lissen, and H. Schmid-Schönbein. The red cell as a fluid droplet: tank tread-like motion of the human erythrocyte membrane in shear flow. *Science*, 202:894–896, 1978.

[6] A. R. Pries, T. W. Secomb, and P. Gaethgens. Biophysical aspects of blood flow in the microvasculature. *Cardiovasc. Res.*, 32:654–667, 1996.

[7] M. Abkarian, M. Faivre, and H. A. Stone. High-speed microfluidic differential manometer for cellular-scale hydrodynamics. *PNAS*, 103:538, 2006.

[8] M. Abkarian, M. Faivre, and A. Viallat. Swinging of red blood cells under shear flow. *Phys. Rev. Lett.*, 98:188302, 2007.

[9] V. Vitkova, M.-A. Mader, B. Polack, C. Misbah, and T. Podgorski. Micro-macro link in rheology of erythrocyte and vesicle suspensions. *Biophys. J.*, 95:33, 2008.

[10] Badr Kaoui, George Biros, and Chaouqi Misbah. Why do red blood cells have asymmetric shapes even in a symmetric flow? *Phys. Rev. Lett.*, 103:188101, 2009.

[11] M. Abkarian, M. Faivre, R. Horton, K. Smistrup, C. A. Best-Popescu, and H. A. Stone. Cellular-scale hydrodynamics. *Biomed. Mater.*, 3:034011, 2008.

[12] Duc Bach Nguyen Jue Wang Lisa Wagner-Britz Achim Jung Christian Wagner Ingolf Bernhardt Lars Kaestner, Patrick Steffen. Lysophosphatidic acid induced red blood cell aggregation in vitro. *Bioelectrochemistry*, Under press, 2011.

[13] Pries A.R. Gaehtgens P Alonso, C. Time-dependent rheological behavior of blood at low shear in narrow vertical tubes. *American Journal of Physiology - Heart and Circulatory Physiology*, Volume 265, Issue 2 34-2, ,1993:1993, 1993.

[14] Albert L. Lehninger et al. *Principlesl of Biochemistry: The Molecular Basis of Cell Structure and Function*. Worth Pub, July 1, 1978.

[15] Udo Seifert. Configurations of fluid membranes and vesicles. *Advances in Physics*, 46(1):13–137, 1997.

[16] Evan. Evans and David. Needham. Physical properties of surfactant bilayer membranes: thermal transitions, elasticity, rigidity, cohesion and colloidal interactions. *The Journal of Physical Chemistry*, 91(16):4219–4228, 1987.

[17] Needham Evans. Structure and mechanical properties of giant lipid (dmpc) vesicle bilayers from 20 "c below to 10 "c above the liquid crystal-crystalline phase transition at 24 c. 27 (21),:pp 82618269, 1988.

[18] Méléard et al. Bending elasticities of model membranes: Influences of temperature and sterol content. *Biophysical Journal*, Volume 72, Issue 6,:Pages 2616–2629, 1997.

[19] P. Méléard, C. Gerbeaud, P. Bardusco, N. Jeandaine, M. D. Mitov, and L. Fernandez-Puente. Mechanical properties of model membranes studied from shape transformations of giant vesicles. *Biochimie*, 80(5-6):401 – 413, 1998.

[20] E. Evans and W. Rawicz. Entropy-driven tension and bending elasticity in condensed-fluid membranes. *Phys. Rev. Lett.*, 64:2094–2097, Apr 1990.

[21] U. Seifert, K. Berndl, and R. Lipowsky. Shape transformations of vesicles: Phase diagram for spontaneous- curvature and bilayer-coupling models. *Phys. Rev. A*, 44(2):1182–1202, Jul 1991.

[22] R. Dimova, B. Pouligny, and C. Dietrich. Pretransitional effects in dimyristoylphosphatidylcholine vesicle membranes: Optical dynamometry study. *Biophys J*, 79:340–356, 2000.

[23] K. Velikov, C. Dietrich, A. Hadjiisky, K. Danov, and B. Pouligny. Motion of a massive microsphere bound to a spherical vesicle. *EPL (Europhysics Letters)*, 40(4):405, 1997.

[24] R. Dimova, C. Dietrich, A. Hadjiisky, K. Danov, and B. Pouligny. Falling ball viscosimetry of giant vesicle membranes: Finite-size effects. *The European Physical Journal B - Condensed Matter and Complex Systems*, 12:589–598, 1999. 10.1007/s100510051042.

[25] K. Olbrich, W. Rawicz, D. Needham, and E. Evans. Water permeability and mechanical strength of polyunsaturated lipid bilayers. *Biophys. J.*, 79:321, 2000.

[26] John F. Nagle. Theory of passive permeability through lipid bilayers. *The Rockefeller University Press*, 2008.

[27] Narla Mohandas. Mechanical properties of the red cell membrane in relation to molecular structure and genetic defects. *Annu. Rev. Biophys. Biomol. Struet.*, 23:787–818, 1994.

[28] Guillaume Lenormand. Direct measurement of the area expansion and shear moduli of the human red blood cell membrane skeleton. *Biophysical Journal*, 81:43–56, 2001.

[29] Thomas M Fischer. Shape memory of human red blood cells. *Biophysical Journal*, 86(5):3304–3313, 2004.

[30] R. M. Hochmuth. Erythrocyte membrane elasticity and viscosity. *Ann. Rev. Physiol.*, 49:209–19, 1987.

[31] John Sleep. Elasticity of the red cell membrane and its relation to hemolytic disorders: An optical tweezers study. *Biophysical Journal*, Volume 77, Issue 6,:Pages 3085–3095, 1999.

[32] Worthy P. R. Evans E. A. Hochmuth, R. M. Red cell extensional recovery and the determination of membrane viscosity. *Biophys. J.*, 26:101–14, 1979.

[33] T C Terwilliger and A K Solomon. Osmotic water permeability of human red cells. *The Journal of General Physiology*, 77(5):549–570, 1981.

[34] Victor W. Sidel and A. K. Solomon. Entrance of water into human red cells under an osmotic pressure gradient. *The Journal of General Physiology*, 41(2):243–257, 1957.

[35] http://www.microscopyu.com/articles/phasecontrast/phasemicroscopy.html.

[36] Dongqing Li David Erickson. Integrated microfluidic devices. *Microfluidics and Lab - On - a - Chip*, Volume 507, Issue 1:Pages 11–26, 2003.

[37] Jongin Hong. Micro- and nanofluidic systems for high-throughput biological screening. *Drug Discover y Today*, Volume 14,:Pages 134–146, 2009.

[38] J. K. Chang. Fabrication of the pdms microchip for serially diluting sample with buffer. *Microsystem Technologies Springer*, Volume 9,:Number 8, 555–558, 2003.

[39] F Szoka and D Papahadjopoulos. Procedure for preparation of liposomes with large internal aqueous space and high capture by reverse-phase evaporation. *Proceedings of the National Academy of Sciences*, 75(9):4194–4198, 1978.

[40] L.D. Mayer, M.J. Hope, and P.R. Cullis. Vesicles of variable sizes produced by a rapid extrusion procedure. *Biochimica et Biophysica Acta (BBA) - Biomembranes*, 858(1):161 – 168, 1986.

[41] John P. Reeves and Robert M. Dowben. Formation and properties of thin-walled phospholipid vesicles. *Journal of Cellular Physiology*, 73(1):49–60, 1969.

[42] Dimitrov Angelova M., Dimiter S. Liposome electro formation. *Faraday Discuss. Chem. Soc.*, 81:303–311, 1986.

[43] D.S. Dimitrov and M.I. Angelova. Lipid swelling and liposome formation mediated by electric fields. *Journal of Electroanalytical Chemistry and Interfacial Electrochemistry*, 253(2):323 – 336, 1988.

[44] A. Srivastav, T. Podgorski, and G. Coupier. Efficiency of size-dependent separation by pinched flow fractionation. *Submited to Microfluidics and nanofluidics*, 2012.

[45] N. Pamme. Continuous flow separations in microfluidic devices. *Lab on a chip*, 7:1644–1659, 2007.

[46] M. Yamada, M. Nakashima, and M. Seki. Pinched flow fractionation: Continuous size separation of particles utilizing a laminar flow profile in a pinched microchannel. *Anal. Chem.*, 76:5465, 2004.

[47] A. L. Vig and A. Kristensen. Separation enhancement in pinched flow fractionation. *Appl. Phys. Lett.*, 93:203507, 2008.

[48] H. Maenaka, M. Yamada, M. Yasuda, and M. Seki. Continuous and size-dependent sorting of emulsion droplets using hydrodynamics in pinched microchannels. *Langmuir*, 24:4405–4410, 2008.

[49] J. Takagi, M. Yamada, M. Yasuda, and M. Seki. Continuous particle separation in a microchannel having asymmetrically arranged multiple branches. *Lab Chip*, 5:778–784, 2005.

[50] Y. Sai, M. Yamada, M. Yasuda, and M. Seki. Continuous separation of particles using a microfluidic device equipped with flow rate control valves. *J. Chrom. A*, 1127:214, 2006.

[51] X. Zhang, J. M. Cooper, P. B. Monaghan, and S. J. Haswell. Continuous flow separation of particles within an asymmetric microfluidic device. *Lab Chip*, 6:561–566, 2006.

[52] A. Jain and J. D. Posner. Particle dispersion and separation resolution of pinched flow fractionation. *Anal. Chem.*, 80:1641–1648, 2008.

[53] J. R. Keller and R. Skalak. Motion of a tank-treading ellipsoidal particle in a shear flow. *J. Fluid. Mech.*, 120:27, 1982.

[54] G. Jeffery. The motion of ellipsoidal particles immersed in a viscous fluid. *Proc. R. Soc. Lond. Ser. A*, 102:161–179, 1922.

[55] T. Biben, C. Misbah, A. Leyrat, and C. Verdier. An advected-field approach to the dynamics of fluid interfaces. *Europhys. Lett.*, 63:623–629, 2003.

[56] J. Beaucourt, F. Rioual, T. Séon, T. Biben, and C. Misbah. Steady to unsteady dynamics of a vesicle in a flow. *Phys. Rev. E*, 69:011906, 2004.

[57] Vasiliy Kantsler and Victor Steinberg. Orientation and dynamics of a vesicle in tank-treading motion in shear flow. *Phys. Rev. Lett.*, 95:258101, 2005.

[58] M. Mader, V. Vitkova, M. Abkarian, A. Viallat, and T. Podgorski. Dynamics of viscous vesicles in shear flow. *The European Physical Journal E: Soft Matter and Biological Physics*, 19:389–397, 2006.

[59] Thierry Biben, Alexander Farutin, and Chaouqi Misbah. Three-dimensional vesicles under shear flow: Numerical study of dynamics and phase diagram. *Phys. Rev. E*, 83:031921, Mar 2011.

[60] C. Misbah. Vacillating breathing and tumbling of vesicles under shear flow. *Phys. Rev. Lett.*, 96:028104, 2006.

[61] V. Kantsler and V. Steinberg. Transition to tumbling and two regimes of tumbling motion of a vesicle in shear flow. *Phys. Rev. Lett.*, 96:036001, 2006.

[62] P. M. Vlahovska and R. Serral Gracia. Dynamics of a viscous vesicle in linear flows. *Phys. Rev. E*, 75:016313, 2007.

[63] V. V. Lebedev, K. S. Turitsyn, and S. S. Vergeles. Dynamics of nearly spherical vesicles in an external flow. *Phys.Rev. Lett.*, 99:218101, 2007.

[64] H. Noguchi and G. Gompper. Swinging and tumbling of fluid vesicles in shear flow. *Phys. Rev. Lett.*, 98:128103, 2007.

[65] Gerrit Danker, Thierry Biben, Thomas Podgorski, Claude Verdier, and Chaouqi Misbah. Dynamics and rheology of a dilute suspension of vesicles: Higher-order theory. *Phys. Rev. E*, 76:041905, 2007.

[66] A. Farutin, T. Biben, and C. Misbah. Analytical progress in the theory of vesicles under linear flow. *Phys. Rev. E*, 81:061904, 2010.

[67] Ghigliotti, Giovanni, Selmi, Hassib, Kaoui, Badr, Biros, George, and Misbah, Chaouqi. Dynamics and rheology of highly deflated vesicles. *ESAIM: Proc.*, 28:211–226, 2009.

[68] J. Kas and E. Sackmann. Shape transitions and shape stability of giant phospholipid vesicles in pure water induced by area-to-volume changes. *Biophysical Journal*, 60(4):825 – 844, 1991.

[69] E. Sackmann. Membrane bending energy concept of vesicle- and cell-shapes and shape-transitions. *Elsevier Science Publisher*, Volume 346, Issue 1,:Pages 3–16, 1994.

[70] Kitty de Jong and Peter Ott. Membrane phospholipid asymmetry in dmpc-induced human red cell vesicles. *FEBS Letters*, 334(2):183 – 188, 1993.

[71] P.B. and Canham. The minimum energy of bending as a possible explanation of the biconcave shape of the human red blood cell. *Journal of Theoretical Biology*, 26(1):61 – 81, 1970.

[72] W.Helfrich H.J.Deuling. The curvature elasticity of fluid membranes : A catalogue of vesicle shapes. *Le Journal de Physique*, 37:1335–1345, 1976.

[73] Michael P. Sheetz and S. J. Singer. Biological membranes as bilayer couples. a molecular mechanism of drug-erythrocyte interactions. *Proceedings of the National Academy of Sciences*, 71(11):4457–4461, 1974.

[74] S. Svetina, Angela Ottova-Leitmannov, and R. Glaser. Membrane bending energy in relation to bilayer couples concept of red blood cell shape transformations. *Journal of Theoretical Biology*, 94(1):13 – 23, 1982.

[75] S.Svetina and B. Zek. Membrane bending energy and shape determination of phospholipid vesicles and red blood cells. *European biophysics journal*, Feb-1989.

[76] K. Berndl, J. Ks, R. Lipowsky, E. Sackmann, and U. Seifert. Shape transformations of giant vesicles: Extreme sensitivity to bilayer asymmetry. *EPL (Europhysics Letters)*, 13(7):659, 1990.

[77] G. K. Batchelor. The stress generated in a non-dilute suspension of elongated particles by pure straining motion. *Journal of Fluid Mechanics*, 46(04):813–829, 1971.

[78] G. K. Batchelor and J. T. Green. The hydrodynamic interaction of two small freely-moving spheres in a linear flow field. *Journal of Fluid Mechanics*, 56(02):375–400, 1972.

[79] L. Van Wijngaarden and D. J. Jeffrey. Hydrodynamic interaction between gas bubbles in liquid. *Journal of Fluid Mechanics*, 77(01):27–44, 1976.

[80] A. Biesheuvel and L. Wijngaarden. The motion of pairs of gas bubbles in a perfect liquid. *Journal of Engineering Mathematics*, 16:349–365, 1982.

[81] E. J. Hinch. An averaged-equation approach to particle interactions in a fluid suspension. *Journal of Fluid Mechanics*, 83(04):695–720, 1977.

[82] A.Z. Zinchenko. Effect of hydrodynamic interactions between the particles on the rheological properties of dilute emulsions. *Journal of Applied Mathematics and Mechanics*, 48(2):198 – 206, 1984.

[83] F. R. Da Cunha and E. J. Hinch. Shear-induced dispersion in a dilute suspension of rough spheres. *Journal of Fluid Mechanics*, 309:211–223, 1996.

[84] M. Loewenberg and E.J. Hinch. Collision of two deformable drops in shear flow. *J. Fluid Mech.*, 338:299, 1997.

[85] E. Lac, A. Morel, and D. Barthès-Biesel. Hydrodynamic interaction between two identical capsules in simple shear flow. *J. Fluid. Mech.*, 573:149, 2007.

[86] Y. Wang, R. Mauri, and A. Acrivos. The transverse shear-induced liquid and particle tracer diffusivities of a dilute suspension of spheres undergoing a simple shear flow. *Journal of Fluid Mechanics*, 327:255–272, 1996.

[87] Y. Wang, R. Mauri, and Acrivos.A. Transverse shear-induced gradient diffusion in a dilute suspension of spheres. *Journal of Fluid Mechanics*, 357:279–287, 1998.

[88] A. Acrivos, G. K. Batchelor, E. J. Hinch, D. L. Koch, and R. Mauri. Longitudinal shear-induced diffusion of spheres in a dilute suspension. *Journal of Fluid Mechanics*, 240:651–657, 1992.

[89] V. Kantsler, E. Segre, and V. Steinberg. Dynamics of interacting vesicles and rheology of vesicle suspension in shear flow. *Europhys. Lett.*, 82:58005, 2008.

[90] Thomas Podgorski, Natacha Callens, Christophe Minetti, Gwennou Coupier, Frank Dubois, and Chaouqi Misbah. Dynamics of Vesicle Suspensions in Shear Flow Between Walls. *MICROGRAVITY SCIENCE AND TECHNOLOGY*, 23(2):263–270, FEB 2011. Biennial Symposium of the European-Low-Gravity-Research-Association (ELGRA), Bonn, GERMANY, SEP 01-04, 2009.

[91] N. Callens, C. Minetti, G. Coupier, M.-A. Mader, F. Dubois, C. Misbah, and T. Podgorski. Hydrodynamic lift of vesicles under shear flow in microgravity. *Europhys. Lett.*, 83:24002, 2008.

[92] G. Coupier, B. Kaoui, T. Podgorski, and C. Misbah. Noninertial lateral migration of vesicles in bounded Poiseuille flow. *Phys. Fluids*, 20:111702, 2008.

[93] P. Olla. The lift on a tank-treading ellipsoidal cell in a shear flow. *J. Phys. II France*, 7:1533–1540, 1997.

[94] N. Callens, C. Minetti, G. Coupier, M.-A. Mader, F. Dubois, C. Misbah, and T. Podgorski. Hydrodynamic lift of vesicles under shear flow in microgravity. *EPL (Europhysics Letters)*, 83(2):24002, 2008.

[95] Geoffrey Taylor. Dispersion of soluble matter in solvent flowing slowly through a tube. *Proceedings of the Royal Society of London. Series A. Mathematical and Physical Sciences*, 219(1137):186–203, 1953.

[96] Eugene C. Eckstein, Douglas G. Bailey, and Ascher H. Shapiro. Self-diffusion of particles in shear flow of a suspension. *Journal of Fluid Mechanics*, 79(01):191–208, 1977.

[97] Roberto Rusconi and Howard A. Stone. Shear-induced diffusion of platelike particles in microchannels. *Phys. Rev. Lett.*, 101:254502, Dec 2008.

[98] John M. Higgins, David T. Eddington, Sangeeta N. Bhatia, and L. Mahadevan. Statistical dynamics of flowing red blood cells by morphological image processing. *PLoS Comput Biol*, 5(2):e1000288, 02 2009.

List of Figures

List of Tables

Abstract

Blood is a complex suspension of deformable particles, red blood cells, which exhibits a sophisticated dynamics when flowing in the microvasculature. Most of these complex phenomena, non-linear rheology, structuration of the suspension, heterogeneities of the hematocrit distribution, are directly connected to the rich microscopic dynamics of individual red blood cells, and their hydrodynamics interactions. We investigate a few aspects of the dynamics of red blood cells and giant vesicles - a simple model for RBCs.

A study on the dynamics of very deflated vesicles, with shapes similar to those of red blood cells, shows that these objects which haven't received a lot of attention so far can exhibit richer than expected dynamics.

We then mainly focus on the still unexplored problem of hydrodynamic interactions between vesicles or red blood cells and their consequences at the scale of the suspension. An experimental study of the interaction of two identical vesicles in shear flow shows that there is a net repulsion between the cells that leads to an increase of the distance between vesicles in a suspension. Scaling arguments are proposed for this interaction and a comparison with numerical results is performed and a quantitative estimation of a shear induced diffusion coefficient obtained by averaging the results for pair interactions is found.

Finally, we investigate the diffusion of a cloud of red blood cells in Poiseuille flow in order to directly determine diffusion coefficients. The experiment shows that the cloud widens when traveling along the channel with a power law behaviour indicating sub-diffusion. This effect is confirmed by a theoretical analysis of a few limit cases.

Résumé

Le sang est une suspension de particules déformables, les globules rouges, qui possède une dynamique riche lorsqu'il s'écoule dans la microvasculature. La plupart des ces phénomènes complexes, comme la rhéologie non-linéaire, la structuration inhomogène de la suspension, ou l'hétérogénéité de l'hématocrite dans les différents vaisseaux, sont directement liés à la dynamique individuelle des globules rouges, elle-même très riche, ainsi qu'à leurs interactions hydrodynamiques. Nous nous intéressons à quelques aspects de cette dynamique, en considérant des globules mais aussi des vésicules lipidiques géantes, un modèle simple de globules.

Une première étude sur des vésicules de forme semblable à celle des globules montre que ces objets jusqu'à présent peu étudiés peuvent présenter une dynamique plus riche qu'attendu.

Nous nous focalisons ensuite principalement sur le problème encore ouvert de l'interaction hydrodynamique entre vésicules ou entre globules, et sur ses conséquences à l'échelle de la suspension. Une étude expérimentale de l'interaction de deux vésicules identiques placées dans un écoulement de cisaillement nous permet de metttre en évidence une répulsion entre les deux objets, ce qui conduit à un éloignement des vésicules en suspension. Une loi d'échelle est proposée afin de caractériser cette interaction et est comparée à nos expériences et à des simulations numériques. Une estimation quantitative du coefficient de diffusion associé à cette interaction est alors fournie.

Enfin, nous étudions la diffusion d'un amas de globules rouges dans un écoulement de Poiseuille afin de mesurer directement les coefficients de diffusion. Les expériences montrent que l'amas s'élargit en s'écoulant le long du canal, en suivant une loi de puissance indiquant un comportement sous-diffusif. Cet effet est confirmé par une analyse théorique de quelques cas limites.